Assembly of charged gold nanocrystals at electrodes and liquid/liquid interfaces

Cover: Photographic image of charge-stabilised colloidal gold solutions in water. The diameter of the particles ranges from 4.5 nm (left vial) to several hundred nanometers (right vial). For more information see chapter 2, section 2.2.

Assembly of charged gold nanocrystals at electrodes and liquid/liquid interfaces

Assemblages van geladen goud nanokristallen op elektroden en aan vloeistof/vloeistof grensvlakken

(met een samenvatting in het Nederlands)

Proefschrift

ter verkrijging van de graad doctor aan de Universiteit Utrecht op gezag van de Rector Magnificus, Prof. dr. W.H. Gispen, ingevolge het besluit van het College voor Promoties in het openbaar te verdedigen op maandag 26 januari 2004 des middags te 2.30 uur

door

François Henri Reincke

geboren op 30 augustus 1976, te Leidschendam

Promotor: Prof. dr. D. Vanmaekelbergh,
Prof. dr. J. J. Kelly,

Co-promotor: dr. W. K. Kegel

Allen verbonden aan de Faculteit Scheikunde van de Universiteit Utrecht

Druk: Labor Grafimedia B.V., Utrecht

ISBN 90-393-3577-X

Contents

CHAPTER 1

Introduction

In the field of nanoscience it has long been a goal to control and structure matter at the molecular level, *i.e.* at the nanometre scale, with the ultimate aim to produce nanostructured functional systems, such as lasers[**1, 2**], magnetic storage media[**3**], and nanometre-sized electronic devices (nanoelectronics)[**4**]. Although some methods of manipulation at the atomic level are known, see for instance the well-known "IBM" logo of Xe atoms [**5**], these essentially involve one-molecule-at-a-time and cannot produce large-scale devices within any reasonable time scale. Optical methods, like photolithography[**6**], can produce extended devices within an acceptable production time, but cannot produce structures smaller than approximately 100 nm[**6**].

There is, therefore, a large interest in systems which have a propensity to self-assemble; they contain building blocks that order themselves in a regular and controlled fashion due to interactions at the molecular level. This scheme can be compared to building a house. First, the 'bricks', the nanocrystals (or the organic equivalent: a polymer/macromolecule), are synthesised from a molecular precursor. These nanocrystals preferably have a defined shape and size and are stable (*i.e.* do not coagulate) in solution. Preparation and storage of such nanocrystals (molecular precursors) is not trivial and these requirements will be discussed later in this introduction. In the second stage, the nanocrystals must self-assemble into a well-defined structure.

1. Stability of colloidal suspensions

A suspension of colloidal particles in a liquid is typically in a metastable state; in the absence of stabilisation, the particles collect (aggregate and/or sedimentate) at the bottom of the vial due to gravity, since the solid phase has a higher density than the surrounding solvent. There are many ways in which particle aggregation can occur [**7**]. Stabilisation methods have been developed, designed to keep the particles separated. There are two distinct ways the colloidal solution can be stabilised; through *steric stabilisation* (section 1.1) and *charge stabilisation* (section 1.2). These two methods will be discussed in the following sections. To place this in the right context, we first discuss the most important inter-particle interactions, such as van der Waals attraction, Born repulsion, and double-layer repulsion.

1.1. Steric stabilisation. The London-van der Waals forces, which we will refer to as van der Waals forces, originate from quantum-mechanical local fluctuations in the electron density allowing atoms, molecules and colloidal particles to have a temporal dipole moment; this can induce a dipole moment of opposite sign on a neighbouring atom, molecule or colloidal particle. The dipole moments interact to give an attractive force $\mathcal{F}_{vdWaals}$. In the case of two identical atoms (molecules) $\mathcal{F}_{vdWaals}$ is given approximately by [**7**]:

$$\mathcal{F}_{vdWaals} = -\frac{\frac{9}{2}h\nu\alpha^2}{r^7} \tag{1.1}$$

where r is the atom (or particle) separation (in metres), h is Planck's constant ($6.63\ 10^{-34}\ Js$), α (in m^{-3}) the polarisability of the atom or molecule, and ν (Hz) is a characteristic frequency corresponding to the first ionization potential.

The work required to bring together reversibly two molecules from a distance $r = \infty$ to a distance $r = r$, via van der Waals attraction is given by:

$$\Delta W_{attr} = \int_{\infty}^{r} \mathcal{F}_{vdWaals}\ dr = -\frac{\frac{3}{4}h\nu\alpha^2}{r^6} \tag{1.2}$$

Colloidal particles, however, consist of many atoms. Equation 1.2 can be applied at large separation between two particles (in that case the particles are approximately point masses), but it cannot be used to describe colloidal particles at small separation ($x/R \ll 1$, where R is the particle radius and $x = r - 2R$ is the surface-to-surface distance). An atom at the particle centre interacts less strongly with the another particle than an atom at the surface facing that other particle. The van der Waals attraction of one atom with a particle is calculated by integrating $\mathcal{F}_{vdWaals}$ over all volume elements v_2 of the attracted particle, $\int_{V_2} \mathcal{F}_{vdWaals}(\overrightarrow{r})\ dv_2$. The attraction between two particles is found by integrating the previous result over the volume of the attracting particle:

$$\Delta W_{vdWaals} = \int_{V_1}\int_{V_2} \mathcal{F}_{vdWaals}(\overrightarrow{r})\ dv_2\, dv_1 \tag{1.3}$$

At close separation $x/R \ll 1$, the particles can be approximated by two infinitely large parallel plates. The work per unit area required to bring the plates to a separation x is [**7**]:

$$\Delta W_{vdWaals} = -\frac{H}{12\pi x^2} \tag{1.4}$$

with H the Hamaker constant, which is a measure for the van der Waals interaction energy between two materials; H is given approximately by Lifshitz theory[**8**]:

$$H \approx \frac{3}{4}kT\left(\frac{\varepsilon_1-\varepsilon_3}{\varepsilon_1+\varepsilon_3}\right)^2+\frac{3h\nu_e}{16\sqrt{2}}\frac{(n_1^2-n_3^2)^2}{(n_1^2+n_3^2)^{3/2}} \tag{1.5}$$

with k the Boltzmann constant, and T the absolute temperature. The two dielectric media, the particle(s) and the solvent, are approximated by a simplified model that only depends on three values: the static dielectric constant ε; the refractive index n (measured using visible light); and the main electronic absorption frequency of the medium in the UV ν_e. Subscripts 1 and 3 refer to the colloidal particle and the solvent, respectively.

Equation 1.4 is plotted in curve (a) of figure 1. In this introduction, we will only discuss the parallel plate approximation. Later, in chapter 4, the solution for spherical particles will be considered.

Comparing equations 1.2 and 1.4 one can see that the attraction between colloidal particles decreases much more slowly with increasing distance than the attraction between atoms. The van der Waals interaction would, if no repulsive force is present, drive all the particles to coalescence. However, as the particles touch the electron clouds overlap, a repulsive force $\mathcal{F}_{Born}$, referred to as Born or steric repulsion, occurs. The Born interaction is intrinsically quantum mechanical in nature. In practice the Born repulsion force can be approximated by:

$$\mathcal{F}_{Born}=\frac{B}{x^{13}} \tag{1.6}$$

where B is a constant.

The work due to Born repulsion is therefore given by:

$$\Delta W_{Born}=\frac{B}{12x^{12}} \tag{1.7}$$

which is plotted in curve (b) figure 1.

The total work $\Delta W_{tot}=\Delta W_{Born}+\Delta W_{vdWaals}$ is plotted in curve (c) of figure 1. This interaction curve has a shape similar to the well-known Lennard-Jones potential curve.

In the previous section it was implicitly assumed that only Born repulsion occurred when two particles touch. It is also possible, however, that two colloidal particles contacting each other form a (chemical) bond. This is one of the ways in which particles can aggregate irreversibly. Even when $\Delta W_{vdWaals} \ll \Delta W_{Born}$ there is still a finite chance that particles touch. Therefore capping molecules, such as alkanethiols[**9**] and polymers[**10**], are introduced into the colloidal system. Capping molecules are chosen such that they attach to the particle surface, but do not bond to each other. The capping molecules spontaneously form a layer of width δ around the particle,

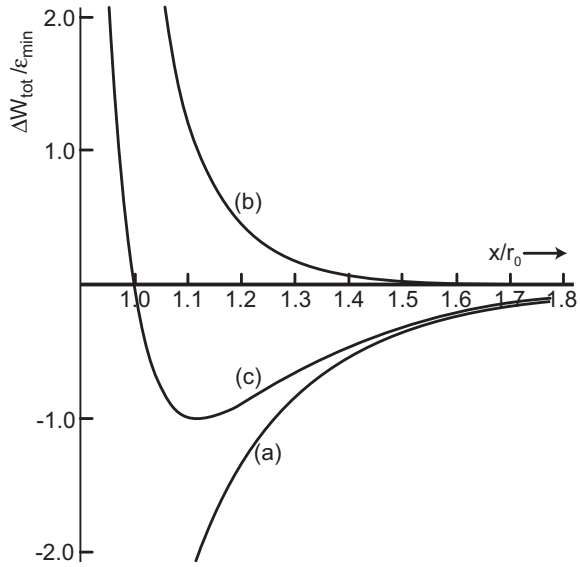

Figure 1. Change of the free energy due to the interaction of two spherical particles. **a.** van der Waals attraction, **b.** Born repulsion, **c.** van der Waals and Born interactions combined. $\varepsilon_{min} = \Delta W_{tot}$ at the minimum of curve **c**. Reproduced from Colloid Science[**7**].

which is, in fact, a case of self-assembly. As the particles touch ($x \leq 2\delta$), the capping molecules exert a steric repulsion, see figure 2a. When the capping is chemically similar to the surrounding solvent, *e.g.* a capping made from alkyl chains in an organic solvent, the van der Waals attraction between capping and solvent is nearly equal to the attraction between the capping molecules of two colloidal particles which are in close proximity. Hence, there is little or no extra van der Waals attraction due to the introduction of the capping. This can also be seen in equation 1.5. Chemically similar compounds have similar dielectric properties, thus $\varepsilon_1 \approx \varepsilon_3$ and $n_1 \approx n_3$, leading to a small van der Waals interaction energy. The capping molecules thus lead to a considerable decrease of the driving force for aggregation.

Since the stabilisation is due to steric repulsion, these particles are said to be *sterically stabilised*. Generally, this is not a hard-shell interaction as depicted in figure 2a, situation (i), since the layers formed around the molecules are flexible and often have an open structure. This may be an intrinsic property of the capping[**7**] or may be due to the curvature of the particle[**11**]. Pressing these two capping layers together forces the capping molecules into a fixed position, which causes a loss of entropy and leads to entropic repulsion. In addition, the openings are filled with solvent, which is squeezed out against the osmotic pressure when the capping layer is compressed.

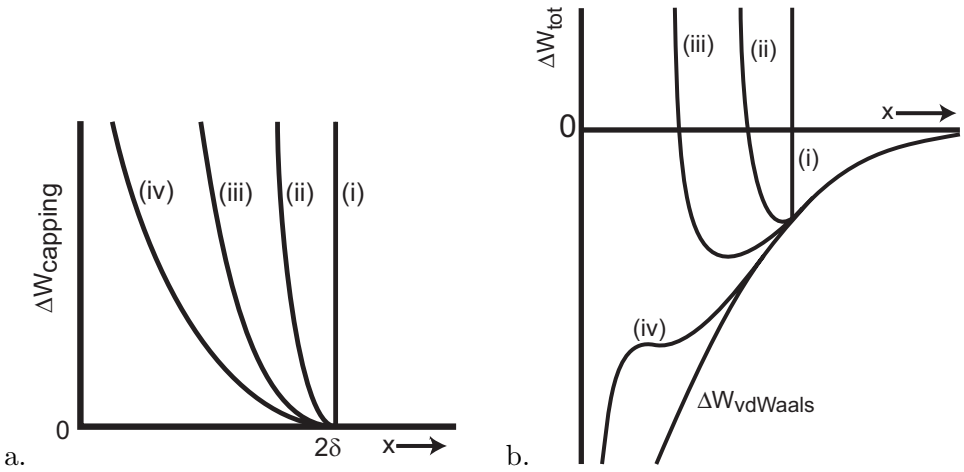

Figure 2. **a.** Repulsion of two capped particles (layer thickness δ) for capping going from very dense in (i) to very porous in (iv). **b.** The effect of van der Waals attraction (figure 1, curve (a)) combined with the effect of the capping. Reproduced from Colloid Science[**7**].

As can be seen in figure 2b, situation (iv), if the density of capping molecules on the particle surface is insufficient or the capping layer is too thin (δ too small), steric stabilisation is unable to prevent aggregation. Therefore, particles capped with longer and/or more rigid capping molecules are more stable. *However*, a colloidal solution with a sufficiently long/dense capping can still aggregate. As can be seen in figure 2b, situation (iii), there is a minimum (ΔW_{min}) close to $x = 2\delta$. If the difference between ΔW_{min} and $\Delta W(x \to \infty)$ is larger than kT the particles have a low probability to dissociate after aggregation has occurred. Long capping molecules are therefore better for stabilising uncharged particles, since the repulsive interaction occurs at larger x where the van der Waals attraction is relatively small.

The function of the capping goes beyond providing stability for the colloidal solution. Capping molecules also play an important role in the synthesis of the colloidal solution, *e.g.* the relative amount of capping agent versus reactants determines the size of the particles formed[**12, 13**]. The capping also strongly influences the surface chemistry of the particles; for instance, it determines the type of solvent in which the particles are stable[**12, 14**]. Fortunately, the capping can be replaced after synthesis without aggregation of the colloidal solution by repetitive exposure to an excess of the desired capping molecule[**15**], provided that the capping is in an adsorption/desoprtion equilibrium with the surrounding solvent.

1.2. Charge stabilisation. Some particles are charged during their synthesis due to a surface reaction (*e.g.* surface oxidation or reduction) or due to preferential adsorption of charged species from the surrounding solution[**7**].

According to Coulomb's law the force between two charged bodies with charge q_1 and q_2 separated by a distance r is expressed as:

$$\mathcal{F}_{Coulomb} = \frac{q_1 q_2}{4\pi\varepsilon\varepsilon_0 r^2} \tag{1.8}$$

with ε and ε_0 the relative dielectric constant of the surrounding medium and the permittivity of vacuum, respectively.

The electric field produced by the charges affects the distribution of ions close to the particle. The local concentration of ions can be calculated from the average value of the electrical potential $\psi(d)$, at a given distance $d = r - R$ from the particle surface, relative to the potential far away from the particle $\psi(d = \infty) \equiv 0$, using Boltzmann's theorem:

$$\left.\begin{array}{l} c_+(d) = c_0\ e^{-z_+ \mathbf{e}\psi(d)/kT} \\ c_-(d) = c_0\ e^{+z_- \mathbf{e}\psi(d)/kT} \end{array}\right\} \tag{1.9}$$

where c_0 is the bulk salt concentration, $c_+(d)$ and $c_-(d)$ the local concentrations of the positive and negative ions, z_+ and z_- the valence of the positive and negative ion, and $\mathbf{e}$ is the electron charge.

In figure 3a the concentrations of positive and negative ions are shown for a negatively charged particle in a $z_+ = z_-$ electrolyte solution. Close to the particle there is a depletion of negative ions, whereas there is an accumulation of positive ions. The effective charge of the diffuse double layer is therefore always opposite to the charge of the particle, see figure 3b. Since the colloidal solution as a whole must be electrically neutral, the total charge of the double layer must be equal to the particle charge.

The Poisson equation relates the spatial variation of $\psi(d)$ to the density of excess charge $\rho = z(c_+ - c_-)$. For the one-dimensional case, we have:

$$\frac{\partial^2 \psi(d)}{\partial d^2} = \frac{-\rho(d)}{\varepsilon\varepsilon_0} \tag{1.10}$$

After combining and solving equations 1.9 and 1.10 for $z\mathbf{e}\psi/4kT \ll 1$ one obtains the solution of the so-called linearised Poisson-Bolzmann equation:

$$\psi(d) = \psi^0 e^{-d/L_D} \tag{1.11}$$

with $\psi^0 = \psi(d = 0)$ the potential at the particle surface.

The electrical double layer is therefore characterised by two quantities: the electrostatic surface potential (determined by the particle charge) and the Debye screening length L_D; the first determines the strength of the double layer (through ψ^0), the latter is a measure for the spatial extension,

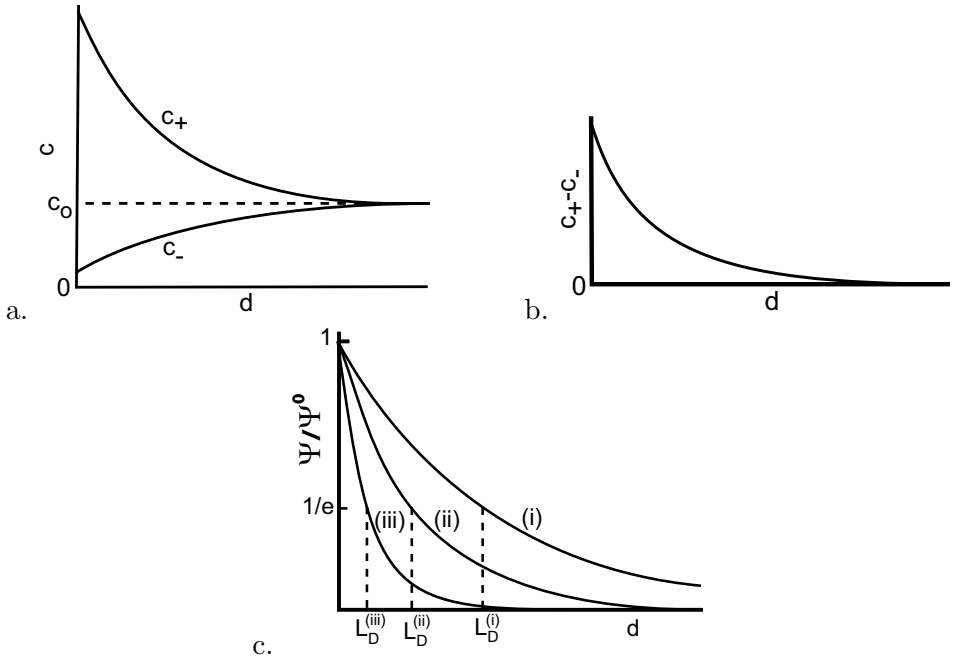

Figure 3. Double layer around a negatively charged colloidal particle in a $z-z$ valent electrolyte solution as a function of distance d from the particle surface. **a.** Concentration of positive (c_+) and negative (c_-) ions. **b.** Effective charge $c_+ - c_-$. **c.** Potential ψ for ionic strengths ranging from low (i) to high (iii). Reproduced from Colloid Science[**7**].

the width, of the double layer. The Debye screening length L_D, the length at which $\psi(d = L_D) = \psi^0/e \approx 0.36\,\psi^0$, is given by:

$$L_D = \sqrt{\frac{\varepsilon\varepsilon_0 kT}{2N_A \mathbf{e}^2 I}} \tag{1.12}$$

with N_A is Avogadro's number, and $I = \frac{1}{2}\sum_i c_i z_i^2$ the ionic strength. It should be noted that c_i and I are in units of mol/m^3.

In figure 3c the potential is shown as a function of d. As the concentration of salt in the solution is increased (going from situation (i) to (iii)), the width of the double layer decreases. Consider, for instance, an aqueous $NaCl$ electrolyte solution at $25°C$. The values of L_D are: 30.4 nm at 10^{-4} M, 9.6 nm at 10^{-3} M, 3.0 nm at 10^{-2} M, and 0.96 nm at 10^{-1} M.

As two charged particles approach each other, the diffuse double layers overlap. The overlap area will approximately have the summed charge of both double layers, depicted in figure 4a, which is energetically unfavourable.

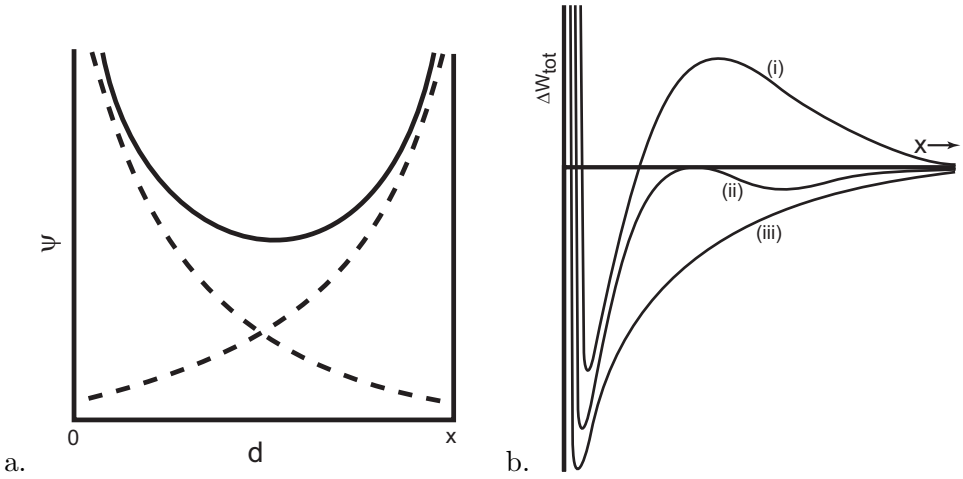

Figure 4. **a.** Potential profile due to the interaction of two double layers. **b.** Total free energy due to Born repulsion, van der Waals attraction and double layer repulsion for three different electrolyte concentrations ranging from (i) low to (iii) high. Reproduced from Colloid Science[**7**].

The work per area that is needed to bring two charged parallel plates together to a distance x due to the repulsion of the double layers is[a]:

$$\Delta W_{dl} = 16 N_A c_0 z \mathbf{e} \psi^0 L_D kT \, e^{-x/L_D} \tag{1.13}$$

which can be used as an approximation to describe the repulsion between two spherical particles at close separation.

When the free-energy contribution corresponding to double-layer repulsion is combined with the free-energy contributions for van der Waals attraction and Born repulsion (the "DLVO potential"), curves as shown in figure 4b are obtained. Looking at figure 4b situation (i), we see that an approaching particle (decreasing x) first encounters a potential barrier due the double-layer repulsion. If this barrier is in the order of several kT, the colloidal solution is stable. If not (situation (ii)), the barrier can be overcome after which van der Waals attraction drives the particles to contact, which will ultimately lead to complete coagulation of the colloidal solution.

It can be easily seen that a highly charged particle is likely to be more stable in solution than a particle with a low charge, since the energy barrier is larger in the former case. The width of the double layer is also an important factor in particle stability. When L_D is small, the double-layer repulsion occurs at the same length scale as the van der Waals attraction, where the repulsive effects are cancelled by the van der Waals attraction, see figure 4b, situation (iii). Therefore, L_D must be sufficiently large, so that the

[a] As before, c_0 is in units of mol/m^3

double layer repulsion is still appreciable at large x, where the van der Waals attraction is smallest, see figure 4b, situation (i). That the double layer width is inversely proportional to the square root of the salt concentration explains the well-known effect of particle coagulation on salt addition.

Since it is often difficult to raise the particle charge experimentally, it is possible to synthesise colloidal particles which are both sterically and charge stabilised. One employs a capping molecule with two functional groups. The first attaches to the particle and the second readily dissociates in the solvent, see *e.g.* references [**9, 14**].

2. Self-assembly of colloidal suspensions

Now that the colloidal 'building blocks' have been introduced, it is time to build the house. As you cannot build a (stable) house without mortar, there must be an inter-particle attraction which induces self-assembly. Here, we disregard the case in which assembly is driven purely by entropy, *i.e.* the crystallisation increases the free volume of the system[**16, 17**].

In the next section the interactions that cause self-assembly are outlined. Next, we will look at three different types of particles, which are widely used as model systems for self-assembly:

- Uncharged, non-magnetic particles
- Magnetic particles, both sterically and charge-stabilised
- Charge-stabilised particles

2.1. Interactions important for self-assembly. Let us first look at the self-assembly in two dimensions which can occur at the interface between a solid and a liquid or between two liquids. The first driving force for self-assembly is chemical bond formation. For this, a molecule with two functional groups at either end is required. One functional group bonds chemically to the substrate whereas the second bonds chemically to the colloidal particle. Self-assembly occurs when the substrate, pre-treated with the aforementioned molecule, is immersed in the colloidal solution. The mechanism of self-assembly is best compared to flies which are caught by sticky flypaper. The sulfide-gold and thiol-gold bond is often used in this respect, but also hydrogen bonds [**18**] and acid-base reactions [**19**] can be used. We have explored another type of molecules, *i.e.* oligo(cyclohexylidene)s as molecular bridges between a gold substrate and the colloidal particles. The motivation for this is that these molecules form extremely well-ordered self-assembled monolayers (SAMs)on gold surfaces, and they show a large electrical conductivity[**20**].

Another way to self-assemble colloidal particles into monolayers is by controlled evaporation of the colloidal solution. Logically, the amount of material in solution must be carefully selected so as not to exceed a monolayer. Self-assembly is aided by two effects that cause contraction of the

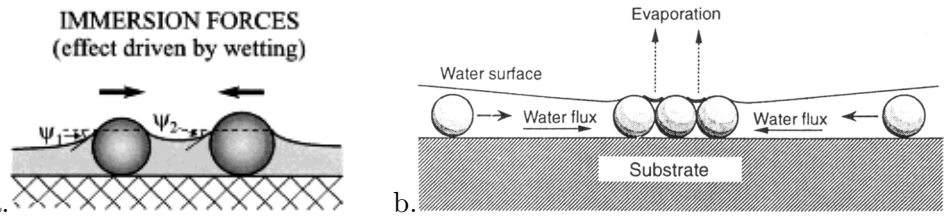

a. b.

Figure 5. Processes occurring in a particle-filled film whose thickness is smaller than the particle diameter. **a.** Capillary attraction due to wetting. Reproduced from Denkov *et al.*[**21**]. **b.** Particle assembly driven by the liquid flow. Reproduced from Kralchevski *et al.*[**22**]

sub-monolayer of particles, while the fluid film is drying. Firstly, when the thickness of the solvent layer is smaller than the particle diameter, the interface between two apolar particles becomes curved due to the wetting of the particles, see figure 5a. This curvature causes a capillary force, termed the immersion force, driving the particles together [**21, 23**]. The immersion force can be significant even for particles as small as 2 nm[**22**]. Secondly, a flux of solvent passing from the bulk to the aggregates, takes individual particles to the aggregate [**21**], see figure 5b.

Besides assembly at solid substrates, it is also possible to assemble 2-D structures at the interface of two immiscible liquids. Here, 2-D self-assembly is driven by a reduction of surface energy. Take for instance the self-assembly at a water/organic interface. If the electrostatic effects and line tension are disregarded, the interfacial (Helmholtz) free energy of a particle in the interface is:

$$F_{int} = A_{c/o}\gamma_{c/o} + A_{c/w}\gamma_{c/w} + (A_{o/w} - A_{occupied})\gamma_{o/w} \tag{1.14}$$

with γ the surface tension and A the area of the different interfaces, indicated with subscripts c/w for colloidal particle/water, c/o for colloidal particle/organic and o/w for the water/organic interface, respectively; $A_{occupied} = \pi R^2 \sin^2\theta$ is the area of the water/organic interface occupied by the particle[b]; θ is the three-phase contact angle as defined in figure 6a and R is the particle radius.

The interfacial energy of the system with the particle in the aqueous phase is given by:

$$F_{bulk} = 4\pi R^2 \gamma_{c/w} + A_{o/w}\gamma_{o/w} \tag{1.15}$$

The energy needed to move a particle from the interface into the aqueous phase is [**24**]:

$$F_{bulk} - F_{int} = A_{c/o}(\gamma_{c/w} - \gamma_{c/o}) - A_{occupied}\gamma_{o/w} \tag{1.16}$$

[b] *i.e.* the cross-sectional area of particle with the organic/water interface

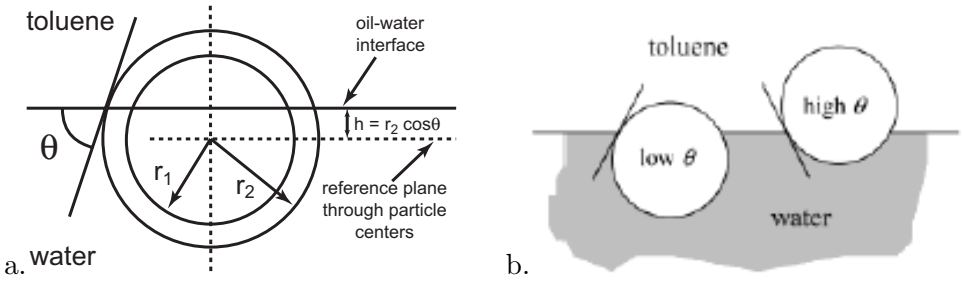

Figure 6. **a.** At equilibrium, a particle at the water/toluene interface is positioned such that the angle is equal to the three-phase angle θ. **b.** Position at the interface of a particle with a low and a high θ. Reproduced form Binks *et al.*[**26**]

After applying the Young-Dupré equation, $\cos\theta = (\gamma_{c/o} - \gamma_{c/w})/\gamma_{o/w}$, together with $A_{occupied} = \pi R^2 \sin^2\theta$ and $A_{c/o} = 2\pi R^2(1 - \cos\theta)$, equation 1.16 to simplifies to:

$$F_{bulk} - F_{int} = \pi R^2 \, \gamma_{o/w} \, (1 - \cos\theta)^2 \tag{1.17}$$

Equation 1.17 also shows that the three-phase contact angle θ is an important parameter. For $\theta = 0°$(completely hydrophilic particles) and $\theta = 180°$(completely hydrophobic particles) there is no energy difference between the bulk and the interface, hence no attachment occurs. For $0° < \theta < 180°$ the free energy of the interface is lower than that of the bulk $F_{bulk} > F_{int}$; in other words, energy is required to move a particle from the interface to the bulk. If $F_{bulk} - F_{int}$ is larger than kT, the interface effectively acts as a trap, localising particles until the interface is full. When line tension is taken into account, it was found that the previous statement holds except for θ close to 0 or 180 degrees for which the particles are not stable (*i.e.* $F_{bulk} < F_{int}$) in the interface[**25**].

At equilibrium and when no other forces act on the particle, the interface is flat and intersects the particle at an angle θ [**26**], see figure 6a and b.

Three-dimensional self-assembly can be achieved with the same interactions as involved in 2-D self-assembly, such as chemical interactions [**18, 27**] and controlled evaporation [**28**]. Controlled 3-D self-assembly is usually achieved by destabilisation of the colloidal solution, specifically by the addition of a "non-solvent". A non-solvent is a liquid that is miscible with the liquid surrounding the particles, but in which the particle is not stable. The non-solvent is typically a liquid with a different polarity than that of the colloidal solvent.

For example, take a colloidal solution of uncharged particles sterically stabilised with an apolar capping, which is stable in non-polar (organic)

solvents. To this solution a polar non-solvent is added. At a certain concentration, the polarity of the sovent/non-solvent mixture is high enough to cause a phase separation between the colloidal particles and the surrounding fluid. Due to van der Waals attraction between the capping molecules, the capping of adjacent particles tend to interdigitate[**29**]. Hence, there are two types of van der Waals attractions at play here: the van der Waals attraction between particles as described in section 1.1 and the van der Waals attraction between the capping molecules of two adjacent particles. In order to maximise both interactions, the geometry with the highest contact area is favoured.

2.2. Self-assembly of uncharged, non-magnetic particles. On gradual destabilisation in a polydisperse colloidal solution, the larger particles aggregate first, since the contact area between these is larger than for small particles [**30**] although in one instance the opposite structure (small particles surrounded by large ones) has also been reported[**31**]. This property is frequently used to reduce the polydispersity[c] of colloidal solutions. In this *size-selective crystallisation* procedure[**13, 32, 33**], just enough non-solvent is added to the colloidal solution to initiate aggregation. As the aggregates settle out, the supernatant, containing the fraction of smaller particles, is removed. The precipitate, with larger particles, is redissolved by adding solvent. This procedure can be repeated for a further reduction of the polydispersity.

When the polydispersity is lowered to below 5 to 10 %, crystal-like close-packed structures are formed from these colloidal solutions[**34**]. Due to the regular ordering of these particles this structure is also referred to as a *colloidal crystal*. The maximum polydispersity which still allows ordered lattices of particles was confirmed by calculations on hard-sphere particles [**35**–**37**].

When a mixure of two monodisperse colloidal solutions[d] with different particles sizes, termed a bimodal solution, is allowed to crystallise on a substrate and the particle sizes are very different $R_A/R_B < 0.27$ (where A and B are small and large particles, respectively) phase separation occurs[**29**]. As can be seen in figure 7a, both phases are hexagonally ordered. However, when the size ratio R_A/R_B is raised to 0.58 a mixed phase is formed, see figure 7b, where the small particles are locked within the lattice structure of the large particles as in ionic crystals. Since the atoms in the particles are themselves arranged in a crystal lattice, these patterns of colloidal particles are often referred to as superlattices. For monolayers, both a cubic AB and a hexagonal AB_2 (shown in figure 7b) superlattices were found, depending on the ratio R_A/R_B[**38**].

[c] the mean of the particle size distribution divided by its standard deviation

[d] a colloidal solution with a sufficiently low polydispersity

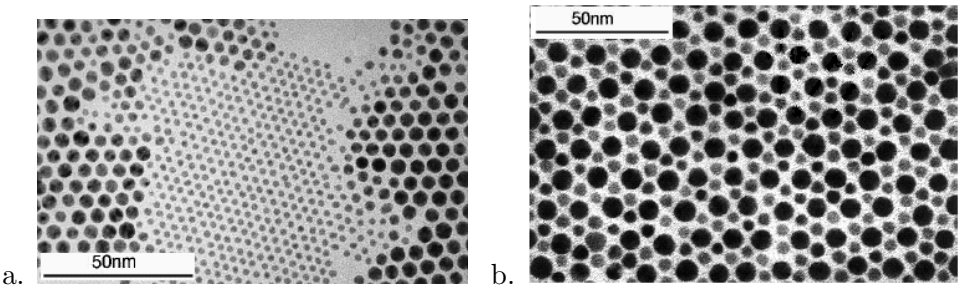

Figure 7. Two-dimensional self-assemblies of mixtures of two monodisperse Au nanocrystals of different size, with size ratios **a.** $R_A/R_B \approx 0.47$ and **b.** $R_A/R_B = 0.58$. Reproduced from Kiely *et al.*[**29**].

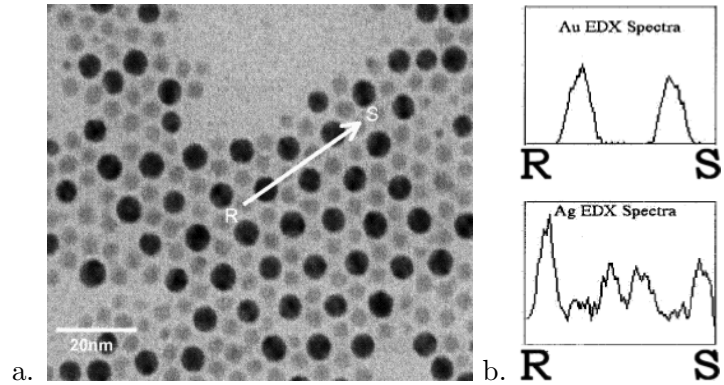

Figure 8. **a.** TEM image of Au and Ag nanocrystals capped with $C_{10}H_{21}SH$ in an AB_2 self-assembled 2D structure ($R_{Au}/R_{Ag} = 0.625$). **b.** Energy Dispersive X-ray (EDX) measurements sensitive for Au (top) and Ag (bottom) taken across the line R-S. Reproduced from Kiely *et al.*[**38**].

These mixed colloidal superlattices can also be made from two chemically different particles with the same capping [**38**]. In figure 8, a mixed monolayer of Au and Ag nanocrystals in an AB_2 structure is shown. As can be seen from the contrast of the particles in the TEM image and from the EDX spectra in figure 8b, each type of particle occupies a very distinct position in the superlattice.

Three-dimensional superstructures can also be formed from bimodal solutions. Several superlattices, such as AB_2[**39**], AB_4[**40**], AB_5[**41**] and AB_{13}[**39**], were found for different size ratios. The AB_2, AB_5 and AB_{13} superlattices resemble AlB_2, $CaCu_5$ and $NaZn_{13}$ crystals, respectively. In fact, the monolayer in figure 7b can be viewed as a crystal plane from either the AB_2 or AB_5 colloidal crystal[**29**]. These colloidal crystals were made

using particles of different materials, such as latex[**41**] and polymethylmethacrylate (PMMA)[**42**], and are even found in naturally occurring samples of Brazilian opals[**43**].

Murray *et al.* [**44**] modelled these systems by calculating the volume of a unit cell for several superlattices (AB, AB_2 and AB_{13}; AB_4 and AB_5 were not investigated) as a function of the R_A/R_B ratio. It was assumed that the more compact superlattice has the most contact area. The most compact superlattice, called the "stable" phase, is therefore preferentially formed. It was found that the AB superlattice, resembling $NaCl$, is stable in the range $0.24 < R_A/R_B < 0.458$ and the AB_2 superlattice in the range $0.482 < R_A/R_B < 0.624$. The AB_{13} superlattice was found to be unstable, unless a slight modification of the structure occurs. With this information phase diagrams were calculated.

In the formation of colloidal crystals, the capping is very important. Multilayers of monodisperse gold nanocrystals capped with tetraoctyl ammonium bromide ($[N(C_8H_{17})_4]^+ Br^-$) did not stack in a hexagonal close-packed structure[**28**]. This was ascribed to the local charge separation within the capping.

To conclude this section on sterically stabilised particles, we focus on the two-dimensional assembly of capped metal nanocrystals at liquid/liquid interfaces. Self-assembly at the interface is especially interesting since the interaction between the particles can be varied by applying a lateral pressure, while the structure can be probed optically[**45**] and electronically[**46**]. It is also possible to transfer these layers onto a solid substrate without destroying the essential features of the layers, using the Langmuir-Schäfer technique[**11**].

In a 2-D layer of metallic nanocrystals the conductive metal particles are separated by a potential barrier (the non-conductive capping). Since this barrier is small enough to allow electron tunnelling, it was found that lateral conduction through the layer occurs by sequential tunneling[**46, 47**]. When the layer is formed at a liquid interface the distance between the particles can be decreased without collapsing the layer [**11**] when flexible capping molecules are used. As the capping between the particles is compressed, the barrier is reduced and the conductivity becomes metal-like[**45, 46**]. This insulator-to-metal transition is reversible; when the lateral pressure is removed, the layer relaxes and the sequential tunnelling-type conductivity returns.

Free metallic particles, which are smaller than the wavelength of light, have a colour that differs from that of bulk metal. Although the origin of this phenomenon was elucidated by Mie [**48, 49**] in 1908, the finer details are still being discussed [**50**]. However, when the colloidal solution aggregates, the colour changes depending on the structure formed [**50**], but also on the

distance between the metal particles [**51**]. After self-assembly, the colour of the interfacial monolayer can be observed with the naked eye, even for small particles [**45**], due to the strong optical absorption. Upon lateral compression, the insulator-to-metal transition was observed in the non-linear optical response [**52**].

2.3. Self-assembly of magnetic particles. Both charge-stabilised [**53**] and sterically stabilised [**54**] magnetic nanocrystals can be synthesised. Charge-stabilised magnetic nanocrystals can be transferred to non-polar solvents by adding an apolar capping molecule, effectively transforming the charge-stabilised particle into a sterically stabilised magnetic particle [**53**].

Small magnetic particles (1-10 nm) consist of a single domain. At low temperatures (in the order of a few Kelvin), the magnetic dipole moment is fixed to a single crystal axis [**54**]. However, when the temperature is raised above the so-called blocking temperature the magnetic moments can rotate freely within the nanocrystal[**54**]. There are two ways to align a colloidal particle in an external magnetic field: rotation of the complete particle or realignment of the magnetic moment within the particle. If the nanocrystal is locked within the lattice of a colloidal crystal, the first option is not available. It was found that the energy barrier for a change of magnetic moment within the nanocrystal is equal to KV, where K is the anisotropy constant (a material constant) and V the volume of the particle. When the energy of thermal motion (kT) is smaller than KV, the magnetic moment is 'locked' unless an external magnetic field is applied. At these temperatures the magnetic colloidal crystal shows a magnetisation with a hysteresis towards an external magnetic field. Larger particles (larger V) show a larger hysteresis. Alternately, when $kT > KV$ the magnetic dipole fluctuates readily by thermal fluctuations and no hysteresis is found.

When the external magnetic field over a magnetic colloidal crystal is switched off, the magnetisation M decays as $M(t) \propto e^{-t/\tau}$, where τ is exponentially proportional to KV, provided the magnetic moments of the nanocrystals do not interact. This double exponential dependance on V necessitates a narrow size distribution; otherwise significant broadening of the blocking transition occurs[**54**]. The synthesis of charge-stabilised magnetic nanocrystals produces particles with a polydispersity larger than that of sterically stabilised nanocrystals (charge stabilised $\approx 50\%$ [**53**], sterically stabilised $\approx 10\%$ [**54**]) and size-selective precipitation is intricate for charge-stabilised magnetic particles [**53**]. Consequently, there is a stronger interest in capped magnetic nanocrystals than in uncapped, charge-stabilised ones.

In general, the (maximum) interaction of two magnetic dipoles is smaller than or comparable to the van der Waals attraction. The assembly of sterically stabilised magnetic particles is, therefore, very similar to that

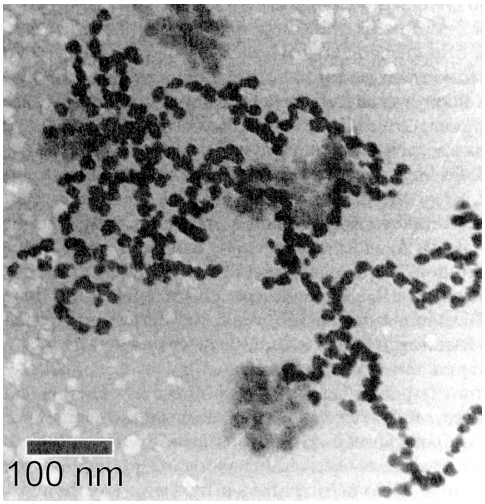

Figure 9. Cryo-TEM image of 8.2 ± 1.5 nm polyisobutene capped magnetite Fe_2O_3 particles. Reproduced from Butter *et al.*[**57**]

of non-magnetic particles. Hexagonal close-packed monolayers[**54**], three-dimensional colloidal crystals[**55**] and even mixed AB_2 and AB_{13} colloidal crystals of magnetic (A = γ-Fe_2O_3) and semiconductor (B = CdSe) nanocrystals have been reported[**56**].

As far back as 1970 it was theoretically predicted that these magnetic particles should form strings in the absence of van der Waals forces and an external magnetic field [**58**]; this was later supported by model calculations [**59**]. However, experimental confirmation of these structures in magnetic colloidal systems has proved experimentally challenging. These strings were only recently (2003) imaged by cryo-TEM [**57**], see figure 9. In these measurements magnetic particles with a large capping were used. Repulsion due to the capping starts at a large distance from the particle surface, where the van der Waals attraction is relatively small. A thin film of this colloidal solution was "vitrified", *i.e.* rapidly cooled to below the freezing point, effectively freezing all Brownian motion. Next, the film was imaged with a low intensity TEM beam, to avoid melting of the layer. It was found that the particle size is vital. Since the van der Waals interactions increase less quickly with increasing partcile size than dipolar interactions[**57**], dipolar effects are stronger for larger particles. It was found that small particles did not form strings, whereas large particles did.

2.4. Self-assembly of charge-stabilised particles. Although some work has been done on 3-D assemblies of charge-stabilised particles [**27,**

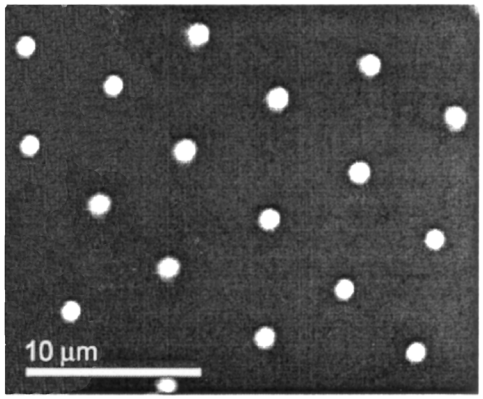

Figure 10. 0.75 μm charge-stabilised poly(methyl methacylate) (PMMA) particles with a fluorescent core, self-assembled at the water/decalin interface. Reproduced from Nikolaides *et al.*[**63**]

60, 61] and 2-D assemblies on substrates[**27**], the self-assembly of charge-stabilised colloidal particles at the interface of two immiscible liquids has attracted most scientific interest. This interest arises from the complex nature of the interactions between charged particles at the interface. In addition, the particle interactions can be controlled by lateral compression of the 2-D array in a Langmuir trough[**62**].

Colloidal particles attach to the liquid/liquid or liquid/air interface because of a decrease in surface energy[**24**], see section 2.1. Due to their charge, two-dimensional close-packed structures will not be formed. Instead, a dilute ordered structure is formed when the particles carry the same surface charge, see figure 10. Assembly at the aqueous/air interface is very similar to assembly at the aqueous/organic interface; only the value for the three-phase angle and the dielectric constant differ. Therefore, we will focus on the self-assembly at the aqueous/organic interface.

It was Pieranski [**64**] who suggested that the electrical double layer is only present at the aqueous side of the particle. Since the dipole induced by the double layer is no longer balanced, a nett dipole moment is present, see figure 11a. These dipole moments interact through the unscreened organic phase.

The suggestion of Pieranski was refined by Hurd [**66**], who found that this dipole-dipole interaction has a longer range than the screened Coulomb interactions. The Coulomb repulsion occurs through the aqueous interface which screens most of the charge, whereas the dipolar interaction occurs largely through the organic phase and is therefore unscreened.

In addition, Aveyard *et al.*[**62**] suggested that the particle/organic interface might not be devoid of charge; charged ions, responsible for the surface

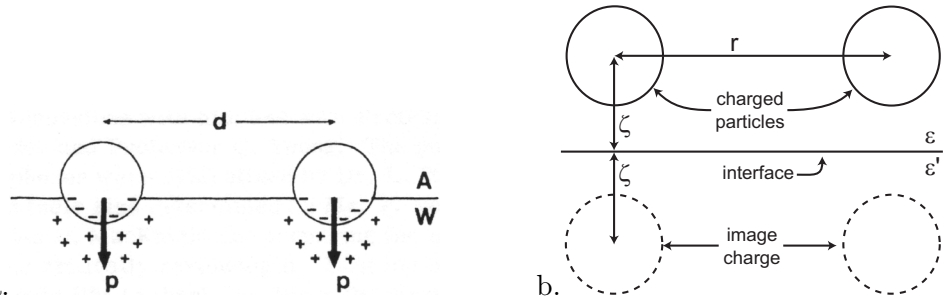

Figure 11. Interactions of charged particles at and near the interface. **a.** Dipolar interaction of two particles at the water(W)/air(A) interface due to incomplete double layers. Reproduced from Pieranski [**64**]. **b.** Enhanced lateral repulsion between two particles near the interface due to image charges. Adapted form [**65**].

charge, could still be present at the particle/organic interface, possibly stabilised by residual traces of water. Since this charge is no longer screened by the aqueous phase, this constitutes a strong long-range Coulomb repulsion between the particles in the interface. Aveyard based his suggestion on the observation that the long-range repulsion between sulfate (SO_4^{2-}) capped polystyrene particles at the water/organic interface (essentially) did not change as a function of the salt concentration[**62**].

Goulding [**65**] showed that (enhanced) repulsion can also occur when particles are close to, but not IN the interface. Consider a charged particle in a solvent with dielectric constant ε close to a phase with dielectric constant ε'. The electrostatic interaction between the particle and the interface can be described by the interaction between the particle and its mirror image, reflected in the interface, see figure 11b. For calculation of the repulsion between two charged particles near the interface one needs to include not only the double layers of the particles, but also the (virtual) double layers of the image particles. It was found that besides a force perpendicular to the surface, there is an enhanced double layer repulsion between the particles.

Such a structure as shown in figure 10 cannot be explained by repulsion alone. Either the interface is restricted such that the particles cannot move from their positions or an attractive force at the same or larger length scale as the repulsion must be present.

The fraction of the particle that is in the organic or aqueous phase is determined by the three-phase angle. If no other forces perpendicular to the interface are acting on the particle the interface between the particles is flat, see figure 6b. However, for very large particles, several hundreds of micrometres in diameter, gravity pulls the particle down, thus curving the

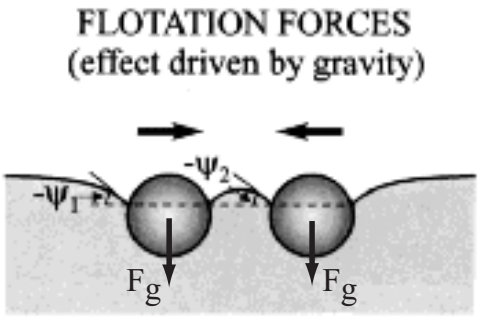

Figure 12. Profile of the water/air interface near two identical particles at the interface. The curvature induced by gravitational pull (F_g) causes attraction by the flotation force. Adapted from Kralchevski *et al.*[**22**]

interface between these particles, see figure 12. This gives rise to attractive capillary forces, called the flotation force[**23, 67**]. The effect of gravity on particles with a radius $R < 5 - 10\ \mu m$ is negligible with respect to thermal motion[**22**]. Since attraction is also observed for particles $R < 5\ \mu m$, another force must operate. The origin of this attractive force is still unclear. In a controversial paper by Nikolaides *et al.* [**63, 68**] the attraction was attributed to a deformation of the interface induced by particle charge and consequent capillary action.

When a layer of charged micrometre-sized latex particles is compressed laterally, a dense, hexagonal close-packed layer is formed[**62**]. Since these particles are not capped, 2-D aggregates remain present at the interface after removal of the lateral pressure. However, what happens just before the formation of the dense monolayer is most interesting. If the lateral pressure on a dilute hexagonal array of particles is increased, the distance between the particles is reduced, but the hexagonal ordering remains intact. If the lateral pressure is further increased, small 2-D islands are formed on the surface in which the particles are in contact. Upon further reduction of the surface area these nuclei continue to grow until a continuous layer, containing large voids, is formed. The voids can be removed by lateral compression and a dense, hexagonally ordered monolayer is formed. 3-D collapse of the layer, *i.e.* the interfacial layer folding back on itself, was not found until the applied lateral pressure was larger than the surface tension of the water/organic interface[**69**]. It was found that the onset of this 2-D aggregation was helped by destabilisation of the particle (addition of salt [**24, 62**]) or the interface (lowering of surface tension with soap [**69**]).

Large micrometre-sized, multivalently charged ions self-assembled at a water/organic interface also exhibited peculiar behaviour when compressed laterally[**70**]. First amphiphilic eicosylamine ($C_{20}H_{43}NH_2$) molecules were

self-assembled at the interface from a solution with $pH = 2$, a pH at which the amine group of the amphiphilic molecule is always fully protonated [**71**]. The orientation of the eicosylamine molecules is similar to that of various soaps: The apolar alkyl chain is in the organic phase and the positively charged polar amino group faces the aqueous phase. Onto this charged layer, large ($\sim 1\ nm^3$ [**72**]) trivalent phosphotungstate anions ($PW_{12}O_{40}^{3-}$) self-assemble through electrostatic interactions. On lateral compression of the layer, the eicosylamine molecules, which have a greater charge per unit area than the phosphotungstate molecules, form a close-packed film at the water/air interface, causing the entire interfacial area to have a positive charge. It was assumed this surplus positive charge was stabilised by a double layer in the aqueous phase.

3. Scope of this thesis

In the previous sections I hope to have shown that the self-assembly of particles into large two- or three dimensional structures is an exciting and therefore 'hot' area of science. These new assemblies hold the promise of novel applications and a better understanding of the physics operating on these small length scales. A particularly interesting topic is the self-assembly of charge-stabilised nanometre-sized particles into monolayers. Until recently[**73, 74**] only particles with sizes in the range of *micrometres* have been studied, mainly because these large particles can be observed individually by optical microscopy [**69**].

We have synthesised charge-stabilised gold nanocrystals, with diameters ranging from a few to several tens of *nanometres*, and studied their self-assembly at the gold/water and water/heptane interfaces.

In chapter 2, charge-stabilised gold nanocrystals have been chemically self-assembled onto various gold (111)/oligo(cyclohexylidene) surfaces, where the oligo(cyclohexylidene)s were modified with various end-functionalities. Unlike alkanethiols, the oligo(cyclohexylidene) molecules exhibit a strong σ-through bond conductivity and can therefore be used as a molecular electronic bridge between the gold substrate and the nanocrystal[**20, 75**]. Due to the semi-rigid structure of the oligo(cyclohexylidene) molecule, the distance between the substrate and the nanocrystal is precisely determined and can be controlled by the number of cyclohexylidene rings. The structure and electrical properties of Au(111)/oligo(cyclohexylidene) and Au(111)/oligo-(cyclohexylidene)/Au_{nc} interfaces were investigated using a combination of electrochemical and scanning probe methods.

In chapter 3, we describe the self-assembly of the same charge-stabilised nanocrystals at the water/heptane interface; the assembly is induced by a slight reduction of the surface charge. We describe here the first well-controlled assembly of charged, uncapped nanometre-sized colloidal particles

at the interface between two immiscible liquids. The interfacial layers were characterised by various *in-situ* and *ex-situ* methods.

Finally, in chapter 4, we have modelled the self-assembly of charge-stabilised gold nanocrystals at the water/heptane interface.

References.

[1] Y. Arakawa and H. Sakaki. *Appl. Phys. Lett.*, **40**-11 (1982) 939.

[2] D. L. Huffaker, G. Park, Z. Zou, O. B. Shchekin, and D. G. Deppe. *Applied Physics Letters*, **73**-18 (1998) 2564–2566.

[3] D. Weller and A. Moser. *Ieee Transactions on Magnetics*, **35**-6 (1999) 4423–4439.

[4] H. Grabert and M. H. Devoret. *Single Charge Tunneling: Coulomb Blockade Phenomena in Nanostructures*, volume 294 of *NATO Asi Series B, Physics*. Plenum, New York, June 1992.

[5] D. M. Eigler and E. K. Schweizer. *Nature*, **344**-6266 (1990) 524–526.

[6] R. A. Cirelli, J. Bude, F. Houlihan, A. Gabor, G. P. Watson, G. R. Weber, F. P. Klemens, J. Sweeney, W. M. Mansfield, and O. Nalamasu. *Microelectronic Engineering*, **53**-1-4 (2000) 87–90.

[7] D.H. Everett. *Colloid Science*. Royal Society of Chemistry Paperbacks, Cambridge, 1988.

[8] Jacob N. Israelachvili. *Intermolecular and Surface Forces*, chapter 11, pages 176–191. Academic Press, London, 2nd edition, 1991.

[9] S.R. Johnson, S.D. Evans, and R. Brydson. *Langmuir*, **14**-23 (1998) 6639.

[10] A.B.R. Mayer and J.E. Mark. *European Polymer Journal*, **34**-1 (1998) 103.

[11] J.R. Heath, C.M. Knobler, and D.V. Leff. *Journal of Physical Chemistry B*, **101**-2 (1997) 189.

[12] M. Brust, M. Walker, D. Bethell, D.J. Schiffrin, and R. Whyman. *Journal of the Chemical Society, Chemical Communications*, (1994) 801.

[13] C. B. Murray, D. J. Norris, and M. G. Bawendi. *Journal of the American Chemical Society*, **115**-19 (1993) 8706–8715.

[14] T. Yonezawa and T. Kunitake. *Colloids and Surfaces A*, **149** (1999) 193.

[15] C. B. Murray, C. R. Kagan, and M. G. Bawendi. *Annual Review of Materials Science*, **30** (2000) 545–610.

[16] W.G. Hoover and F.H. Ree. *J.Chem.Phys.*, **49** (1968) 3609–3617.

[17] W. K. Kegel, H. Reiss, and H. N. W. Lekkerkerker. *Physical Review Letters*, **83**-25 (1999) 5298–5301.

[18] A.K. Boal, F. Ilhan, J.E. DeRouchey, T. Thurn-Albrecht, T.P. Russel, and V.M. Rotello. *Nature*, **404** (2000) 746.

[19] G. Schmid, M. Baumle, and N. Beyer. *Angewandte Chemie, International Edition*, **39**-1 (2000) 181.

[20] E. P. A. M. Bakkers, A. W. Marsman, L. W. Jenneskens, and D. Vanmaekelbergh. *Angewandte Chemie-International Edition*, **39**-13 (2000) 2297–2299.

[21] N. D. Denkov, O. D. Velev, P. A. Kralchevsky, I. B. Ivanov, H. Yoshimura, and K. Nagayama. *Nature*, **361**-6407 (1993) 26–26.

[22] P. A. Kralchevsky and K. Nagayama. *Advances in Colloid and Interface Science*, **85**-2-3 (2000) 145–192.

[23] P. A. Kralchevsky, V. N. Paunov, I. B. Ivanov, and K. Nagayama. *Journal of Colloid and Interface Science*, **151**-1 (1992) 79–94.

[24] D. F. Williams and J. C. Berg. *Journal of Colloid and Interface Science*, **152**-1 (1992) 218–229.

[25] R. Aveyard and J. H. Clint. *Journal of the Chemical Society-Faraday Transactions*, **92**-1 (1996) 85–89.
[26] Bernard P. Binks, John H. Clint, Amro K. F. Dyab, Paul D. I. Fletcher, Mark Kirkland, and Catherine P. Whitby. *Langmuir*, **19**-21 (2003) 8888–8893.
[27] Andrew N. Shipway, Katz Eugenii, and Willner Itamar. *ChemPhysChem*, **1** (2000) 18–52.
[28] John Fink, Christopher J. Kiely, Donald Bethell, and David J. Schriffrin. *Chemistry of Materials*, **10**-3 (1998) 922.
[29] C. J. Kiely, J. Fink, M. Brust, D. Bethell, and D. J. Schiffrin. *Nature*, **396**-6710 (1998) 444–446.
[30] P. C. Ohara, D. V. Leff, J. R. Heath, and W. M. Gelbart. *Physical Review Letters*, **75**-19 (1995) 3466–3469.
[31] S. Murthy, Z. L. Wang, and R. L. Whetten. *Philosophical Magazine Letters*, **75**-5 (1997) 321–327.
[32] R. L. Whetten, J. T. Khoury, M. M. Alvarez, S. Murthy, I. Vezmar, Z. L. Wang, P. W. Stephens, C. L. Cleveland, W. D. Luedtke, and U. Landman. *Advanced Materials*, **8**-5 (1996) 428.
[33] A. Chemseddine and H. Weller. *Berichte Der Bunsen-Gesellschaft-Physical Chemistry Chemical Physics*, **97**-4 (1993) 636–637.
[34] P.N. Pusey and W. van Megen. *Nature*, **320** (1986) 340–342.
[35] P.N. Pusey. *Journal de Physique*, **48** (1987) 709–712.
[36] E. Dickinson and R. Parker. *J. Physique Lett.*, **46** (1985) L–229.
[37] R. McRae and A. D. J. Haymet. *Journal of Chemical Physics*, **88**-2 (1988) 1114–1125.
[38] C. J. Kiely, J. Fink, J. G. Zheng, M. Brust, D. Bethell, and D. J. Schiffrin. *Advanced Materials*, **12**-9 (2000) 640.
[39] M. D. Eldridge, P. A. Madden, and D. Frenkel. *Nature*, **365**-6441 (1993) 35–37.
[40] S. Yoshimura and S. Hachisu. *Progr. Colloid & Polymer Sci.*, **68** (1983) 59–70.
[41] S. Hachisu and S. Yoshimura. *Nature*, **283** (1980) 188–189.
[42] P. Bartlett, R. H. Ottewill, and P. N. Pusey. *Physical Review Letters*, **68**-25 (1992) 3801–3804.
[43] J. V. Sanders. *Phil. Mag. A*, **42**-6 (1980) 705–720.
[44] M. J. Murray and J. V. Sanders. *Phil. Mag. A*, **42**-6 (1980) 721–740.
[45] C.P. Collier, R.J. Saykally, J.J. Shiang, S.E. Henrichs, and J.R. Heath. *Science*, **277** (1997) 1978.
[46] G. Markovich, C.P. Collier, and J.R. Heath. *Physical Review Letters*, **80**-17 (1998) 3807.
[47] R. H. Terrill, T. A. Postlethwaite, C. H. Chen, C. D. Poon, A. Terzis, A. D. Chen, J. E. Hutchison, M. R. Clark, G. Wignall, J. D. Londono, R. Superfine, M. Falvo, C. S. Johnson, E. T. Samulski, and R. W. Murray. *Journal of the American Chemical Society*, **117**-50 (1995) 12537–12548.
[48] Gustav Mie. *Annalen der Physik*, **25** (1908) 25.
[49] J.A.A.J. Perenboom. *Physical Review*, **78** (1981) 173.
[50] U. Kreibig and L. Genzel. *Surface Science*, **156** (1985) 678.
[51] T. Ung, L. M. Liz-Marzan, and P. Mulvaney. *Journal of Physical Chemistry B*, **105**-17 (2001) 3441–3452.
[52] F. Remacle, C.P. Collier, J.R. Heath, and R.D. Levine. *Chemical Physics Letters*, **291** (1998) 453.
[53] S. Lefebure, E. Dubois, V. Cabuil, S. Neveu, and R. Massart. *Journal of Materials Research*, **13**-10 (1998) 2975–2981.
[54] C. B. Murray, S. H. Sun, W. Gaschler, H. Doyle, T. A. Betley, and C. R. Kagan. *Ibm Journal of Research and Development*, **45**-1 (2001) 47–56.

[55] S. H. Sun, C. B. Murray, D. Weller, L. Folks, and A. Moser. *Science*, **287**-5460 (2000) 1989–1992.
[56] F. X. Redl, K. S. Cho, C. B. Murray, and S. O'Brien. *Nature*, **423**-6943 (2003) 968–971.
[57] K. Butter, P. H. H. Bomans, P. M. Frederik, G. J. Vroege, and A. P. Philipse. *Nature Materials*, **2**-2 (2003) 88–91.
[58] P. G. de Gennes and P. A. Pincus. *Phys. Kondens. Materie*, **11** (1970) 189–198.
[59] P. J. Camp, J. C. Shelley, and G. N. Patey. *Physical Review Letters*, **84**-1 (2000) 115–118.
[60] S. H. Wang, S. Sato, and K. Kimura. *Chemistry of Materials*, **15**-12 (2003) 2445–2448.
[61] S. Bharathi, J. Joseph, O. Lev, and Z. Lev. *Electrochemical and Solid State Letters*, **2**-6 (1999) 284–287.
[62] R. Aveyard, J. H. Clint, D. Nees, and V. N. Paunov. *Langmuir*, **16**-4 (2000) 1969–1979.
[63] M. G. Nikolaides, A. R. Bausch, M. F. Hsu, A. D. Dinsmore, M. P. Brenner, and D. A. Weitz. *Nature*, **420**-6913 (2002) 299–301.
[64] P. Pieranski. *Phys. Rev. Lett.*, **45**-7 (1980) 569–572.
[65] D. Goulding and J. P. Hansen. *Molecular Physics*, **95**-3 (1998) 649–655.
[66] A. J. Hurd. *J. Phys. A: Math. Gen.*, **18** (1985) L1055–L1060.
[67] D. Y. C. Chan, J. D. Henry, and J. R. White. *J. Coll. Interf. Sci.*, **79**-2 (1981) 410–418.
[68] M. Megens and J. Aizenberg. *Nature*, **424**-6952 (2003) 1014–1014.
[69] R. Aveyard, J. H. Clint, D. Nees, and N. Quirke. *Langmuir*, **16**-23 (2000) 8820–8828.
[70] N. Cuvillier and F. Rondelez. *Thin Solid Films*, **329** (1998) 19–23.
[71] X. L. Zhao, S. W. Ong, H. F. Wang, and K. B. Eisenthal. *Chemical Physics Letters*, **214**-2 (1993) 203–207.
[72] M. R. Spirlet and W. R. Busing. *Acta Cryst.*, **154** (1987) 137.
[73] A. Kumar, S. Mandal, S. P. Mathew, P. R. Selvakannan, A. B. Mandale, R. V. Chaudhari, and M. Sastry. *Langmuir*, **18**-17 (2002) 6478–6483.
[74] Ashavani Kumar, Priyabrata Mukherjee, Ayon Guha, S.D. Adyantaya, A.B. Mandale, Rajiv Kumar, and Murali Sastry. *Langmuir*, **16**-25 (2000) 9775–9783.
[75] Y. V. Kervennic, D. Vanmaekelbergh, L. P. Kouwenhoven, and H. S. J. Van der Zant. *Applied Physics Letters*, **83**-18 (2003) 3782–3784.

CHAPTER 2

Electrochemical and topological characterization of gold (111)/oligo(cyclohexylidene)/gold nanocrystal interfaces

1. Introduction

Electrical devices in which molecules or molecular crystals are the active element receive considerable interest from chemists and physicists since they are promising candidates for future miniaturized electrical components[**1**]. Single-molecule electrical junctions can be made by mounting a molecule between two closely spaced electrodes on a non-conducting substrate. The fabrication of such a device is, however, still very demanding. Only a few single-molecule electrical devices have been presented[**2**–**6**]. An alternative method, which can be used for investigating electron transport through single molecules, is based on the attachment of the molecules by one end to a conducting substrate, while an electrical contact at the other end of the molecule is obtained with the tip of a scanning tunneling microscope[**7**]. Attaching a nanometer-sized particle with an optical or electrical function to the end of the molecule would be a further step in the fabrication of real molecular junctions. Recently, our group has demonstrated that insulating CdS and CdSe quantum dots can be bound to the thiol or sulfide end-functionality of alkane and oligo(cyclohexylidene) molecules which have been self-assembled on gold. This results in a parallel array of optically and electrically addressable gold/molecule/Q-dot junctions[**8, 9**]. Schiffrin and colleagues reported a self-assembled array of individual and independent molecular junctions, terminated with a gold nanocrystal contact, which show on-off conductance, depending on the electron occupation of a built-in redox system acting as a switch[**10**].

Here, we report on an electrochemical and Scanning Probe Microscopy (SPM) characterization of a nanostructured interface consisting of a parallel array of gold (111)/oligo(cyclohexylidene)/gold nanocrystal molecular junctions. End-functionalized oligo(cyclohexylidene) molecules (see figure 1 and 2 for structure and notation) form an interesting class of molecules for single-molecule electrical devices since

(i) molecules of different length and with a variety of end-functionalities can be prepared,

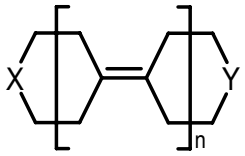

FIGURE 1. General form of an oligo(cyclohexylidene), where X and Y can be S, CH_2, $=N-OH$ (oxime) or $=N-OCH_3$ (methylated oxime). The oligo(cyclohexylidene) group (between square brackets) is repeated n times, where n = 0, 1 or 2. For simplicity, the compounds will be named after their number of rings followed by the nature of their substituents X and Y. For instance, a cyclohexylidene with $n = 1$, $X = S$ and $Y = CH_2$ will be referred to as a dicyclic monosufide. For more examples, see figure 2.

(ii) structural analysis on single crystals and ab-initio calculations showed that these molecules preferentially stack in chair conformation[**11**–**13**]. The molecules are expected to form a well-ordered self-assembled monolayer (SAM) on gold (111).
(iii) MO-theory and two different types of experiments have shown that they exhibit strong s-through-bond coupling making them possible candidates for molecular wires[**8**].

We performed a layer-by-layer characterization. First, we investigated the possible formation of self-assembled mono- and difunctionalized oligo(cyclohexylidene) layers on Au(111) surfaces (sections 3.1 and 3.2, respectively) using classical electrochemical methods *i.e.* by measurement of the interfacial capacitance and by cyclic voltammetry in the presence of a redox system ($Fe(CN)_6^{3-/4-}$). We employed STM, contact- and tapping mode AFM to investigate the topology of the SAMs on gold. Second, the attachment of gold nanocrystals (Au_{nc}) to the molecular layers was studied by in-situ measurement of the electrochemical capacitance and by ex-situ AFM (section 3.3).

2. Methods

Chemicals were obtained from Aldrich (pentamethylene sulfide 99%, hydrogen tetrachloroaurate(III) trihydrate, sodium citrate dihydrate 99%), Lancaster (1,4-dithiane 98%) and Merck (potassium chloride p.a., sodium perchlorate monohydrate p.a., potassium hexacyanoferrate(II) trihydrate p.a.). All solutions were made using purified water (16 $M\Omega\ cm$) from the Purite Bio Select. The end-functionalized oligo(cyclohexylidene)s were prepared following previously published studies[**11**–**14**].

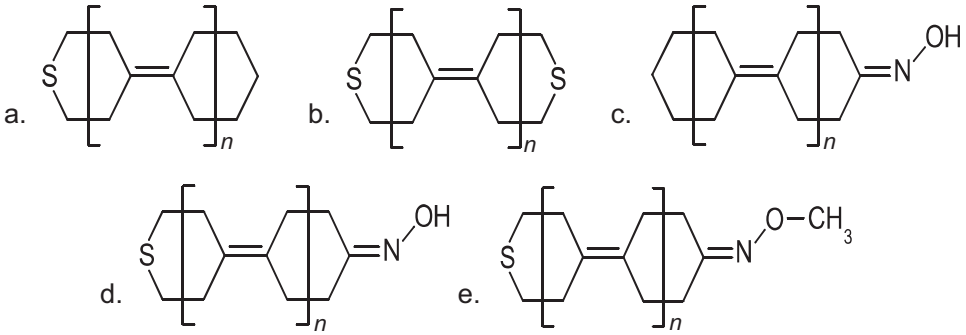

Figure 2. The end-functionalized oligo(cyclohexylidene) molecules used in this study. For simplicity we refer to these molecules by their functional groups, *viz.* a. monosulfide, b. disulfide, c. oxime, d. oxime-sulfide, and e. methylated oxime-sulfide. The oligo(cyclohexylidene) group (between square brackets) is repeated n times, where n is 0, 1 or 2.

2.1. SAM preparation and electrochemical setup. A standard three electrode cell was employed, with a Pt counter and a saturated calomel electrode (SCE) as reference. The working electrodes employed consisted of a 1 by 3 cm wide, 1 mm thick borosilicate glass ("pyrex") slides onto which 2.5 nm of Cr and 200 nm Au were evaporated. Before use, the electrodes were annealed by heating in a hydrogen flame followed by rapid cooling under an Ar flow. Self-assembled monolayers were formed by immersion of the electrode in an ethanolic cyclohexylidene solution at 60 $^{\circ}C$ for for at least 2 days.

2.2. Gold nanocrystal synthesis. Aqueous suspensions of gold nanocrystals were prepared according to the method employed by Frens[**15**]. A typical synthesis for obtaining charge-stabilised gold particles with a diameter of 16 nm is described below. In a volumetric flask 5 ml of an aqueous 1 % w/w $HAuCl_4$ solution was diluted to 50 ml. This faintly yellow solution was transferred to a 250 ml conical flask and heated to boiling. Under vigorous stirring, 1 ml 0.1 % w/w trisodium citrate solution was added. The solution was stirred and kept boiling until the reaction had ended. The colour changed from slight yellow to intense blue, purple and orange-red.

Larger nanocrystals were prepared by adding smaller amounts of the citrate solution to the same amount of $HAuCl_4$ solution. Particles smaller than 16 nm were synthesized by injecting a freshly prepared mixture of 1 ml 0.1 % w/w sodium borohydride + 1 ml 0.1 % w/w trisodium citrate into the boiling $HAuCl_4$ solution. Since borohydride readily decomposes

TABLE 1. Influence of citrate and bororhydride on particle size and polydispersity. Particle sizes were determined from TEM images over at least 200 particle counts.

μl citrate	μl $NaBH_4$	size (nm)	std.dev.	polydisp.(%)	colour
200	0	44	7.5	17.2	blue
300	0	40	5.9	14.8	purple
400	0	32	4.3	13.6	pink
1000	0	16.6	1.9	11.4	ruby-red
1000	1000	4.2	0.74	17.4	orange-brown

in water, the concentration of borohydride cannot be rigorously controlled. This results in a particle size that differs with each attempt.

Information on particle sizes was obtained from TEM images, see table 1[a]. As can be seen in figure 3c, the 44 nm particles are highly faceted and elongated in one direction. The difference between the shortest and longest axis could be as much as 10 nm. In contrast the 4.2 nm nanocrystals (figure 3a) show no sign of faceting and the particles are nearly spherical. The intermediate sized particles, see figure 3b, are nearly spherical although some facets are still visible.

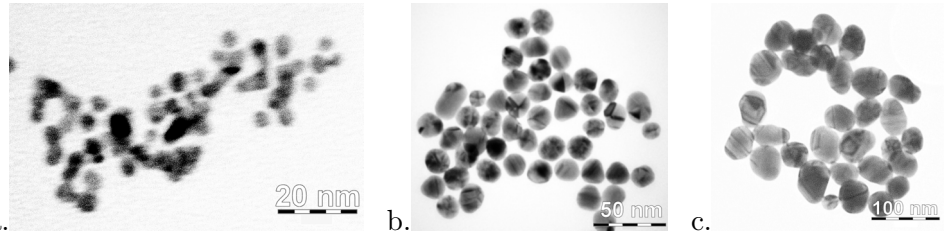

FIGURE 3. Tunneling Electron Microscope (TEM) images of Au nanocrystals made by the Frens method. Reducing agents added were **a.** 1 ml 0.1% w/w $NaBH_4$ + 1 ml 0.1 % w/w trisodium citrate, **b.** 1 ml and **c.** 0.2 ml 0.1 % w/w trisodium citrate.

When the larger particles ($> 16\ nm$) are attached to a cyclohexylidene-modified Au(111) surface, the exact contact area cannot be known due to the peculiar shape of these particles. Therefore the larger particles were not used in the following experiments.

2.3. Cyclic Voltammetry. Cyclic voltammetry was performed using an EG&G 273A galvanostat/potentiostat in 1 M electrolyte solutions of KCl or $NaClO_4$, and also with 10 mM $FeCN_6^{4-}$ in the solution.

[a]A colour photograph of the solutions described in table 1 has been printed on the front cover

2.4. Electrical Impedance Spectroscopy. In Electrical Impedance Spectroscopy (EIS), or Impedance for short, a small sinusoidal perturbation E_{mod} (typically 5-10 mV), of amplitude A_E and radial frequency ω ($= 2\pi f$, with f the perturbation frequency), is superimposed onto a constant potential E_{const} applied to the electrode, see figure 4a, top.

$$E_{EIS} = E_{const} + E_{mod} = E_{const} + A_E\, e^{i\omega t} \tag{2.1}$$

The current response (i_{EIS}) to this perturbation will also be a constant current i_{const} with a superimposed sinusoidal variation i_{mod}. This sinusoidal wave has the same frequency ω, but may be delayed by a phase vector φ, see figure 4a, bottom.

$$i_{EIS} = i_{const} + i_{mod} = i_{const} + A_i\, e^{i(\omega t+\varphi)} \tag{2.2}$$

where A_i is the amplitude of the sinusoidal signal.

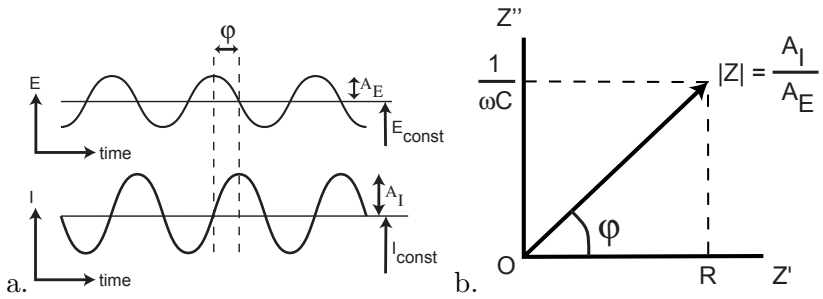

Figure 4. Electrical Impedance Plot *a.* top: Applied potential; bottom: Resulting current; *b.* Impedance vector. Variables as explained in the text.

The electrical impendence $\overrightarrow{Z}$ is defined as the ratio of the modulated current to the modulated potential.

$$Z = \frac{i_{mod}}{E_{mod}} = \frac{A_i}{A_E}\, e^{i\varphi} \tag{2.3}$$

Equation 2.3 shows that the impedance is a time-independent vector in the imaginary plane, as schematically shown in figure 4b. The length of the vector $\overrightarrow{Z}$ is given by the ratio A_i/A_E and the angle with respect to the real axis is φ. The real axis Z' is equal to the total resistance of the system, whereas the imaginary axis Z'' is related to the total capacitance C as $Z'' = 1/(\omega C)$.

Measurements were performed using the Solartron 1255B Frequency Response Analyzer. During a measurement typically 40 different frequencies were applied ranging from $f = 1.3$ to 13000 Hz, 10 in each decade. These frequencies were chosen such that no single frequency was close to a multiple

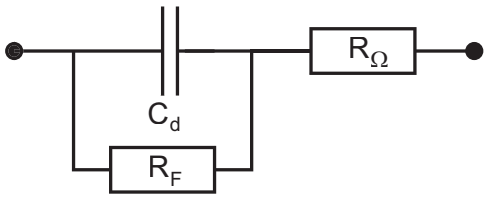

FIGURE 5. Equivalent circuit used to fit the EIS measurements. Variables as in the text.

of 50 Hz to avoid interference from the mains. Next, the data was fitted to the equivalent circuit shown in figure 5, where R_Ω is the cell resistance, C_d the interfacial capacitance and R_F the charge transfer resistance. This was done for several potentials ranging typically from -0.7 to +0.7 V vs. SCE.

2.5. Potential Step. In contrast to Electrical Impedance Spectroscopy where a sinusoidal perturbation is applied, the potential of the working electrode is instantaneously stepped from E to $E + \Delta E$, see figure 6a. ΔE was chosen as 0.05 V after it was confirmed that the results are independent of the amplitude of the potential step.

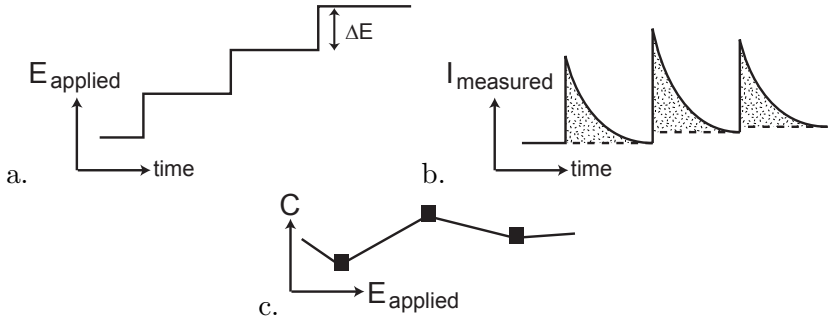

FIGURE 6. Image to explain the potential step experiment

After each potential step current flows to compensate for the potential step, see figure 6b. This charging current density i_c induced by the potential step is related the interfacial capacitance C_d as

$$i_c = \frac{dq}{dt} = \frac{dq}{dE}\,\frac{dE}{dt} = C_d \frac{dE}{dt} \tag{2.4}$$

where q is the charge density of the electrode.

Integrating the current measured between time t_1 before the potential step and t_2 after the system has reequilibrated yields the interfacial capacitance times the potential step.

$$\int_{t_1}^{t_2} i_c\, dt = C_d \int_{E(t_1)}^{E(t_2)} dE = C_d\, \Delta E \tag{2.5}$$

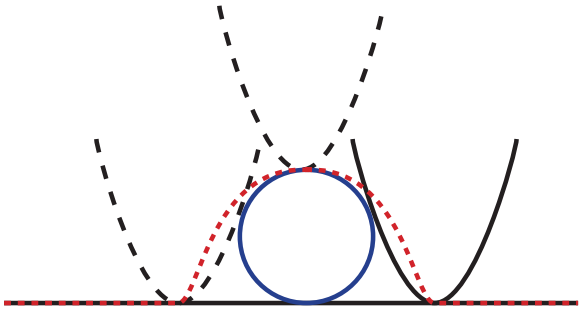

Figure 7. Behavior of an AFM tip around a large object. The dotted line is the measured height profile. Due to the width of the AFM tip objects seem larger in the X-Y direction. The height of the object is not distorted.

The determined value is therefore the double layer capacitance at $E + \frac{1}{2}\Delta E$. The capacitance data is then plotted against potential (figure 6c).

The setup is identical to that used for cyclic voltammetry. Transients were checked visually for signs of overlap between consecutive pulses. Since the electrode is perturbed with a single pulse, this method can be compared with EIS with a large(r) amplitude pulse and a frequency close to zero ($\omega \to 0$).

2.6. Atomic Force Microscopy. Atomic Force Microscopy (AFM) images were made using the Digital Instruments Nanoscope IIIa. The substrates (10x10x1 mm) were either the same as those used for the electrochemical investigations or were obtained from Arrandee[b], formerly Metallhandel Schröer GmbH.

Atomic Force Microscope uses the mechanical interaction of the tip with a substrate. By scanning the tip over the substrate an image of the topology can be obtained. Two types of AFM were employed.

- "Contact mode" AFM (cmAFM) utilizes a sharp tip mounted on a wedge-shaped cantilever. When pressed onto a substrate the deflection of the cantilever can be measured using a focussed laser beam. The interaction of the tip with the substrate is very strong, and may sometimes induce structural changes in the substrate.
- In "Tapping mode" AFM (tmAFM) a sharpened cantilever is brought into resonant oscillation. This oscillation is monitored by a laser beam focused on the cantilever. As the cantilever touches the substrate, the oscillation is dampened and the amplitude of the oscillation decreases.

[b]Arrandee website: http://www.arrandee.com/

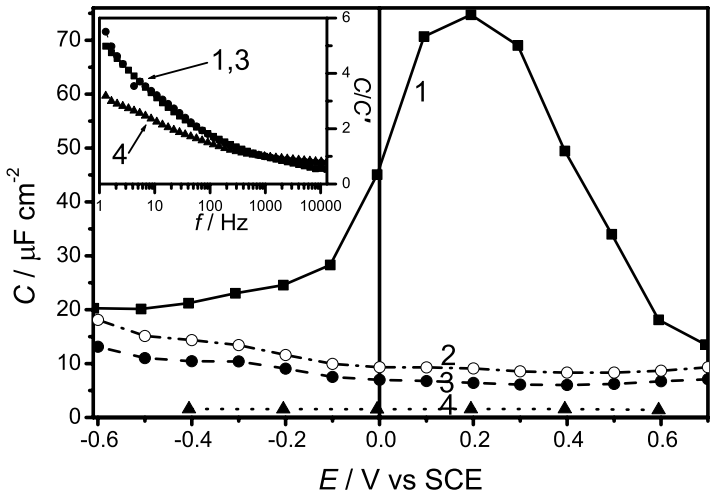

FIGURE 8. The interfacial capacitance (measured at 1000 Hz) of a gold (111) electrode in an aqueous solution of 1 M KCl at 25°C as a function of electrode potential after pretreatment with ethanolic solutions of oligo(cyclohexylidene)s with different end-functionalities. (1, —■—) an untreated, bare gold (111) electrode. (2,– · ○ · –) after immersion in pure ethanol for 12 hours. (3,– – ● – –) after immersion in an oxime (figure 2c; n=1)/ethanol solution for 24 hours. (4,· · ▲ · ·) after immersion in a monosulfide (figure 2a; n=1)/ethanol solution for 24 hours. The insert shows the capacitance C at 0 V vs. SCE (normalized with respect to that measured at 1000 Hz, denoted C') as a function of the modulation frequency.

The resolution of both methods is limited by the size of the tip apex. This causes the so-called tip convolution effect. The size of all objects in the plane of the substrate (the X-Y direction) seem enlarged by approximately the tip diameter, see figure 7. As a result, the dimensions of any feature on the substrate can only be accurately determined in the Z direction. The convolution effect is more prominent for small features, since the distortion will be relatively large.

3. Results

3.1. Monofunctionalized oligo(cyclohexylidene)s. We first investigated the possibility of forming self-assembled monolayers with monofunctionalized oligo(cyclohexylidene)s, specifically the two ring monosulfide and oxime (figure 2a and c, respectively, both with n=1). Figure 8 curve 1 shows

the interfacial capacitance of a bare gold (111) electrode in an aqueous 1 M KCl solution as a function of the electrode potential, together with the capacitance measured after application of the monosulfide (figure 8, curve 4) and the oxime (figure 8, curve 3). The frequency dependence of the measured capacitances at 0 V vs. SCE is shown in the insert. The capacitance (normalized with respect to the capacitance at 1000 Hz) of the bare electrode increases considerably with decreasing modulation frequency. A strong frequency dependence of the interfacial capacitance in concentrated aqueous electrolytes has been reported before [**16**]. This frequency dispersion is most likely due to surface roughness[**17**] and/or specific adsorption of the anion[**18, 19**]. It was not possible to account for the frequency dependence by a constant phase element. We therefore present the capacitance measured at a frequency of 1000 Hz for further discussion. The bare Au(111) electrode shows a pronounced maximum at +0.2 V, close to the potential of zero charge. The maximum capacitance in a 1 M KCl solution varied from sample to sample (68 $\mu F\, cm^{-2} \pm 15$ % at 1000 Hz). Negative with respect to the maximum, the capacitance decreased to a constant value equal to 20 $\mu F\, cm^{-2}$. Positive of the potential of zero charge the capacitance decreased to 9 - 15 $\mu F\, cm^{-2}$ at 0.7 V. The capacitance plot of Au(111) in 1 M $NaClO_4$, see figure 9, has the same features; however the maximum is much less pronounced than for KCl. The maximum in the capacitance is observed at +0.3 V vs. SCE, which is close to the point of zero charge E_{pzc} of +0.33 V vs. SCE found in the literature[**20**–**24**]. The C vs. E plot shows an asymmetric peak in KCl, very probably due to chemisorption of Cl^- ions at the electrode surface in the potential range positive of E_{pzc}. Similar results (an increase of the maximum capacitance and shift of the maximum to more negative potentials with increasing specific adsorption) have been reported in the literature[**16, 18, 19**].

The capacitance of the gold electrode measured in a 1 M KCl solution after a prolonged immersion in an ethanolic solution of oxime (figure 8, curve 3) is reduced considerably compared to that of a bare electrode, and a maximum is not found in the capacitance-potential curve. A similar reduction of the interfacial capacitance is, however, found after placing the electrode for one night in pure ethanol, see figure 8, curve 2. Note that the frequency dependence of the interfacial capacitance of a bare and an oxime-treated electrode is identical (insert figure 8). We infer that the interfacial capacitance is reduced with respect to that of a bare electrode due to physisorption of ethanol or oxime molecules and that a robust SAM is not formed. In contrast, the capacitance of the gold electrode in a 1 M KCl solution is extremely low ($C < 1$ $\mu F\, cm^{-2}$) in the entire potential range after application of a monosulfide (figure 8, curve 4). The capacitance decreases with increasing length of the monosulfide (figure 2a; n=0,1). This is at odds with what was found with functionalized n-alkanethiol SAMs[**25**–**27**]. This

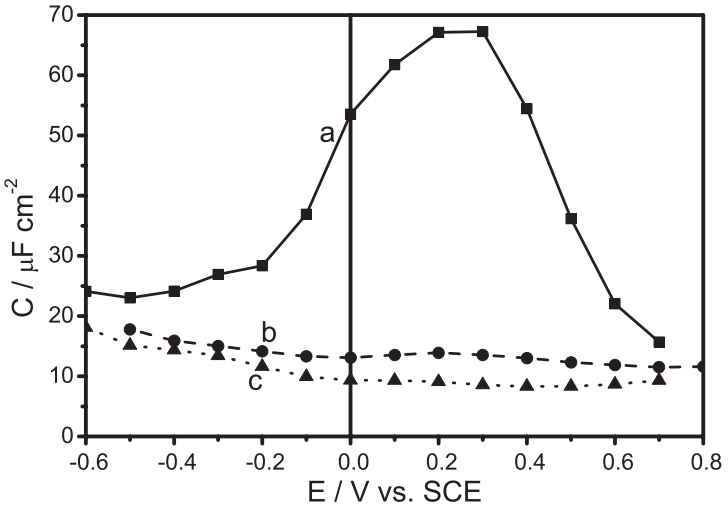

FIGURE 9. The interfacial capacitance (measured at 1000 Hz) of a gold (111) electrode in an aqueous solution of 1 M KCl (curve a and c) and 1 M $NaClO_4$ (curve b) at 25°C as a function of electrode potential. The electrodes of curves a and b were untreated, whereas the electrode of curve c was immersed in pure ethanol for 12 hours before use.

indicates that monosulfides form well-ordered SAMs that cover the entire electrode. This has been confirmed by ex-situ tapping mode AFM, contact mode AFM and STM characterization of such layers. No defects could be found in the layers, and the atomic steps of the Au(111) surface were visible on the images.

The contrast between the effect of monosulfides and oximes (figure 2a and c, respectively) on Au(111) is also illustrated by the cyclic voltammograms shown in figure 10. With the bare gold electrode the difference between the reduction and oxidation peaks of $Fe(CN)_6^{3-/4-}$ in a 1 M KCl solution is 110 mV, whereas 58 mV is expected for a reversible reaction. The reaction is thus quasi-reversible at a scan rate of 100 mV/s. Similar results have been reported in the literature[**28**]. After immersion of the gold sample in ethanol or an oxime in ethanol solution, the reaction becomes more irreversible, indicating that oxime or ethanol molecules cover (partly) the electrode surface. However, the cyclic voltammogram tends to that of a bare electrode when the electrode potential is scanned for a longer time, indicating that the ethanol or oxime molecules are weakly physisorbed and can be removed electrochemically. On the other hand, when the gold electrode was treated with a monosulfide (figure 2a; n=1) dissolved in ethanol, the oxidation/reduction reaction is strongly inhibited with respect to that at a bare gold electrode. Pinholes in the SAM are rarely observed with STM;

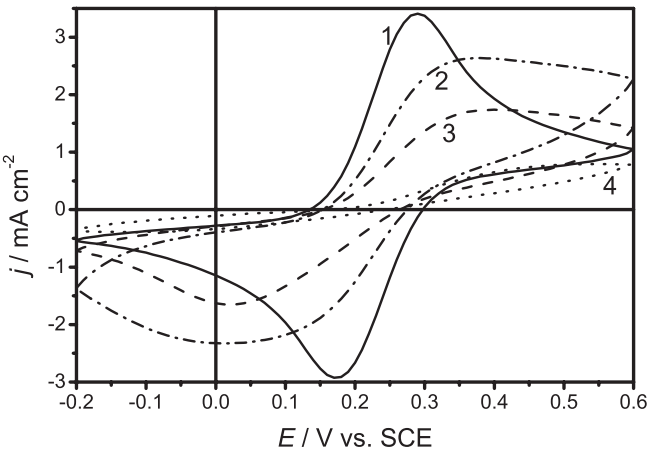

Figure 10. Cyclic voltammograms measured in a 10 mM $FeCN_6^{4-}$ / 1 M KCl solution after several pretreatments. (1,—) an untreated, bare gold (111) electrode. (2,– · – ·) after immersion in a pure ethanol solution for 12 hours. (3,– – –) after immersion in an oxime (figure 2c; $n = 1$)/ethanol solution for 24 hours. (4,· · ·) after immersion in a monosulfide (figure 2a; $n = 1$)/ethanol solution for 24 hours.

thus it is likely that the remaining Faradaic current is due to electron transfer through the oligo(cyclohexylidene) SAM. We conclude that monosulfide oligo(cyclohexylidene)s form well-ordered SAMs, with a strong gold-sulfur bond. It is clear that the oxime function does not bind chemically to gold.

3.2. Difunctionalized oligo(cyclohexylidene)s. Next, we investigated the possible formation of SAMs by difunctionalized oligo(cyclohexylidene)s, *i.e.* disulfides, oxime-sulfides and methylated oxime-sulfides, on Au(111). After treatment of the gold surface with a disulfide (figure 2b; n=0), the interfacial capacitance in 1 M KCl reduces to a value of about 6 $\mu F\ cm^{-2}$ at 1000 Hz, independent of the electrode potential. In addition, the cyclic voltammograms show a strong attenuation of interfacial electron transfer. This points to the formation of a well-ordered oligo(cyclohexylidene) disulfide SAM covering the entire gold surface; this conclusion is supported by AFM measurements. The results obtained after application of the oxime-sulfides (figure 2d; n=0) and methylated oxime-sulfides (figure 2e; n=0) are shown in figures 11 and 12. After application of the oxime-sulfide, the capacitance is moderately reduced with respect to that of a bare gold electrode measured in KCl solution (compare curves 1 and 2 of figure 11).

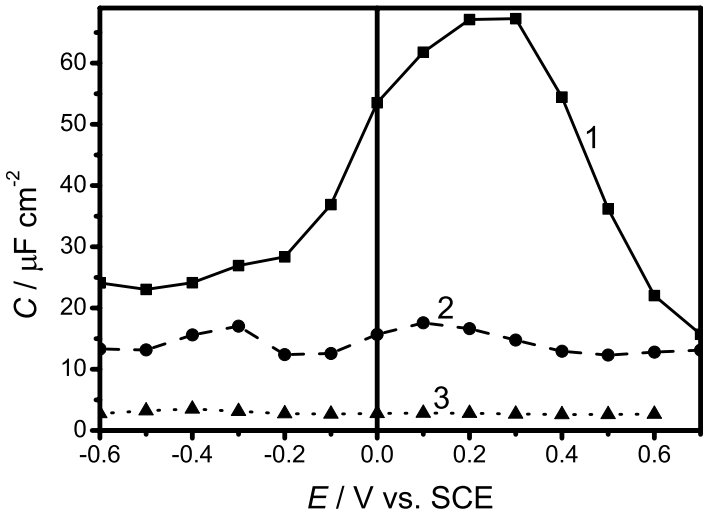

FIGURE 11. The interfacial capacitance (measured at 1000 Hz) of a gold (111) electrode in an aqueous solution of 1 M KCl at 25°C as a function of electrode potential after pre-treatment with ethanolic solutions of oligo(cyclohexylidene)s with different end-functionalized. (1,—■—) an untreated, bare gold (111) electrode. (2, – – • – –) after immersion in a oxime-sulfide (figure 2d; n=0)/ethanol solution for over 48 hours. (3,· · ▲ · ·) after immersion in a methylated oxime-sulfide (figure 2e; n=0)/ethanol solution for 24 hours.

The capacitance is in the range of 15-20 $\mu F\, cm^{-2}$; a value smaller than 10 $\mu F\, cm^{-2}$ is expected for a well-ordered SAM. Moreover, the $Fe(CN)_6^{3-/4-}$ peak currents in the voltammogram for a 1 M KCl solution are reduced to only half the values found with a bare electrode (figure 12, curves 1 and 2). These results suggest that oxime-sulfides do not form a well-ordered SAM on Au(111). This is unexpected, since the sulfide function binds strongly to gold, resulting in well-ordered SAMs with the mono and disulfide. The oxime $=N\text{-}OH$ function seems to hinder SAM formation. This is supported by the results shown in figure 11 (curve 3) and 11 (curve 3), obtained with methylated oxime-sulfides (figure 2e; n=0). The capacitance reduces to a value of 4 $\mu F\, cm^{-2}$ at 1000 Hz, even slightly lower than that of a disulfide. In addition, the reduction/oxidation of the redox system is strongly inhibited. It is not yet clear why the $=N\text{-}OH$ end-functionality has such a strong inhibiting effect on the formation of a SAM layer. It may be related to the fact that the $=N\text{-}OH$ group can form hydrogen bonds with ethanol or another oxime molecule.

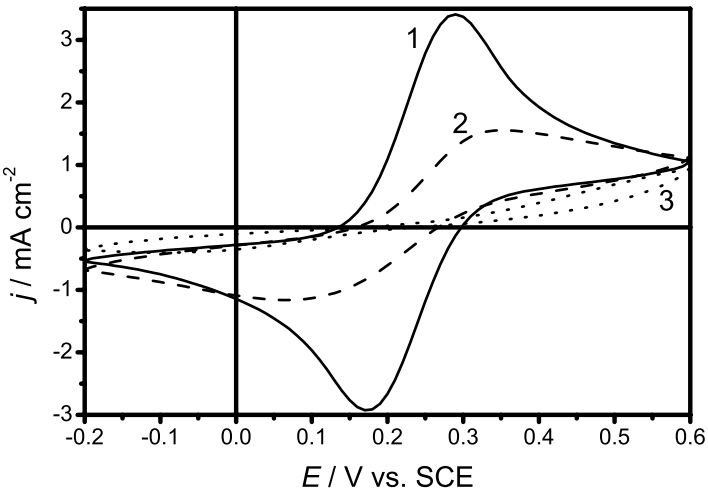

Figure 12. Cyclic voltammograms measured in a 10 mM $FeCN_6^{4-}$ / 1M KCl solution after different pretreatments. (1,—) an untreated, bare gold (111) electrode. (2,– – –) after immersion in a oxime-sulfide (figure 2d; $n = 0$)/ethanol solution for over 48 hours. (3,· · ·) after immersion in a methylated oxime-sulfide (figure 2e; $n = 0$)/ethanol solution for 24 hours.

3.3. Gold nanocrystal attachment. We investigated whether the gold (111)/disulfide system can be used in preparing gold (111)/oligo(cyclohexylidene)/Au_{nc} molecular junctions. Charge-stabilized gold nanocrystals (5-20 nm in size) were adsorbed on a gold (111)/disulfide interface from an aqueous colloidal suspension[**15**]. The size of the nanocrystals was checked by UV-VIS spectroscopy, TEM and tapping mode AFM. Figure 13a shows a tapping-mode AFM picture of a Au/disulfide interface which is covered with gold nanocrystals. From the cross-section (inset) it follows that the height of the nanocrystals is 15 nm which is in agreement with the particle size in solution. The same agreement was found for a Au/disulfide/Au_{nc} interface with Au nanocrystals of 8 nm in size, see figure 13b. Interestingly, the nanocrystals attach as individual particles to the disulfide SAM; no clustering is observed. The nanocrystals cannot be moved along the surface by the tapping-mode tip indicating strong bonding and formation of a robust Au(111)/disulfide/Au_{nc} junction. Charge-stabilized nanocrystals were also observed to adhere to some extent to an alkyl-terminated monosulfide (figure 2a; n=0) SAM. Figure 13c shows the result after immersion of the gold with a monosulfide SAM in colloidal suspension. Individual nanocrystals are observed on the SAM. However, when the tip/substrate interaction is

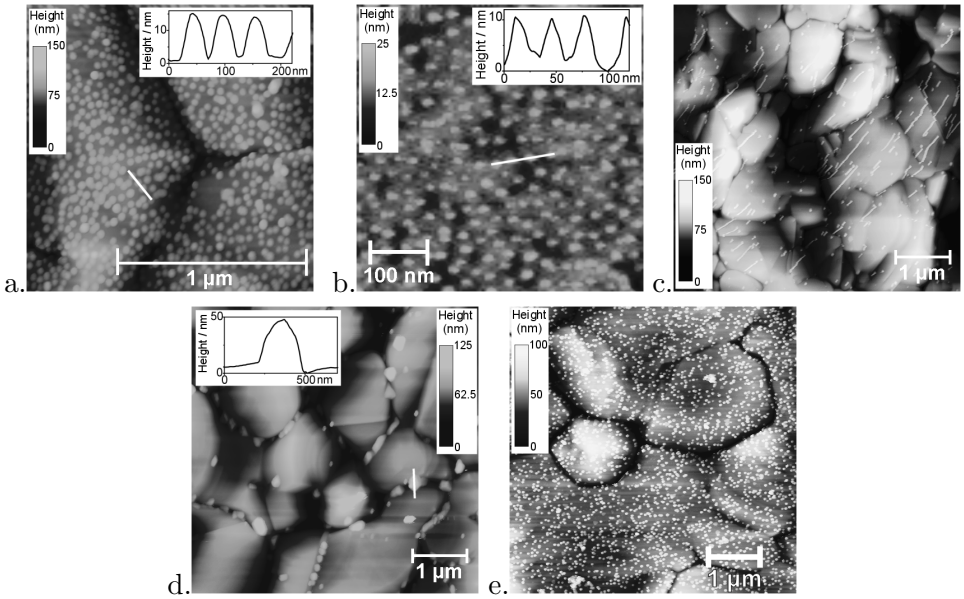

FIGURE 13. Tapping mode AFM images of bare and oligo-(cyclohexylidene)-covered Au(111) surfaces after immersion in an aqueous colloidal solution of charge-stabilized gold nanocrystals (size 5-20 nm). See figure 2 for cyclohexylidene nomenclature. **a.** A gold (111)/disulfide (n=0) surface after immersion for 4 hours in the colloidal gold solution (diameter 16 nm). The height of the particle forms a good estimate of the particle size (see inset). **b.** Same as **a.**, but with 8 nm gold particles. **c.** A gold (111)/monosulfide (n=0) surface after immersion for 1 hour in 16 nm colloidal gold solution. **d.** A bare gold (111) surface after immersion in a 16 nm colloidal gold solution for 1 hour. **e.** A Au(111)/oxime-sulfide (n=0) surface after immersion for 2 hours in 16 nm colloidal gold solution.

increased (low setpoint) the gold nanocrystals can be moved along the surface by the tapping-mode tip (resulting in the 'stripes' going from top-right to bottom-left in figure 13c), indicating that they are van der Waals-bound to the surface. Interestingly, charge-stabilized gold nanocrystals do not attach to a bare Au(111) surface under open-circuit conditions. The result of prolonged immersion of bare gold in a colloidal solution is shown in figure 13d: only some large agglomerates are visible at the grain boundaries.

As has been previously shown, self-assembly of a oxime-sulfide (figure 2d; n=0) on gold (111) leads to a disordered layer, most likely due to the formation of hydrogen bonds. These hydrogen bonds can give rise to the

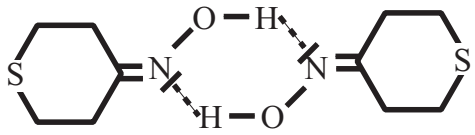

Figure 14. Dimer of two oxime-sulfides molecules through hydrogen bonds.

formation of oxime dimers[**29**], see figure 14. If a sufficient amount of dimers attach to the gold (111) surface a gold nanocrystal can be securely attached to the interface. In figure 13e a sulfide-oxime modified gold (111) electrode was immersed in a 16 nm Au_{nc} solution. The gold nanocrystals cannot be moved by the tapping mode AFM tip, suggesting that the gold nanocrystals are firmly attached to the Au(111)/oxime-sulfide cyclohexylidene surface.

We were unable to image nanocrystals attached to an oligo(cyclohexylidene) SAM with Scanning Probe Microscopy (SPM) methods other than with tapping mode AFM. The force applied by *contact mode* AFM and STM tips proved to be enough to break the adhesion between the surface and the nanocrystal. Probing an individual nanocrystal attached to a cyclohexylidene SAM will therefore not be possible. However, probing all the nanocrystals simultaneously by electrochemical means should still be feasible.

In figure 15 the interfacial capacitance of a Au(111)/disulfide/Au_{nc} interface in a 1 M KCl solution is plotted as a function of electrode potential. The capacitance of the bare electrode is considerably reduced after application of the disulfide to the Au(111) surface (compare curves 1 and 2 of figure 15), again demonstrating the quality of the disulfide SAM on gold. When gold nanocrystals are anchored to the SAM, the capacitance increases in the entire potential range; the increase is most pronounced at around the potential of zero charge (curve 3); the capacitance of the nanostructured Au(111)/disulfide/Au_{nc} interface shows a maximum as a function of the potential, similar to that of a bare gold electrode. We conclude that the attachment of gold nanocrystals to the SAM leads to the formation of an additional gold/water interface which can be charged/discharged by electron transfer through the molecular layer. A simple model to explain this effect qualitatively will be discussed below.

We used the increase of the interfacial capacitance $C(\omega \to 0, E \approx E_{pzc})$ as a quantitative measure to follow in real time and in-situ (*i.e.* in the colloidal gold suspension) the anchoring of gold nanocrystals (15 nm in size) to a gold/disulfide SAM. In figure 16 the relative increase in capacitance $\theta = \Delta C/\Delta C_{max}$, which is a measure for the surface coverage, is plotted versus time. A justification of this procedure is given in the discussion. Initially, the surface concentration of Au_{nc} on the SAM layer increases linearly with time; the addition rate decreases at longer times and finally becomes very

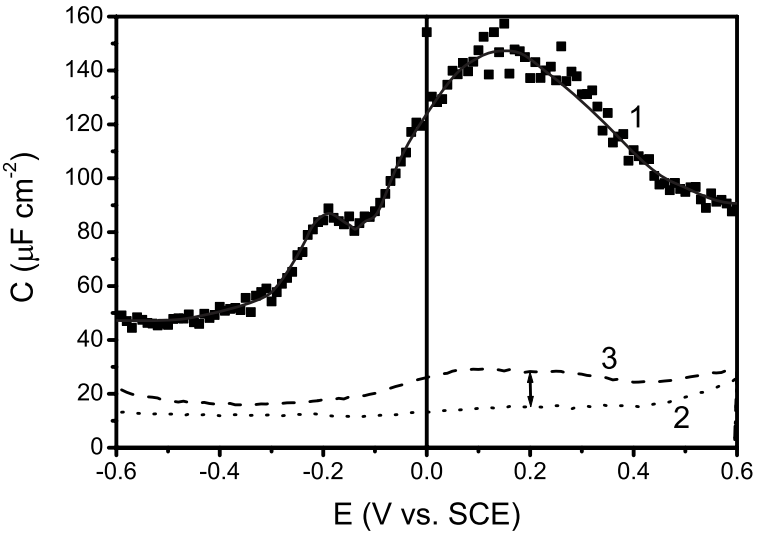

FIGURE 15. The low-frequency limit of the interfacial capacitance of a gold (111) electrode after different pretreatments in a 1M KCl solution at $25°C$ as a function of the electrode potential. The capacitance was obtained from the charging/discharging response to small-amplitude potential step. (1, —■—) an untreated, bare gold (111) electrode. (2,· · ·) after immersion of the gold (111) electrode in an ethanolic solution of disulfide (figure 2b; n=0). (3,− − −) after immersion of the gold (111)/disulfide electrode in a colloidal gold suspension for 4 hours. The ↕ shows the increase in the capacitance due to the gold nanocrystal attachment.

low. We note that the maximum coverage observed in the saturation range is about 75 $particles/\mu m^2$, corresponding to an average centre-to-centre distance of about 97 nm between two nanocrystals (A local mapping is given in the inset of figure 13a). Assuming an attachment rate independent of the surface coverage, *i.e.* interparticle interactions are ignored, we can describe the rate $d\theta/dt$ as:

$$\frac{d\theta}{dt} = k_a c\,(1-\theta) - k_d\theta \tag{2.6}$$

where θ is the fraction of the surface sites occupied by a nanocrystal, c is the concentration of nanocrystals and k_a and k_d the pseudo-first order rate constants for nanocrystal adsorption and desorption, respectively. At equilibrium ($d\theta/dt = 0$) equation 2.6 simplifies to the well-known Langmuir isotherm, which is used to describe reversible (monolayer) adsorption onto surfaces.

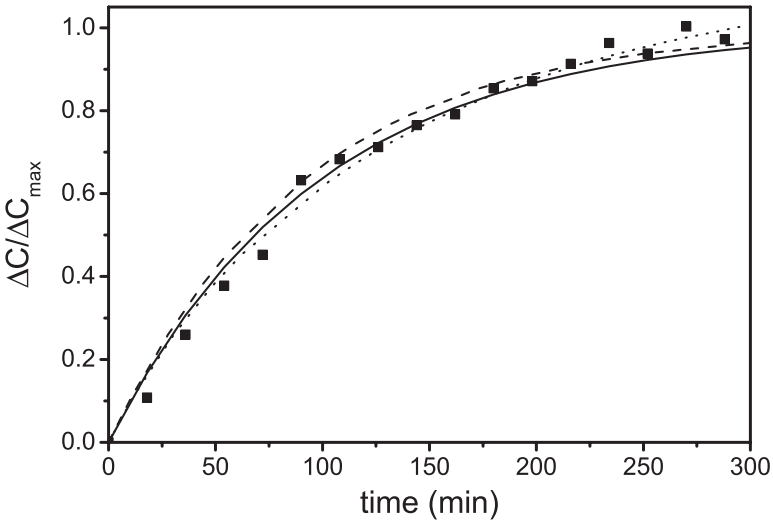

Figure 16. The relative surface coverage $\theta = \Delta C/\Delta C_{max}$ of gold nanocrystals on a gold (111)/disulfide (figure 2b; n=0) SAM attachment obtained from the increase in the interfacial capacitance (see arrow in figure 15) measured in-situ during nanocrystal attachment. The data (■) have been fitted with equation 2.6 (——), equation 2.7 (− − −) and equation 2.7 with C_{max} taken as 1.17 times the highest measured capacitance ($\cdots$).

A fit of the addition kinetics according to equation 2.6 is included in the figure 16 (drawn line). It can be seen that this simple law describes the kinetics of particle addition reasonably well, except for the longer times, *i.e.* at high coverage. This is probably due to the electrostatic interactions between the adsorbed particles, which is important at high coverage. Therefore a Frumkin-type exponential factor is incorporated in equation 2.6.

$$\frac{d\theta}{dt} = k_a c\,(1-\theta)e^{-f\theta} - k_d\theta \tag{2.7}$$

At equilibrium ($d\theta/dt = 0$) equation 2.7 yields the Frumkin isotherm. The Frumkin parameter f takes into account the fact that the apparent free energy of binding to the substrate changes linearly with surface coverage[**30**]. When $f < 0$, the interaction between the particle and the (particle covered) surface is repulsive, whereas $f > 0$ when this force is attractive.

The exponential factor in equation 2.7 causes the fit to level off later (at higher t), as can be seen in figure 16, dashed curve. Unfortunately, this does not increase the accuracy of the fit. In the previous section we assumed that the highest measured capacitance corresponds to C_{max}. However, since this equilibrium value is only slowly reached the true maximum may be higher.

When C_{max} was increased by 17.6% the fit was obtained as shown in figure 16, dotted curve. This fit describes satisfactory the attachment of particles.

It should be remarked that the attachment of gold nanocrystals is likely to be an irreversible process, *i.e.* $k_d \cong 0$. This may also explain why the gold nanocrystals do not form ordered two-dimensional arrays on the gold/disulfide surface.

4. Discussion and Conclusions

The interfacial capacitance of a gold (111) electrode covered with an oligo(cyclohexylidene) SAM is very much reduced compared to that of a bare gold electrode; in addition it shows a different dependence on the electrode potential and modulation frequency. The capacitance features change again when gold nanocrystals become attached to the SAM. The highly polarizable double layer structure (*i.e.* jellium layer) of the metal, itself arising from electrons that spill over the surface layer of gold core ions, plays a key role in the total capacitance[**31, 32**]. There is still debate on the applicability of the jellium model to noble metals. Here, we take the jellium model as a basis to rationalize the experimental results presented in the foregoing section. The capacitance of a bare gold (111) electrode measured in 1 M KCl and 1 M $NaClO_4$ aqueous solutions shows a pronounced and asymmetric peak when plotted as a function of the electrode potential and a relatively strong frequency dependence. The peak can be accounted for by the capacitance of the metal double layer C_M that is in series with the capacitance of the first water layer C_{sol}, see figure 17a. The interfacial capacitance of a bare gold electrode is then given by equation 2.8:

$$C = \frac{|C_M| C_{sol}}{|C_M| - C_{sol}} \tag{2.8}$$

The peak in the interfacial capacitance C at around E_{pzc} can be explained by assuming

(i) that C_{sol} does not depend strongly on the charge density and hence on the electrode potential, and

(ii) that $|C_M| - C_{sol}$ is positive in the entire potential region and has a minimum at around E_{pzc}.

The maximum interfacial capacitance depends sensitively on the difference $|C_M| - C_{sol}$ around the point of zero charge. This explains the strong influence of the nature of the metal and exposed crystal surface on the maximum interfacial capacitance close to E_{pzc}, reported in the literature[**32**]. In 1 M KCl and 1 M $NaClO_4$, E_{pzc} is +0.2 and +0.3 V vs. SCE, respectively. This is somewhat more negative than in fluoride electrolytes ($E_{pzc} = +0.33$ V vs. SCE[**20**–**24**]) indicating specific Cl^- and to lesser extent ClO_4^- adsorption on the gold (111) surface. The frequency dispersion of a bare electrode is more pronounced than that of a gold electrode covered with a SAM (see

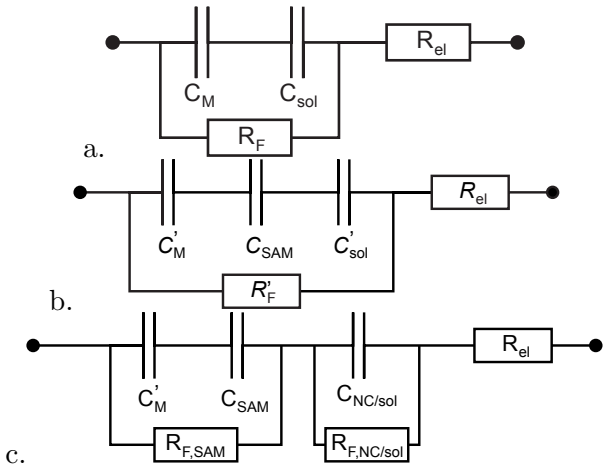

FIGURE 17. Randle's equivalent circuit for **a.** a bare metal electrode, **b.** a metal electrode covered with a self-assembled monolayer, and **c.** a disulphide modified Au(111) electrode covered with a gold nanocrystal, all in contact with a polar electrolyte solution. For explanation of the electrical components see text.

insert of figure 8). This suggests that the frequency dispersion of bare gold electrodes is due partly to anion adsorption[**19**]. At potentials negative with respect to E_{pzc} the capacitance of the bare electrode decreases to a nearly constant value of 20 $\mu F\, cm^{-2}$ at 1000 Hz, indicating that $C_M \gg C_{sol} \cong 20$ $\mu F\, cm^{-2}$ when the charge density on the gold surface is negative (see also figure 8).

Oligo(cyclohexylidene) mono- and disulfide molecules, and methylated oxime-sulfide molecules (figure 2a, b and e, respectively) form well-ordered SAMs on gold (111) surfaces, characterized by a low and nearly potential-independent capacitance ($C \leq 6$ $\mu F\, cm^{-2}$). The structure of the double layer is schematically presented in figure 17b. The capacitance of the metal double layer can be influenced by the large density of Au-S bonds; C'_M is used instead of C_M to denote this capacitance. Similarly, we use C'_{sol} (instead of C_{sol}) for the capacitance of the solvent layer in contact with the SAM. The total interfacial capacitance is now given by equation 2.9:

$$C = \frac{|C'_M| C'_{sol} C_{SAM}}{|C'_M|(C'_{sol} + C_{SAM}) - C_{SAM} C'_{sol}} \tag{2.9}$$

The interfacial capacitance is nearly equal to that of the SAM monolayer for the case in which $C'_M > C_{sol} > C_{SAM}$:

$$C \cong C_{SAM} = \frac{\varepsilon_{SAM} \varepsilon_0}{d_{SAM}} \tag{2.10}$$

where ε_{SAM} is the dielectric constant and d_{SAM} the thickness of the SAM. Equation 2.10 explains why the observed capacitance of the SAM covered gold electrode is low and does not show a peak at around E_{pzc}. We should remark here that there are subtle, but reproducible differences between sulfide oligo(cyclohexylidene)s of the same length (n=0,1) but with different end-functionalities at the water side; the capacitance of the alkyl-terminated SAM is smaller than that of a methylated oxime-sulfide (figure 2e) terminated SAM, which is, in turn, slightly smaller than that of a sulfide-terminated (figure 2b) SAM. This may be due partly to a difference in ε_{SAM}, partly to a different ordering of the first water layers contacting the hydrophobic and less hydrophobic end-functionalities of these oligo(cyclohexylidene) molecules. A dependence on the end-functionality has also been reported in the literature [**25, 26**]. We also note that the capacitance decreases with increasing length of the molecules in the SAM, which is in qualitative agreement with equation 2.10.

When a gold nanocrystal (Au_{nc}) is anchored to an S-terminated oligo-(cyclohexylidene) SAM layer a nanometer-sized electrical junction is formed with an impedance represented in figure 17c. This impedance replaces that of a non-occupied site shown in figure 17b. Since the entire system consists of both occupied and non-occupied sites, the total electrical equivalent circuit for the Au(111)/oligo(cyclohexylidene)/Au_{nc} interface is formed by a parallel connection of figure 17b and c. The impedance of a gold (111)/oligo(cyclohexylidene)/Au_{nc}/water structure shown in figure 17c accounts for charging of the gold nanocrystal through the molecular SAM layer (Faradaic resistance $R_{F,SAM}$) and the formation of an electrochemical double layer at the gold nanocrystal/water interface (capacitance $R_{F,NC/sol}$). At sufficiently low frequencies, the nanocrystal/water interface can be charged/discharged, and the interfacial capacitance will be larger than that of a gold (111)/oligo(cyclohexylidene)/water site. Although the scheme presented in figure 17b-c for the nanostructured interface is perhaps naive, it can be used to understand the increase of the interfacial capacitance of the gold electrode upon attachment of gold nanocrystals to the SAM layer (figure 15 and 16).

From the above discussion, we may conclude that the electrochemical capacitance provides a plausible description of a bare gold (111)/water, a gold (111)/oligo(cyclohexylidene)/water and a gold (111)/oligo(cyclohexylidene)/Au_{nc}/water interface. The self-assembly of end-functionalized alkane molecules on metal surfaces (mostly alkanethiols on gold surfaces) has been studied extensively by other research groups[**7, 33, 34**]; similar conclusions concerning the usefulness of electrochemistry have been drawn. The novelty of our work lies in the choice of the molecules, *i.e.* oligo(cyclohexylidene)s, and in the striking effects found with different end-functionalities. Oligo(cyclohexylidene) molecules have a rigid C-skeleton with a chair conformation. This enables the formation of well-ordered SAMs, even with short molecules,

with one cyclohexyl ring (*i.e.* n = 0). In addition, both chemical end-functionalities play a key role in the possible formation of oligo(cyclohexylidene) SAMs on gold (111) surfaces. We found that oligo(cyclohexylidene) molecules terminated with one or two sulfide-end functions form well-ordered SAMs on gold (111). Even the shortest oligo(cyclohexylidene) molecule led to a low and potential-independent capacitance and a considerable reduction of the rate of interfacial electron transfer. The electrochemical results show that oxime-terminated oligo(cyclohexylidene) molecules do not form a SAM on gold (111). The oxime-gold interaction is too weak. Surprisingly, oligo-(cyclohexylidene) molecules with a sulfide and oxime function also do not form well-ordered SAMs. This is not well understood at present, but the results clearly indicate that the oxime termination inhibits the formation of well-ordered layers.

A second new aspect in this work is that we show that the attachment of Au nanocrystals to a gold/oligo(cyclohexylidene) SAM can be followed in-situ by measurement of the interfacial capacitance. Attachment of a gold nanocrystal to the SAM leads to a new gold/water nanointerface that can be charged by electron transport through the molecular layer. Similarly, photo-induced electron transfer through oligo(cyclohexylidene) molecules mounted between an insulating quantum dot and gold has been observed [**8**]. By measurement of this additional charge, we were able to follow the adsorption kinetics. A simple law is found; the rate of adsorption of the nanocrystals on the SAM is proportional to the density of free sites on the SAM surface. Under conditions of saturation, we find with tapping mode AFM a disordered array of individual gold nanocrystals, still corresponding to a relatively low coverage. Most likely, the attachment of nanocrystals is an irreversible process. The low coverage may be due to the charged double layer around the nanocrystals. This also explains why there is no clustering of individual nanocrystals. It should be noted here that charge-stabilized gold nanocrystals do not attach to bare gold, but only form some clusters at the grain boundaries. We suggest that the electron spill-over region (jellium layer) of the bare gold (111) surface repels the negatively charged gold nanocrystals. Interestingly, when the gold (111) surface is covered with an alkyl-terminated SAM, gold nanocrystals do attach to the surface. With tapping mode AFM, we show that these nanocrystals can be moved easily along the surface, a clear indication of weak adsorption. This is in clear contrast to the nanocrystals attached to a sulfide-terminated surface, which are chemically bound.

References.

[1] C. Joachim, J. K. Gimzewski, and A. Aviram. *Nature*, **408**-6812 (2000) 541–548.

[2] Danny Porath, Alexey Bezryadin, Simon De Vries, and Cees Dekker. *Nature*, **403**-6770 (2000) 635–638.

[3] Zhen Yao, Charles L. Kane, and Cees Dekker. *Phys. Rev. Lett.*, **84**-13 (2000) 2941–2944.
[4] Sander J. Tans and Cees Dekker. *Nature*, **404**-6780 (2000) 834–835.
[5] J. Chen, M. A. Reed, A. M. Rawlett, and J. M. Tour. *Science*, **286**-5444 (1999) 1550–1552.
[6] M. A. Reed, C. Zhou, C. J. Muller, T. P. Burgin, and J. M. Tour. *Science*, **278**-5336 (1997) 252–254.
[7] P. S. Weiss, L. A. Bumm, T. D. Dunbar, T. P. Burgin, J. M. Tour, and D. L. Allara. *Ann. N. Y. Acad. Sci.*, **852**-Molecular Electronics: Science and Technology (1998) 145–168.
[8] Erik P. A. M. Bakkers, Albert W. Marsman, Leonardus W. Jenneskens, and Daniel Vanmaekelbergh. *Angew. Chem., Int. Ed.*, **39**-13 (2000) 2297–2299.
[9] E. P. A. M. Bakkers, A. L. Roest, A. W. Marsman, L. W. Jenneskens, L. I. De Jong-Van Steensel, J. J. Kelly, and D. Vanmaekelbergh. *J. Phys. Chem. B*, **104**-31 (2000) 7266–7272.
[10] David I. Gittins, Donald Bethell, David J. Schiffrin, and Richard J. Nichols. *Nature*, **408**-6808 (2000) 67–69.
[11] F. J. Hoogesteger, R. W. A. Havenith, J. W. Zwikker, L. W. Jenneskens, H. Kooijman, N. Veldman, and A. L. Spek. *Journal of Organic Chemistry*, **60**-14 (1995) 4375–4384.
[12] F. J. Hoogesteger, D. M. Grove, L. W. Jenneskens, T. J. M. deBruin, and B. A. J. Jansen. *Journal of the Chemical Society-Perkin Transactions 2*, -11 (1996) 2327–2334.
[13] A. W. Marsman, R. W. A. Havenith, S. Bethke, L. W. Jenneskens, R. Gleiter, J. H. van Lenthe, M. Lutz, and A. L. Spek. *Journal of Organic Chemistry*, **65**-15 (2000) 4584–4592.
[14] A. W. Marsman, R. W. A. Havenith, S. Bethke, L. W. Jenneskens, R. Gleiter, and J. H. van Lenthe. *European Journal of Organic Chemistry*, -14 (2000) 2629–2641.
[15] G. Frens. *Nature (Phys. Sci.)*, **241** (1973) 20–22.
[16] D. Eberhardt, E. Santos, and Wolfgang Schmickler. *Journal of Electroanalytical Chemistry*, **419** (1996) 23–31.
[17] T. Pajkossy. *Journal of Electroanalytical Chemistry*, **364**-1-2 (1994) 111–125.
[18] A. Hamelin, T. Vitanov, E. Sevastyanov, and A. Popov. *Journal of Electroanalytical Chemistry*, **145** (1983) 225.
[19] T. Pajkossy, T. Wandlowski, and D. M. Kolb. *Journal of Electroanalytical Chemistry*, **414**-2 (1996) 209–220.
[20] J. Lecoeur and A. Hamelin. *C.R. Acad. Sci.*, **279C** (1974) 1081.
[21] J. Lecoeur, C. Sella, L. Tertain, and A. Hamelin. *C.R. Acad. Sci.*, **280C** (1975) 247.
[22] J. Lecoeur, C. Sella, J.C. Martin, L. Tertain, and J. Deschamps. *C.R. Acad. Sci.*, **281C** (1975) 71.
[23] A. Hamelin and J. Lecoeur. *Surf. Sci.*, **57** (1976) 771.
[24] J. Lecoeur, J. Andro, and R. Parsons. *Surf. Sci.*, **114** (1982) 320.
[25] M. J. Esplandiu, H. Hagenstrom, and D. M. Kolb. *Langmuir*, **17**-3 (2001) 828–838.
[26] C. E. D. Chidsey and D. N. Loiacono. *Langmuir*, **6**-3 (1990) 682–691.
[27] C. A. Widrig, C. Chung, and M. D. Porter. *Journal of Electroanalytical Chemistry*, **310**-1-2 (1991) 335–359.
[28] R. P. Janek, W. R. Fawcett, and A. Ulman. *Langmuir*, **14**-11 (1998) 3011–3018.
[29] L. I. de Jong-van Steensel, M. M. E. Snel, G. J. K. van den Berg, L. W. Jenneskens, and Jpjm van der Eerden. *Crystal Growth and Design*, **1**-5 (2001) 347–353.
[30] C. D. Keating, M. D. Musick, M. H. Keefe, and M. J. Natan. *Journal of Chemical Education*, **76**-7 (1999) 949–955.
[31] N.D. Lang and W. Kohn. *Physical Review B*, **1**-12 (1970) 4555–4568.
[32] Wolfgang Schmickler. *Chemical Reviews*, **96**-8 (1996) 3177–3200.

[33] C. E. D. Chidsey. *Science*, **251**-4996 (1991) 919–922.
[34] A. Ulman. *Chemical Reviews*, **96**-4 (1996) 1533–1554.

CHAPTER 3

Self-assembly of charged, amphiphilic Au nanocrystals at a polar/apolar liquid interface

1. Introduction

In the last decades colloidal gold nanocrystals have received considerable attention due to their interesting electronic [**1**–**5**] and optical [**5**–**8**] properties. Two methods of synthesizing these nanocrystals have been widely employed. The first is the method developed by Brust *et al.*[**9**]. This yields uncharged metal nanocrystals capped with alkyl thiols soluble in apolar solvents. The thermodynamic stability of the *colloidal solution* is due to the fact that the interaction between the capping molecules of the particles is smaller or equal to the capping-solvent interaction. Evaporation of the solvent leads to the formation of assemblies which show long-range order, if the size-dispersion is sufficiently small. The strong interdigitation of the alkyl chains indicates that the formation of such nanocrystalline 2-D and 3-D solids [**10, 11**] is driven by the large decrease in enthalpy due to the van der Waals interactions between the capping alkyl molecules.

Another method used to form gold nanocrystals is based on the reduction of aqueous hydrogen tetrachloroaurate at 100 $^{\circ}C$ by citrate[**12, 13**]. The resulting nanocrystals have a negative surface charge which is due to citrate and chloride adsorption [**14, 15**]. This charge induces a diffuse layer of counter charge, the electrical double layer. Since the overlap of two double layers leads to an increase in free energy [**16**], the solution is kinetically stabilized against aggregation. Adsorbed citrate also provides a short-range steric barrier [**15**]. Decrease of the width of the diffuse double layer L_D by salt addition leads to destabilisation of the sol and (irreversible) coagulation of the gold particles.

Here, we report the spontaneous formation of a 2-D array of charged gold nanocrystals at the interface of a polar solvent (water) and an immiscible apolar solvent (heptane). When a heptane phase is brought into contact with an aqueous colloidal gold solution no visible change is observed. Very strikingly, a dense gold film forms promptly after addition of only a few milliliters of ethanol.[a] Figure 1 shows an image of the gold sol(5

[a]For the interested reader, movies of the film formation have been made available on the bottom of the internet page http://www.phys.uu.nl/~reincke/Amphiphilic.html.

ml)/heptane(2.5 ml) system before (figure 1a) and after (figure 1b and c) addition of 3 ml ethanol. The gold nanocrystals have a diameter of 16nm. Addition of the ethanol has two profound effects. Firstly, the colour of the aqueous phase (bottom) changes from orange-red to purple. Secondly, a blue layer of gold nanocrystals with a high reflectivity is rapidly formed at the water/heptane interface; the layer also moves upwards along the glass within 1 or 2 seconds.

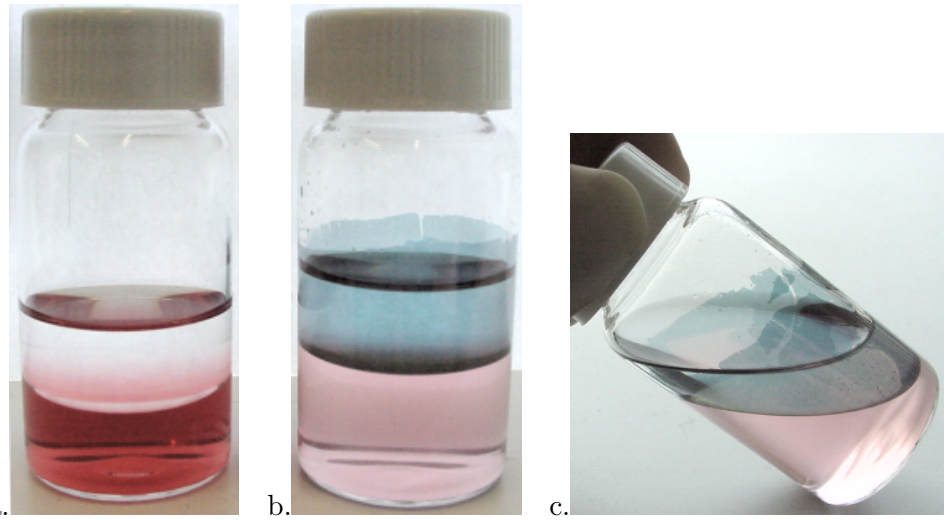

Figure 1. Photograph of the vial filled with 2.5 ml heptane and 5 ml gold sol, before (**a.**) and after (**b.** and **c.**) addition of 3 ml ethanol.

Self-assembly of charged colloidal particles at the polar/apolar interface usually leads to an ordered, but *diluted* array of particles due to the electrostatic repulsion between the particles[**17**]. The distance between the particles is of the order of the width of the diffuse double layer. In addition, Aveyard *et al.* [**18**] showed that *dense* 2-D layers of charged polystyrene spheres (2.6 μm in diameter) could be formed at the octane/water interface by addition of several soaps. When no soap was added, only diluted ordered structures were found. Cuvillier *et al.* [**19**] also found that large phosphotungstate ($PW_{12}O_{40}^{3-}$) ions, which are anchored electrostatically to a eicosylamine, form dense self-assembled monolayers at the aqueous/octane interface.

In section 3 the structure of the layer of charged gold nanocrystals (Au_{nc}) is described; both in-situ (section 3.1) and ex-situ (section 3.2) methods were used. In section 4 the wetting of gold by various liquids is studied. The results of the wetting experiments are extrapolated to the Au_{nc} layers. Next, in section 5, the origin of this layer formation is addressed, where the

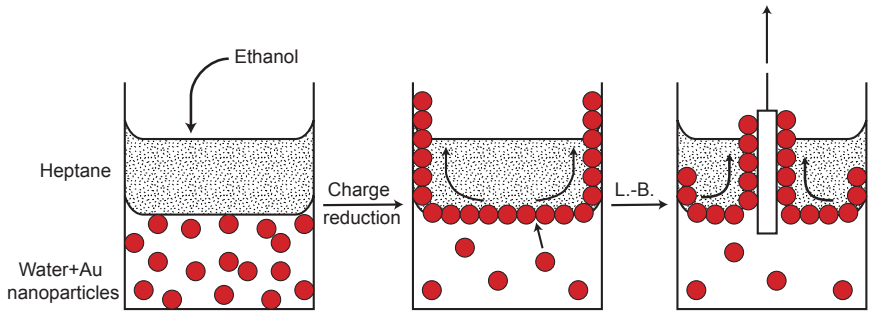

Figure 2. Schematic picture of the layer formation and collection. Left: The addition of ethanol to the heptane/gold sol system. Middle: Particles form a layer at the aqueous/organic interface; the layer extends onto glass. Right: Layer is extracted by the Langmuir-Blodgett technique.

emphasis will be on the reduction of the particle charge (section 5.1), the thickness of the double layer (section 5.2) and adsorption of species on the particle surface (section 5.3). In the Discussion and Conclusions (section 6) the dense interfacial monolayers composed of *charged* nanocrystals are compared to those of *uncharged* nanocrystals.

2. Experimental Methods

2.1. Layer formation. Trisodium citrate trihydrate, sodium borohydride, hydrochloric acid, sulphuric acid and sodium perchlorate monohydrate were obtained from Merck and were of p.a. grade or better. $HAuCl_4$ p.a. was obtained from Sigma-Aldrich and anhydrous ethanol (ACS Reagent; 99%) was obtained from Riedel-de Haën.

The aqueous colloidal gold solutions, or gold sols for short, were prepared as described in chapter 2. Typically, 2.5 ml of organic solvent (usually heptane) is added to 5 ml of gold sol. After addition of several milliliters of ethanol the mixture is vigorously shaken and an unstable water/heptane foam is obtained. During the breakup of this foam, the heptane/aqueous interface shows a clearly visible blue hue. At a certain point the blue interfacial layer extends upwards onto the heptane/glass interface, see figure 1. The intensity of the orange-red colour of the gold sol has decreased considerably, indicating that nanocrystals are transferred to the interface.

When the organic phase was allowed to evaporate the layer remained present on the water/air interface. This layer will be termed the 'dry' layer.

2.2. Layer collection. The 'wet' layers were collected by pulling a substrate vertically through the aqueous/heptane interface using a home-made dipcoater set at a speed of 0.5 cm/min, see figure 2. The substrate was

subsequently dried and analyzed using tapping mode AFM and Transmission Electron Microscopy (TEM). For analysis using tapping mode AFM, we used glass substrates, which were cleaned with piranha mixture (3:1 H_2SO_4/H_2O_2 v/v) and rinsed thoroughly with distilled water before use. For TEM, carbon-coated copper grids were employed as a substrate.

The 'dry' layers were compressed using a custom-built Langmuir trough. During lateral compression of the layer the substrate was moved through the aqueous/air interface, dried and analysed using AFM and TEM. In the Langmuir setup, the surface tension could be measured with a Wilhelmy plate connected to a microbalance.

2.3. Particle charge measurements. For these measurements the Doppler Effect Light Scattering Analyser (Delsa) 440SX was used. The colloidal gold solution is inserted into a 1 mm thick tube. A potential of 20 V is applied along the axis of the tube. The charged gold nanocrystals move in the electric field. Due to this movement, the light scattered by the nanocrystals has a slight Doppler shift, which is measured for five different angles 0°, 8.9°, 17.6°, 26.3°, and 35.2°. This beam perpendicular (0°) to the tube shows no Doppler shift, since there is no nett field in that direction. Therefore the beam at 0° is used as a reference beam.

The beams were focused three times at 0.16 mm below the top and three times at 0.16 mm above the bottom of the tube. In this way the distribution of mobility and zeta potential of the gold particles can be measured and checked for reproducibility. A typical result can be seen in figure 3. The peak at 0 mobility is clearly an artifact, probably caused by stray light that did not pass through the cell and therefore did not exhibit a Doppler shift. The resulting mobility curves were fitted using a Lorentzian and the maximum was recorded. The maxima of the four angles were averaged.

The mobility U is defined as the drift velocity v divided by the applied electric field E. When the width of the double layer L_D is small compared to the particle radius, the surface charge s per particle can be written as:

$$s = L_D^{-1} \eta U \tag{3.1}$$

The solvent viscosity η was measured using the MCR 300 rheometer (Paar Physica) with a double-gap cylindrical probe (DG 26.7; after DIN 54453). The Debye-Hückel screening length L_D is calculated by the well-known formula:

$$L_D = \sqrt{\frac{\varepsilon \varepsilon_0 kT}{2 N_A e^2 I}} \tag{3.2}$$

where N_A is Avogadros constant, e the electron charge, ε and ε_0 the relative permittivity and the permittivity of vacuum, respectively, k the Boltzmann constant, T the absolute temperature and I the ionic strength (in units of

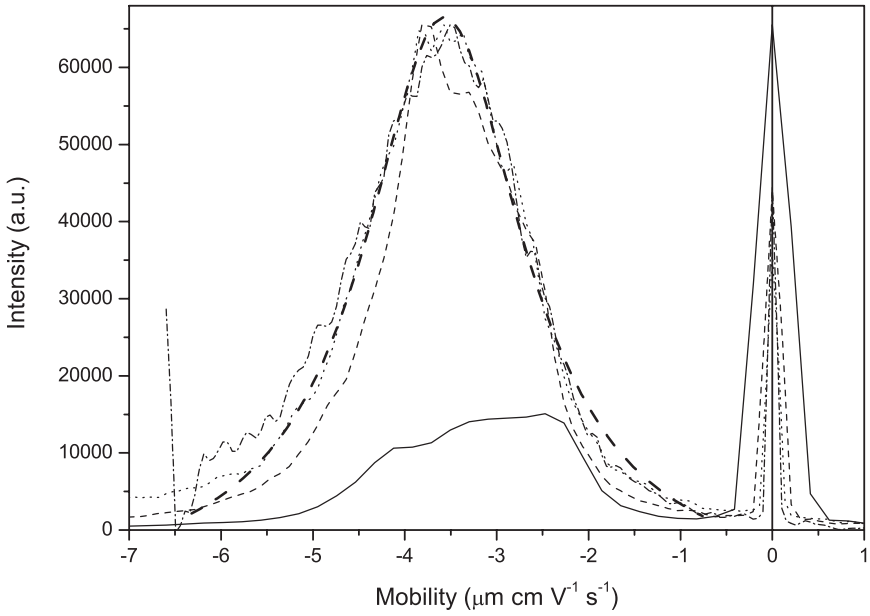

Figure 3. Mobility measurements of charge-stabilised gold nanocrystals in aqueous solution using the DELSA. Measurements were taken at angles of 8.9 (—), 17.6 (− − −), 26.3 (· · ·), and 35.2 (− · − · −) degrees. Thick dashed line: Lorentzian fit to the data at an angle 26.3°.

mol/m^3), which is defined as

$$I = \frac{1}{2}\sum_i c_i z_i^2 \tag{3.3}$$

where c_i and z_i are the concentration and charge of ion i in solution, respectively.

The dielectric constant of the water/ethanol mixtures ε was calculated using an effective medium approach:

$$\varepsilon_{H_2O/Ethanol} = \frac{V_{H_2O}\,\varepsilon_{H_2O} + V_{Ethanol}\,\varepsilon_{Ethanol}}{V_{H_2O} + V_{Ethanol}} \tag{3.4}$$

where V_{H_2O} and $V_{Ethanol}$ are the volumes of water and ethanol and ε_{H_2O} and $\varepsilon_{Ethanol}$ are the dielectric constants of water and ethanol.

2.4. Dynamic Light scattering. A vial was filled with 10 ml gold sol. The vial was irradiated with a 632.8 nm He-Ne laser and the detector was placed at an angle $\Theta = 60°$ with respect to the incoming light beam and the scattered light intensity $i(\overrightarrow{k}, t)$ was measured. A small part of the scattered light was selected using 200 μm pinholes and measured with a

photomultiplier tube (Hamamatsu) in photon-counting mode. The photon counts were autocorrelated using a Flex01-12D digital correlator[b].

Next, 5 ml heptane and 3 ml ethanol was added to the vial. The layer was allowed to form and move up the glass. The light of a He-Ne laser was then pointed at the glass/layer/heptane interface and the measurement was repeated.

2.5. Wetting experiments. Gold substrates, identical to those used for AFM/STM measurements (see chapter 2, section 2.6), were cleaned by flame-annealing in a hydrogen flame. When necessary, the substrates were immersed in a 1 % trisodium citrate solution for 30 min at 50 $^{\circ}C$. Using a level and shock-free granite table as a base, the substrates were placed in a Petri dish filled with heptane. Next, 20 μl of water with varying amounts of ethanol was carefully dropped onto the gold surface. The experiments were repeated three times to check for consistency.

3. Structural characterisation of the layer

3.1. In-situ characterisation.

3.1.1. *Optical microscopy.* The sample was a gold sol+ethanol/heptane mixture in a Petri dish imaged from the topside (through the heptane), as explained in section 2.1. The sample was irradiated from above (through the objective) with white light. In figure 4a an image is shown of a layer after addition of 1 ml of ethanol. Standing out from the dark background, bright aggregates of gold nanocrystals are visible at the interface.

When further ethanol is added, more particles are driven to the interface. As can be seen in figure 4b the islands grow larger until a continuous layer of gold nanocrystals is formed. This layer, however, contains voids. The layer formed from 16 nm nanocrystals or smaller has a blue colour with a strong metallic hue, despite the voids in the layer. Layers made from larger nanocrystals showed a pattern of gray-coloured islands.

3.1.2. *Lateral compression of the layer.* To learn more about the interaction between the particles in the layer, we measured the surface tension as the layer was compressed. The lateral pressure Π is defined as:

$$\Pi = -(\gamma_{layer} - \gamma_{ref}) \tag{3.5}$$

where γ_{layer} is the surface tension of the compressed layer and γ_{ref} the surface tension of the gold sol+ethanol/air interface.

At one point in the compression (for a known macroscopic area) the layer was collected and the number of particles per unit area was determined with TEM. The other area per particle values were extrapolated from the macroscopic area, see also section 2.2.

[b]Correlator website: http://correlator.com

a.
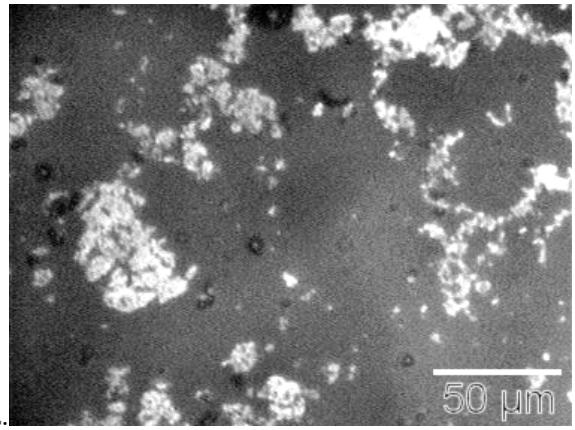

b.
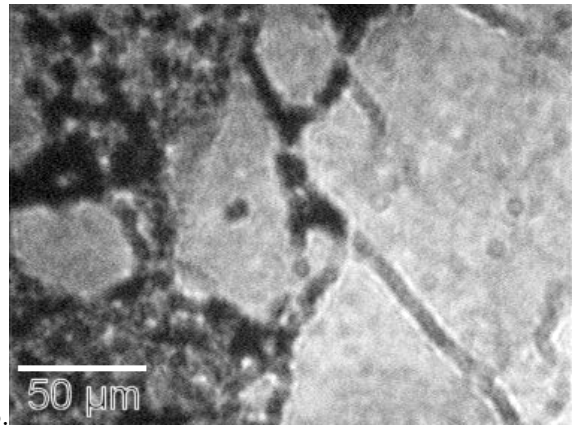

Figure 4. In-situ microscope pictures of 16 nm gold nanocrystals at the gold sol/heptane interface (magnification 20x10), with **a.** 1 ml and **b.** 3 ml ethanol added to 10 ml of gold sol.

Due to the low interfacial tension of a gold sol+ethanol/heptane interface (about 2 mN/m), the surface pressure could not be accurately determined. Therefore the heptane was allowed to evaporate and the surface pressure of a gold sol+ethanol/air interface was measured. Since optically no differences were observed in the layer, it was assumed that the structure of the layer was unaltered by the drying process.

An example of a measurement of Π vs. area/particle for a 'dry' layer (gold sol/layer/air) is shown in figure 5a. For the 16 nm particles no pressure is measured beyond 330 nm^2/particle. The islands can still move independently and the lateral pressure only induces a rearrangement of the islands. Below 330 $nm^2/particle$ the lateral pressure starts to increase. Here the islands have merged into a continuous layer. This layer still contains large

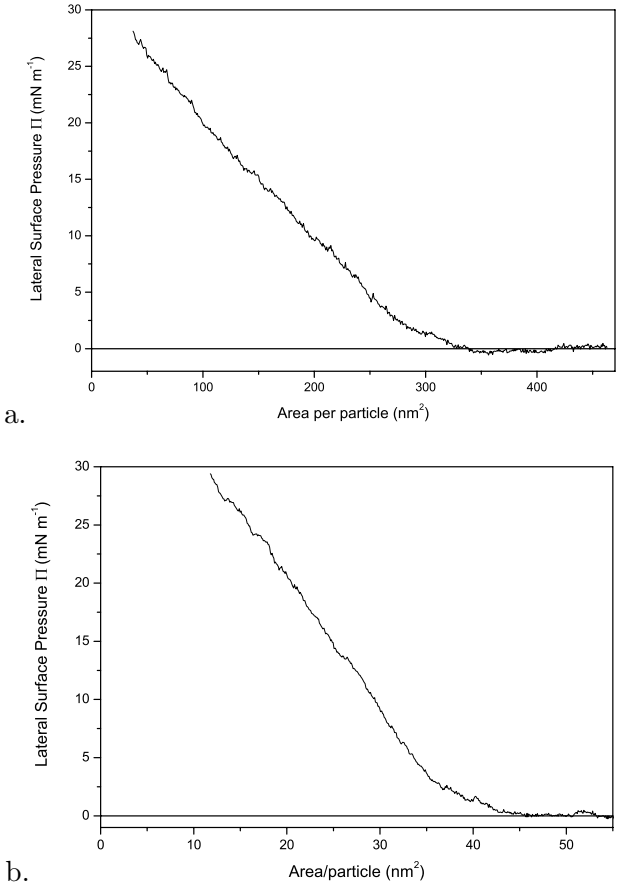

Figure 5. Lateral pressure of the gold sol/layer/air interface. Layers were formed using a colloidal solution of **a.** 16 nm and **b.** 6 nm gold nanocrystals.

voids, since in a hexagonal close-packed monolayer the space filling is $\frac{1}{6}\sqrt{3}\,\pi$ or 91%, which translates to about 221 $nm^2/particle$ for 16 nm particles. When the layer is compressed even further, the pressure increases roughly linearly with decreasing area per particle; fluctuations in the pressure are also visible. This upward trend is found in every measurement. It is tempting to assign these fluctuations to the annealing/removal/collapse of these voids. However, the trend continues well beyond the 220 $nm^2/particle$, the point at which the layer could no longer consist of just one monolayer. This indicates that the lateral pressure induces multilayer formation, otherwise known as collapse. Although annealing of the voids cannot be ruled out, it is not the dominant compression mechanism. Collapse and void annealing are also responsible for the noise in the plot of Π vs. area/particle.

The 6 nm gold nanocrystals (figure 5b) show a similar trend as the 16 nm nanocrystals. The pressure is almost zero down to 42 $nm^2/particle$, and increases nearly linearly far beyond the point corresponding to close-packing (36 $nm^2/particle$).

3.1.3. *Mobility of Au_{nc} in the layer.* The mobility of the particles in the layer can be probed using the technique of dynamic light scattering, see paragraph 2.4. Curve a in figure 6 shows the correlation graph for a 16 nm colloidal gold solution, measured at a scattering angle of 60°. It clearly shows a fluid-like decay at a typical delay time of $t = 0.35\ ms$ (indicated by ↓). At smaller sampling times the fluctuations are strongly correlated while at longer sampling times the correlation is much weaker. In appendix A it is shown that the diffusion constant D of the gold nanocrystals can be obtained from the normalised intensity auto correlation function $\widehat{g}_I(\overrightarrow{k}, t)$:

$$\widehat{g}_I(\overrightarrow{k}, t) = \frac{< i(\overrightarrow{k}, t_0)\ i(\overrightarrow{k}, t + t_0) >}{< i(\overrightarrow{k}, t) >^2} \sim e^{-2Dk^2t} + 1 \qquad (3.6)$$

A fit of curve a using equation 3.6 yielded a diffusion constant of 8.2 10^{-8} cm^2/s. This value is comparable to the value calculated by the Stokes-Einstein equation $D = \frac{k_B T}{6\pi a \eta} = 1.5\ 10^{-7}\ cm^2/s$, using $\eta = 1.13\ 10^{-3}\ kg/(m\ s)$[c] and $a = 13\ nm$[d].

The correlation plot measured for a monolayer of Au_{nc} at the glass/heptane interface is markedly different (see figure 6, curves b and c). The transition occurs at a much larger sampling time ($t = 9.4$ and 140 s for the 40 and 16 nm gold nanocrystals, respectively, indicated by ↓'s in figure 6). The increased correlation time suggests that individual particles in the layer are immobilised, and that only self-assembled islands consisting of many nanocrystals are able to move.

3.2. Ex-situ characterisation. Using the Langmuir-Blodgett technique, see section 2.2, the layers were collected and dried. It was found from Transmission Electron Microscopy (TEM) measurements that the 'wet' layers (collected from the gold sol+ethanol/heptane interface) were similar to the 'dry' ones (collected from the gold sol+ethanol/air interface). Thus, evaporation of the heptane top phase does not change the structure of the layer.

In figure 7a a TEM image is shown of the blue layer of 16 nm particles as collected from the aqueous/organic interface, see section 2.2. A submonolayer of individual gold nanocrystals is formed, with a number of voids. The distance between neighboring particles is typically between 1 and 4 nm, which is smaller than the width of the double layer L_D (4 to 5 nm). Although

[c] The unit $10^{-3}\ kg/(m\ s)$ is better known as the *milli Pascal second* or the *centi Poise*

[d] The hydrodynamic radius a was taken as the sum of the particle radius (8 nm) and the double layer width (5 nm)

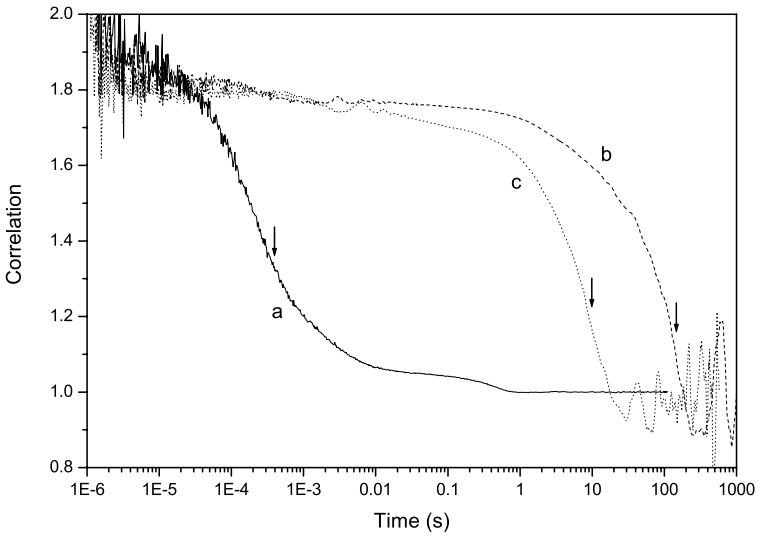

Figure 6. Graph of the intensity auto correlation function versus sampling time of the gold nanocrystals in the as-prepared solution (a) and self-assembled into a 2-D layer at the heptane/glass interface (b and c). Curves a and b were measured for 16 nm and curve c for 40 nm Au_{nc}.

there is some local ordering in the layer, no long-range order can be found. As has been shown in the previous chapter, the polydispersity in the particle size, more than 10%, is too large to allow ordered layers to form[**20, 21**].

Figure 7b shows a layer collected at a lateral pressure of 10 to 15 mN/m (see figure 5). It is clear that this layer consists of monolayers and regions which have collapsed to multilayers. Strikingly, the remaining portions of the monolayer still contain some voids. Due to the low mobility of the particles, lateral pressure is not able to anneal all of the voids.

Similar results were obtained with AFM characterisation, as can be seen in figure 8a. Due to the thickness of the tip the space between adjacent particles cannot be fully probed, but the height difference between the layer and a void in the layer shows that, in the uncompressed state, the interfacial film consists of a monolayer of gold nanocrystals, see figure 8b.

The same topology of the collected layers has been found for smaller (4-8 nm; see figure 9a), and larger nanocrystals (40 nm; figure 9b).

4. Wetting experiments

In the experiment of figure 10a a 20 μl drop of water is placed onto a flame-annealed gold substrate; the substrate and the drop are completely immersed in heptane. The contact angle is clearly negative, indicating that bare gold is predominantly hydrophobic. Adding ethanol to the drop did

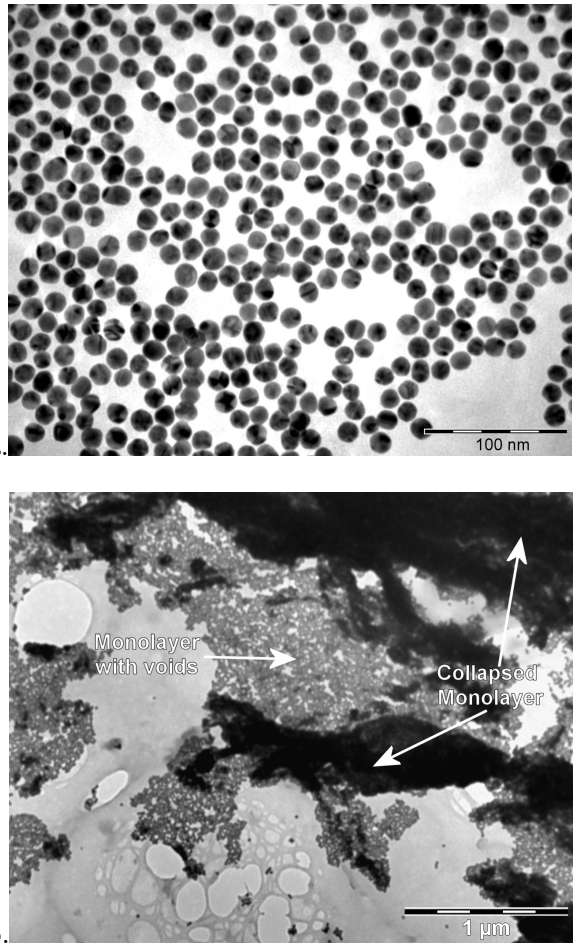

Figure 7. TEM image of a 'dry' layer (Au_{nc} layer at the water+ethanol/heptane interface *after* evaporation of the heptane) collected by the Langmuir-Blodgett technique **a.** before and **b.** after compression by a Langmuir trough.

not significantly change the contact angle, see figure 10b. However, when the gold was pretreated with trisodium citrate the contact angle is nearly 90 degrees, see figure 10c, hence the surface becomes amphiphilic. Again, after addition of ethanol to the drop, figure 10d, the contact angle remained close to 90°. When heptane saturated with ethanol was used is stead of pure heptane the same contact angles were observed. Therefore the gold nanocrystals that form the monolayer at the water/heptane interface are expected to be located halfway through the interface, as schematically drawn in figure 12, regardless of the ethanol concentration.

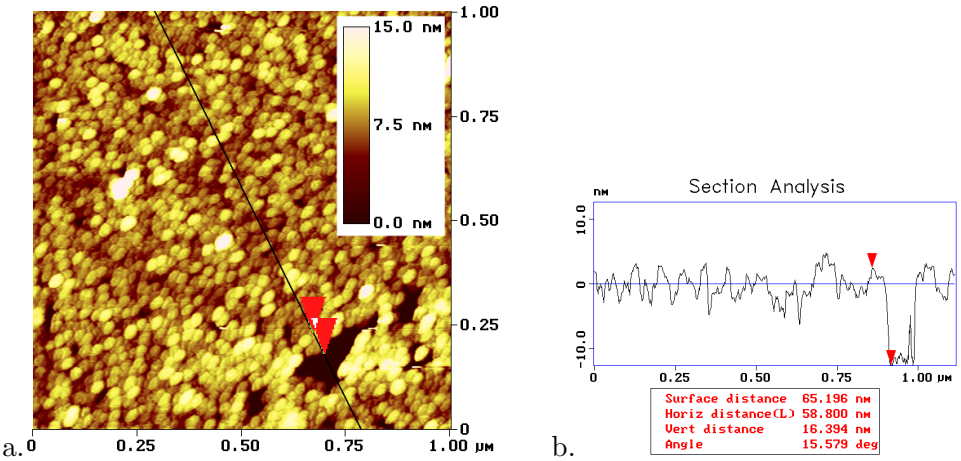

Figure 8. **a.** AFM image of a layer originating from gold sol+ethanol/heptane interface (5, 10 and 3 ml respectively) which was deposited on glass using the Langmuir-Blodgett technique. **b.** Cross section as indicated in **a.**. The numbers correspond to the positions of the arrows. The layer height exactly matches the particle size (16 nm).

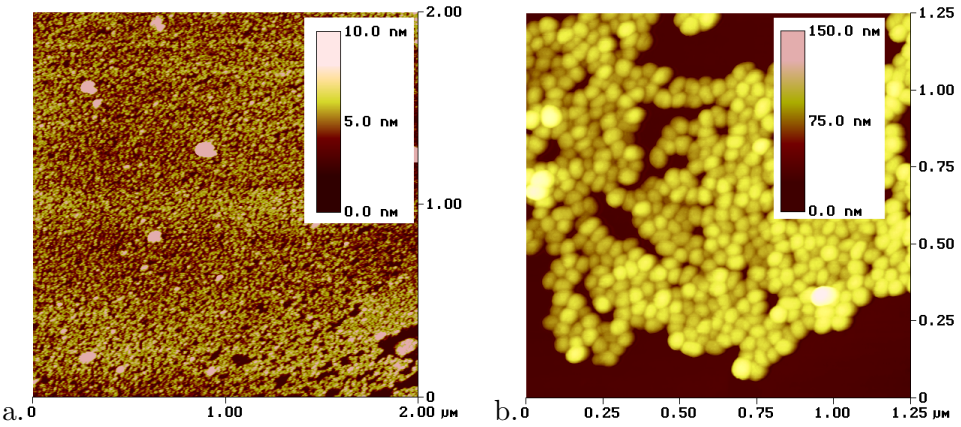

Figure 9. Tapping mode AFM image of a Au_{nc} layer with a diameter of **a.** 8 nm and **b**. 40 nm formed at the water/heptane interface after addition of ethanol

5. Factors important in formation of the interfacial gold layer

In this section we consider why the interfacial layer forms spontaneously after addition of a small amount of ethanol to the aqueous gold sol. Therefore, we have systematically investigated the factors that could influence the formation of the layer: the surface charge density of the particle, the

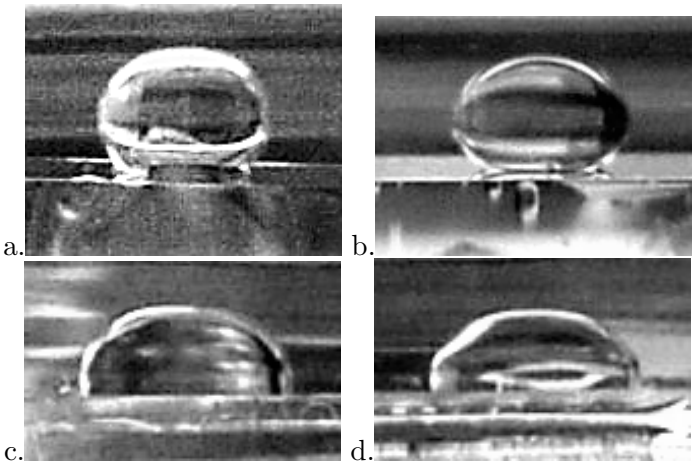

Figure 10. Wetting experiments on gold (111). The entire setup was immersed in heptane. 20 μl drops of distilled water (**a.** and **c.**) and 38% v/v ethanol in water (**b.** and **d.**) were carefully deposited on flame-annealed gold samples which were either unpretreated (**a.** and **b.**) or pretreated by immersion in 0.1% w/w trisodium citrate for 30 min (**c.** and **d.**)

reduction of the double layer width, and adsorption of molecules at the nanocrystal surface.

5.1. Reduction of the surface charge. Dense layers of gold nanocrystals are formed at the aqueous/organic liquid interface upon addition of a moderate amount of ethanol to the aqueous solution. On the moment that the interfacial layer is formed, the gold nanocrystals are still charged. We will assume that their charge is preserved in the layer. As can be seen in figure 7a, the average distance between the particles is close to 1 nm. Using equation 3.2 the lower limit of the Debye screening length L_D was calculated to be 5.0 nm for the particles shown in figure 7, *i.e.* the aqueous gold sol with ethanol added. This value is slightly higher than that of an as-prepared gold sol (4.6 nm). Thus, the distance between two adjacent gold nanocrystals in the layer is smaller than the Debye screening length L_D.

Although the screening length gives the length scale of the Coulomb interactions between the particles, it does not describe the strength of the repulsion, which is determined by the surface charge.

A charged colloidal particle in an electric field moves with a velocity which is proportional to its charge. Therefore, the mobility of the particle is directly related to the surface charge. The mobility of a colloidal particle in solution can be measured with the *Doppler Effect Light Scattering Analyzer* (DELSA). The experiments were performed as described in section 2.3. In

figure 11, the negative surface charge density present on the gold nanocrystals is shown as a function of the amount of ethanol added to the solution. The surface charge decreases considerably upon addition of ethanol, from 10 mC/m^2 to 4 mC/m^2, for both the 6 and 16 nm sized gold nanocrystals. Since the charge on the Au_{nc} surface is mainly due to adsorbed citrate on the surface, ethanol could adsorb more strongly and in this way remove citrate from the surface. However, the surface charge does not go to zero; This could be due to chloride ions which remain present at the nanocrystal surface[**14, 15**].

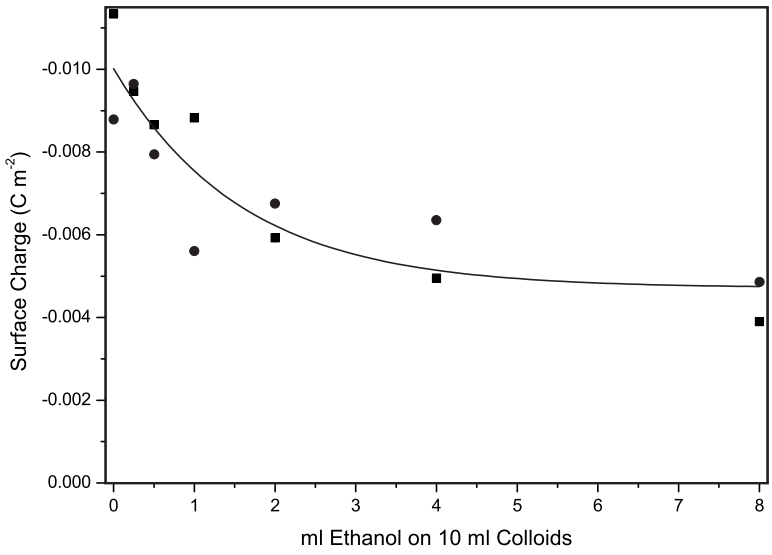

Figure 11. Charge density on the gold nanocrystal surface as measured with the DELSA for 4 nm (■) and 16 nm (●) nanocrystals. The line is a guide to the eye.

However, removal of citrate also changes other interfacial properties, *e.g.* wetting of the nanocrystals. To distinguish clearly between the charge reduction and a change of the gold/water interface we reduced the charge without removing citrate from the surface. This can be accomplished by decreasing the pH, thereby protonating the citrate.

Addition of 2 ml of a 39 mM sulfuric acid solution to the heptane/gold sol mixture leads to formation of a monolayer of individual nanocrystals, similar to those formed by addition of ethanol. Similar results were found after addition of 2.2 ml of 11.0 mM hydrochloric acid. No aggregation was observed in the aqueous phase and this was also not expected since the L_D of particles in solution was only slightly reduced to 3.2 and 4.4 nm after addition of H_2SO_4 and HCl, respectively.

Upon addition of acid the pH of the gold sol decreased from 5.8 to 2.0 and 2.8 for sulfuric and hydrochloric acid, respectively. These values are

lower than the lowest pKa values of citric acid (3.08)[e] showing that most citrate is protonated. Complete removal of the surface charge is unlikely since Cl^- is also present on the nanocrystal surface, and this cannot be protonated.

5.2. The width of the double layer. Besides charge reduction, which does not change or only slightly changes the screening length L_D, increasing the ionic strength also destabilises the nanocrystals, see equation 3.2 and reference [**16**]. An inert salt was added to the gold sol/heptane system. It was found that 0.55 ml of 1M $NaClO_4$ was needed to form a layer. In this solution L_D is 2.5 nm, which is smaller than that in the presence of acid. Layers obtained from this gold sol/heptane/$NaClO_4$ system contained mostly aggregates and no monolayer sections.

When L_D is reduced, the energy barrier for aggregation is reduced, both in the bulk aqueous phase and at the interface. Reducing the double layer introduces two possibilities, *viz.* layer formation and aggregation. These two possibilities will occur simultaneously, producing a layer of aggregates at the interface. The best way to obtain monolayers at the polar/non-polar interface is therefore through charge reduction which only allows layer formation and prevents aggregation.

5.3. Addition of chemisorbing moieties. In the foregoing sections we have used ethanol which physisorbs on the gold nanocrystal, see chapter 2. Since we only need to introduce a moiety that attaches itself more strongly to the Au_{nc} surface than citrate, other chemicals may also invoke layer formation. An obvious choice would be sulphur-containing compounds, which are renowned for their strong chemisorption to gold surfaces.

When several sulphide and thiol moieties[f] were added to the gold sol/heptane system, the aqueous phase changed colour from orange-red to blue within seconds and layers were formed within half a minute. This colour change is evidence for thiol adsorption[**8**]. The amount of thiol or sulphide required for layer formation was found to be relatively small, typically 40 μl of a 10 mM solution in heptane.

Compared to the layers transferred from the gold sol+ethanol/heptane interface, the layers formed by addition of thiols were not so dense; a substantially smaller part of the substrate is covered with a monolayer and a larger number of large ($> 100\ nm$ high) aggregates is present. This is different from the result by Kumar *et al.* [**23**], who showed that a monolayer of individual nanocrystals could be obtained by adding a chemisorbing moiety to a gold sol/heptane system.

To rule out the influence of the substrate (glass) on the layer topology, the experiment was repeated with mica as a substrate. The degree of

[e]The others pKa values are 4.74 and 5.40 [**22**]

[f]We used pentamethylene sulfide, benzylethanethiol, 1-heptanethiol and 1-octanethiol

aggregation did not decrease on mica. After addition of heptanethiol and octadecanethiol, aggregates were observed to form in the aqueous phase. The alkanethiol capping causes the particle to become more apolar, with aggregation in the aqueous phase competing with layer formation, producing a 'clumpy' layer, as seen before.

6. Discussion and Conclusions

Suspensions of sterically stabilized and (nominally) uncharged gold nanocrystals have often been used as a model system for the study of self-assembly. A wealth of gold nanocrystal structures have been reported[**24**–**26**] and their opto-electrical properties are still under investigation. The synthesis of charge-stabilized gold sols is well established. The processing of such sols has focussed on the capping of charged nanocrystals with organic molecules in order to allow transfer to a non-aqueous phase. In addition, the assembly of these nanocrystals into molecular-like structures, covalently linked by organic bridges[**27**] or DNA strands[**28**] has been reported. However, the formation of a *dense* interfacial monolayer of charged gold nanocrystals has, to our knowledge, not been reported.

Charged gold nanocrystals self-assemble at the polar/apolar liquid interface upon a slight reduction of the surface charge. We have shown that a reduction of the surface charge at a constant Debye screening length L_D leads to the formation of monolayers of nanocrystals at the interface between water and heptane without any sign of coagulation. If the screening length is reduced, 3-D aggregation occurs together with layer formation, leading to a 'clumpy' layer. The creation of the layer is fast, in the order of a few seconds. The layer is also remarkably robust, being able to move up vertical glass/heptane interfaces.

The self-assembled interfacial layer of gold nanocrystals consists of dense arrays, interrupted by voids. In the dense parts, the distance between the gold nanocrystals is between 1 and 4 nm, smaller than the Debye screening length L_D. This observation allows us to speculate on the structure of the interfacial Au_{nc} layer. Due to the small interparticle distance it is unlikely that a diffuse double layer is present between the gold nanocrystals. Thus, the diffuse double layer with counter charge is structurally two-dimensional, see figure 12a.

The thermodynamic stability must be due to a number of different interactions. Firstly, the interaction of the gold surface with the heptane phase on one side, and the interaction of the gold with the aqueous phase on the other side, replaces the heptane/water interaction. We will show in the next chapter that this is the major driving force for the formation of an interfacial layer. Secondly, the close proximity between the nanocrystals is likely to give rise to van der Waals interaction between them. Thirdly, due to the difference in dielectric constants, the strength of the electric field in the

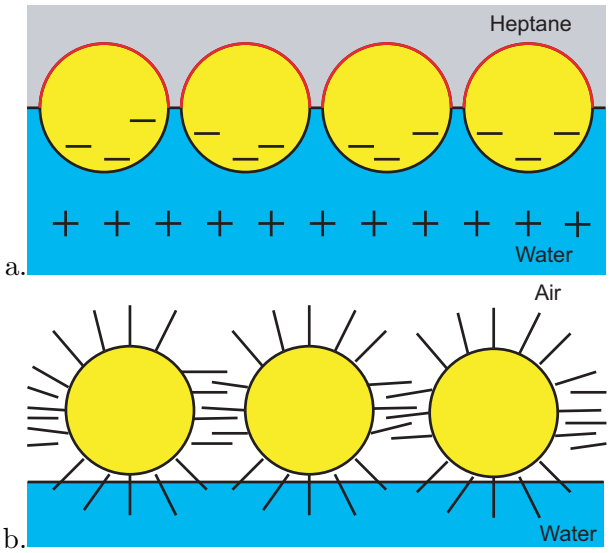

Figure 12. **a.** Schematic representation of the charge distribution of a self-assembled monolayer of charged, uncapped, amphiphilic gold nanocrystals at the heptane/air interface. **b.** Schematic representation of alkanethiol capped, uncharged gold nanocrystals at the aqueous/air interface, for comparison.

organic phase is about 40 times larger than that in the aqueous phase[**17**]. As a result, the free interface between the particles tends towards the oil side, creating a curved interface. This curvature might cause a capillary attraction between the two particles. As the layer consists of charged particles in close proximity, Coulomb-repulsion would partly counteract these stabilizing factors.

The layers show an unexpectedly high mechanical strength. This is best illustrated by the observation that the layer is pushed from the aqueous/heptane interface vertically up the glass for several centimeters within seconds, without collapsing. The stability must also be the cause of the very slow lateral diffusion of the gold nanocrystals in the layer, as was shown with dynamic light scattering experiments.

The stability of alkanthiol-capped films at the aqueous/air interface is mainly determined by the capping. The capping molecules can interact with those of an adjacent particle. The capping molecules of two adjacent particles tend to interdigitate, causing a strong van der Waals interaction between neighboring particles, as can see figure 12b. In addition, the apolar/apolar interaction between the capping and air also constitutes a stabilizing interaction.

Besides the lateral stability of the amphiphilic gold layer, another striking effect is its colour. The colour of charged, individual 16 nm nanocrystals is orange/red [**7, 9**]. However when the nanocrystals are close together, *e.g.* within a layer, the colour becomes more blue[**29**] and would eventually get a distinct golden sheen as if it was a continuous gold layer[**30**]. This effect is attributed to the overlap of electronic orbitals of the individual nanocrystals. In the case of sterically stabilized nanocrystals, the separation between the nanocrystals in the monolayer is usually too large to provide sufficient overlap between the electronic orbitals, due to the size of the capping molecules. An insulator-to-metal transition was only observed, both optically and electronically[**30**], when the layer was compressed laterally. It was found that the layer had metallic properties when the particle separation to diameter ratio ($x/2R$) was below 1.2. For the charge-stabilised layer described in this chapter the distance is already small enough to provide electronic overlap ($x/2R \approx 0.06$), resulting in a blue colour and a golden sheen, despite the fact that holes are present in the layer. The electrical conductivity of the layer will probably be low due to the presence of holes.

Charged colloidal nanocrystals have considerable technological relevance. Many methods are available for the preparation of charge-stabilized sols. Furthermore, it has become clear that even sterically stabilized particles in non-aqueous solvents can carry residual charge[**31**]. The preparation of monolayers of such charged nanocrystals would constitute an important step forwards in the route to the fabrication of two-dimensional and three-dimensional materials for opto-electrical or magnetic applications. We have shown that charged gold nanocrystals self-assemble at the water/oil interface upon gradual reduction of the surface charge density. Since charge reduction can be accomplished in various ways, this method of assembly does not depend on the details of the surface chemistry and should thus be widely applicable.

In the next chapter, a thermodynamic model will be presented which explains the main observations of this chapter.

References.

[1] R.P. Andres, T. Bein, M. Dorogi, S. Feng, J.I. Henderson, C.P. Kubiak, W. Mahoney, R.G. Osifchin, and R. Reifenberger. *Science*, **272** (1996) 1323.

[2] S. Chen, R.S. Ingram, M.J. Hostetler, J.J. Pietron, R.W. Murray, T.G. Schaaff, J.T. Khoury, M.M. Alvarez, and R.L.Whetten. *Science*, **280** (1998) 2098.

[3] R.S. Ingram, M.J. Hostetler, R.W. Murray, T.G. Schaaff, J.T. Khoury, R.L. Whetten, T.P.Bigioni, D.K. Guhrie, and P.N. First. *Journal of the American Chemical Society*, **119** (1997) 9279.

[4] M.Y. Han, L. Zhou, C.H. Queck, S.F.Y. Li, and W. Huang. *Chemical Physics Letters*, **287** (1998) 47.

[5] D. Davidovic and M. Tinkham. *Physical Review Letters*, **83**-8 (1999) 1644.

[6] J.A.A.J. Perenboom. *Physical Review*, **78** (1981) 173.

[7] Gustav Mie. *Annalen der Physik*, **25** (1908) 25.

[8] S. Link and M.A. El-Sayed. *Journal of Physical Chemistry B*, **103**-21 (1999) 4212.
[9] M. Brust, M. Walker, D. Bethell, D.J. Schiffrin, and R. Whyman. *Journal of the Chemical Society, Chemical Communications*, (1994) 801.
[10] R. P. Sear, S. W. Chung, G. Markovich, W. M. Gelbart, and J. R. Heath. *Physical Review E*, **59**-6 (1999) R6255–R6258.
[11] P. C. Ohara, D. V. Leff, J. R. Heath, and W. M. Gelbart. *Physical Review Letters*, **75**-19 (1995) 3466–3469.
[12] G. Frens. *Nature (Phys. Sci.)*, **241** (1973) 20–22.
[13] J. Turkevich, J. Hiller, and P.C. Stevenson. *Disc. Farad. Soc.*, **11** (1951) 55.
[14] M. K. Chow and C. F. Zukoski. *Journal of Colloid and Interface Science*, **165**-1 (1994) 97–109.
[15] S. Biggs, M. K. Chow, C. F. Zukoski, and F. Grieser. *Journal of Colloid and Interface Science*, **160**-2 (1993) 511–513.
[16] D.H. Everett. *Colloid Science*, chapter 3, pages 30–53. Royal Society of Chemistry Paperbacks, Cambridge, 1988.
[17] M. G. Nikolaides, A. R. Bausch, M. F. Hsu, A. D. Dinsmore, M. P. Brenner, and D. A. Weitz. *Nature*, **420**-6913 (2002) 299–301.
[18] R. Aveyard, J. H. Clint, D. Nees, and N. Quirke. *Langmuir*, **16**-23 (2000) 8820–8828.
[19] N. Cuvillier and F. Rondelez. *Thin Solid Films*, **329** (1998) 19–23.
[20] P.N. Pusey. *Journal de Physique*, **48** (1987) 709–712.
[21] R. McRae and A. D. J. Haymet. *Journal of Chemical Physics*, **88**-2 (1988) 1114–1125.
[22] R.C. Weast. *Handbook of Chemisrty and Physics*. Number 10. Chemical Rubber Company, 49th edition, May 1968.
[23] A. Kumar, S. Mandal, S. P. Mathew, P. R. Selvakannan, A. B. Mandale, R. V. Chaudhari, and M. Sastry. *Langmuir*, **18**-17 (2002) 6478–6483.
[24] J.R. Heath, C.M. Knobler, and D.V. Leff. *Journal of Physical Chemistry B*, **101**-2 (1997) 189.
[25] C. J. Kiely, J. Fink, M. Brust, D. Bethell, and D. J. Schiffrin. *Nature*, **396**-6710 (1998) 444–446.
[26] John Fink, Christopher J. Kiely, Donald Bethell, and David J. Schriffrin. *Chemistry of Materials*, **10**-3 (1998) 922.
[27] J. P. Novak and D. L. Feldheim. *Journal of the American Chemical Society*, **122**-16 (2000) 3979–3980.
[28] J. J. Storhoff and C. A. Mirkin. *Chemical Reviews*, **99**-7 (1999) 1849–1862.
[29] T. Ung, L. M. Liz-Marzan, and P. Mulvaney. *Colloids and Surfaces a-Physicochemical and Engineering Aspects*, **202**-2-3 (2002) 119–126.
[30] C.P. Collier, R.J. Saykally, J.J. Shiang, S.E. Henrichs, and J.R. Heath. *Science*, **277** (1997) 1978.
[31] L. N. Donselaar, A. P. Philipse, and J. Suurmond. *Langmuir*, **13**-23 (1997) 6018–6025.

CHAPTER 4

A model for the self-assembly of charged colloidal particles at the water/organic interface

1. Introduction

Charged colloidal particles, with sizes in the micrometer range, are known to self-assemble at polar/apolar interfaces. This can lead, for instance, to the stabilisation of Pickering emulsions of two immiscible liquid phases [**1**].

Charged colloidal particles are stabilised in solution by an electrical double layer. This double layer is characterised by its surface charge density σ and its width (Debye length L_D). The electrical double layer prevents aggregation of the particles in solution. However, if the aqueous solution is covered with an immiscible organic liquid, spontaneous adsorption of charged particles can occur at the water/organic liquid-liquid interface. This is driven by a reduction of the interfacial energy of the water/organic interface[**2**].

With micrometer-sized particles, diluted two-dimensional arrays were observed, often showing long-range order. It was assumed that the particles all carry the same charge, and that the ordering is due to the repulsion of the double layers. Recently, it was suggested that residual charge could still be present at the organic side of the particle surface, which is poorly shielded due to the low dielectric constant of the organic phase[**3**]. Besides regular structures, Aveyard *et al.* [**4**] showed that dense, disordered 2-D layers of charged polystyrene (diameter 2.6 μm) could also be formed at the octane/water interface.

We have shown in chapter 3 that a change of the surface charge density of nanometer-sized gold particles leads to the formation of dense, but disordered, monolayers at the water/organic liquid interface. Thus, assembly of charged colloidal particles at the water/organic interface is an ubiquitous phenomenon. Here we will present a model to describe the properties of these layers. We will follow a route similar to a model of Paunov *et al.*[**5**], and we will derive expressions for the chemical potential for a particle in the aqueous bulk (μ_{bulk}) and at the aqueous/organic interface (μ_{int}). Equating these two chemical potentials, $\mu_{bulk} = \mu_{int}$, we obtain an expression for the system at equilibrium. This expression contains the equilibrium surface fraction ϕ_s^{eq} and the surface charge density σ. Calculation of this equilibrium fraction for several values of σ, yields an ϕ_s^{eq} vs. σ isotherm. This model

can be easily adapted to describe the assembly at the water/air interface by setting the dielectric constant of the organic phase $\varepsilon_{organic}$ to 1.

2. Model

In the next sections the factors contributing to μ_{bulk} (section 2.1) and μ_{int} (section 2.2) will be described.

2.1. Chemical potential of bulk colloidal particles. We consider colloidal solutions which are sufficiently dilute so that, at most, interactions at a pair level play a role. The particles are also assumed to be monodisperse, equally charged and spherical, the latter condition results in translational degrees of freedom only.

With these assumptions, there are three contributions to the bulk (Helmholtz) free energy.

2.1.1. *Ideal solution.* According to statistical thermodynamics, the Helmholz free energy can be written as:

$$F = -k\,T \ln Q \tag{4.1}$$

with k and T Boltzmann's constant and absolute temperature, respectively, and Q is the canonical partition function, *i.e.* the sum of the Boltzmann probabilities of all possible states. For a monoatomic ideal gas with three translational degrees of freedom, Q becomes:

$$Q = \frac{V^N}{N!\,\Lambda^{3N}} \tag{4.2}$$

where V is the total volume of the aqueous phase, and N the number of particles. When a particle is moved over a distance Λ, a new state is reached. In the case of an ideal gas, where the particles are surrounded by vacuum, Λ is the thermal de Broglie wavelength. Since the particles are dispersed in an aqueous matrix, we will use the linear size of water molecules l_w as the length scale Λ[**6**].

Combining equations 4.1 and 4.2 and using the Stirling approximation ($\ln N! = N \ln N - N$) we obtain the ideal gas contribution:

$$F_{id} = N\,k\,T\,(\ln(v_w N/V) - 1) \tag{4.3}$$

with $v_w = l_w^3$ the molecular volume of water.

Using $\mu = (\frac{\partial F}{\partial N})_{T,V}$ we obtain the "ideal colloidal solution" term of the bulk chemical potential:

$$\mu_{id}/k\,T = \ln(v_w \rho) \tag{4.4}$$

with $\rho = N/V$ the particle number density.

2.1.2. *Pair interaction.* The second contribution to the bulk chemical potential comes from interactions between particles at a pair level. This contribution follows from the osmotic pressure $\Pi(\rho) = \rho kT(1 + B_2\rho)$, with B_2 the second virial coefficient. B_2 is, to a good approximation, given by $B_2 = -\int_0^\infty (e^{-u(r)/kT} - 1)2\pi r^2 dr$, where $u(r)$ is the interaction potential between the colloidal particles as a function of their separation r. At large r Coulomb repulsion dominates adding a positive contribution to B_2, whereas at small r van der Waals attraction provides a negative contribution to B_2. The sign of B_2 is therefore determined by the balance of the two. Application of the Gibbs-Duhem equation, *i.e.*, $(\frac{\partial\mu}{\partial\rho})_T = \rho^{-1}(\frac{\partial\Pi}{\partial\rho})_T$, results in

$$\mu/k\,T = \ln(\rho/\rho_0) + 2B_2(\rho - \rho_0) \tag{4.5}$$

When we take $\rho_0 = v_w^{-1}$ it can be seen that the first term is the "ideal colloidal solution" term (see equation 4.4) and the second is the non-ideal term that accounts for the pair interaction energy between the particles. Since the ideal behaviour was already accounted for in equation 4.4 it can be ignored here. Since ρ_0 is the integration constant and since we are only interested in the deviation from ideal behaviour, the chemical potential term due to pair interaction can be written as:

$$\mu_{pair}/k\,T = 2B_2\rho \tag{4.6}$$

2.1.3. *Interfacial energy.* The free energy of the particle-solvent interface is given by

$$F_{c/w} = 4\pi R^2 N\gamma_{c/w} \tag{4.7}$$

where $\gamma_{c/w}$ is the interfacial tension between water (solvent) and colloidal particles, and R the particle radius.

2.1.4. *Bulk chemical potential.* Combining the three contributions of equations 4.4, 4.6 and 4.7 we obtain the chemical potential of a particle in the bulk water phase

$$\mu_{bulk}/k\,T = \ln\left(\frac{v_w}{v_p}\right) + \ln(\phi) + 2\frac{B_2}{v_p}\phi + \frac{4\pi R^2\gamma_{c/w}}{k\,T} \tag{4.8}$$

In this equation, $v_p = \frac{4}{3}\pi R^3$ is the particle volume, and $\phi = v_p\rho$ is the volume fraction of the particles in the water phase.

2.2. Chemical potential of particles adsorbed at the interface. This part consists of four contributions due to: the organic solvent/water, particle/water and particle/organic interfaces in the system; the Coulomb interactions between charges located at the particle/organic interface; van der Waals interactions between the particles; and the translational entropy of the particles at the interface.

2.2.1. *Surface tension.* The interfacial properties depend strongly on the position of particles at the interface. From wetting experiments (chapter 3, section 4) it was shown that the three-phase contact angle between the water+ethanol/heptane interface and the gold nanocrystals is very close to 90°. Therefore we will take the particles to be half in the organic phase and half in the water phase, as shown in figure 1 and figure 12 of chapter 3.

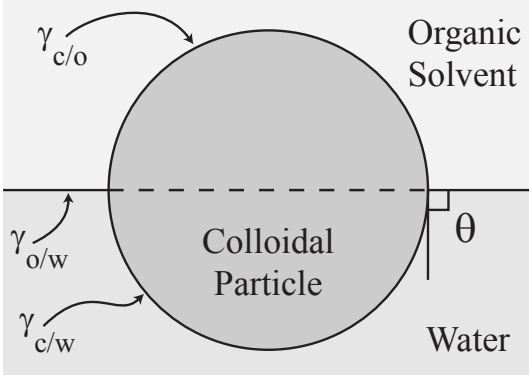

Figure 1. Schematic representation of a colloidal particle at the aqueous/organic interface. Since the particle has the same affinity for the organic and water phases, it is located as shown in the figure with a three-phase contact angle θ of 90°. The interfacial tensions corresponding to the organic/water ($\gamma_{o/w}$), colloidal paricle/organic ($\gamma_{c/o}$) and colloidal partile/water ($\gamma_{c/w}$) interfaces are indicated.

The Helmholtz free energy due to the interfacial tension is given by $F_\gamma = \sum_i A_i \gamma_i$ where A_i and γ_i are the area and interfacial tension of interface i, respectively. In our case this leads to:

$$F_\gamma = (A - \pi R^2 N)\,\gamma_{o/w} + 2\pi R^2 N\,\gamma_{c/o} + 2\pi R^2 N\,\gamma_{c/w} + 2\pi R N\,\gamma_l \qquad (4.9)$$

where $\gamma_{o/w}$, $\gamma_{c/o}$ and $\gamma_{c/w}$ are the interfacial tensions of the aqueous/organic, colloidal particle/organic and colloidal particle/aqueous interfaces, respectively (as indicated in figure 1), and γ_l is the line tension.

A particle in the interface has a three-phase angle θ of 90°, see figure 1. Using the Young-Dupré equation, $\cos\theta = (\gamma_{c/o} - \gamma_{c/w})/\gamma_{o/w}$ (which in our case is $\gamma_{c/o} = \gamma_{c/w}$), equation 4.9 simplifies to:

$$F_\gamma = (A - \pi R^2 N)\,\gamma_{o/w} + 4\pi R^2 N\,\gamma_{c/w} + 2\pi R N\,\gamma_l \qquad (4.10)$$

This assumption also entails some more simplifications, which will be addressed later.

2.2.2. *Electrostatic repulsion.* The screening of the charge on the particle surface differs considerably in the aqueous and the organic phases. The electric field extends further into the organic phase, since the dielectric constant of organic solvents is usually much lower (2-10 as compared to 78 for water) and a double layer is not present in the organic phase. Therefore, most likely residual charge at the particle/organic interface[**3**] determines the Coulomb repulsion in the layer. Some of the surface charge, due to charged species adsorbed at the particle interface, may be transferred to the water phase. Some of the charge could also recombine with its counter-charge. However, some charge is still present at the particle/organic interface. The charge at the aqueous phase will therefore be ignored. We expect that electrostatic interactions are to a good approximation described by Coulomb's law

$$V_{Coulomb} = \frac{q^2}{4\pi\varepsilon\varepsilon_0 x} \approx \frac{4\pi R^4 \alpha^2 \sigma_{ex}^2}{\varepsilon\varepsilon_0 x} \tag{4.11}$$

In this equation, x is the distance between point charges; since the charge is located at the surface, x will be taken as the surface-to-surface distance between the particles, q is the charge at the particle/organic interface, the fraction α indicates the extent to which the charge at the particle/organic interface is reduced with respect to the charge σ_{ex} before adsorption at the water/organic interface and ε and ε_0 are the relative dielectric constant and the vacuum permittivity, respectively.

The electrostatic free energy of the system in principle follows from a Boltzmann weighted sum over the electrostatic energies of all particle configurations. However, due to the long-range nature of the electrostatic interactions, it is prohibitively difficult to calculate the total electrostatic energy: it is not pairwise additive. We will therefore make some simplifications to obtain an analytical expression for the electrostatic free energy. This allows one to consider qualitatively the influence of electrostatic interactions on the adsorption density.

We assume that the particles form a rigid two-dimensional crystal at the organic/water interface, as depicted in figure 2. We also assume that interactions are pairwise additive. In that case the electrostatic free energy may be written as $F_{el} \approx zNV_{Coulomb}(x)/2$ with z the number of nearest neighbours and x the surface-to-surface distance.

In the case of a two-dimensional crystal, the surface volume fraction $\phi_s = N\pi R^2/A$ can be calculated by dividing the area of the circles enclosed by the triangle in figure 2 ($\frac{1}{2}\pi R^2$) by the area of the triangle ($\frac{1}{2}(x + 2R)^2 \sin\beta$):

$$\phi_s = \frac{2}{3}\sqrt{3}\,\pi\,\frac{R^2}{(x+2R)^2} \tag{4.12}$$

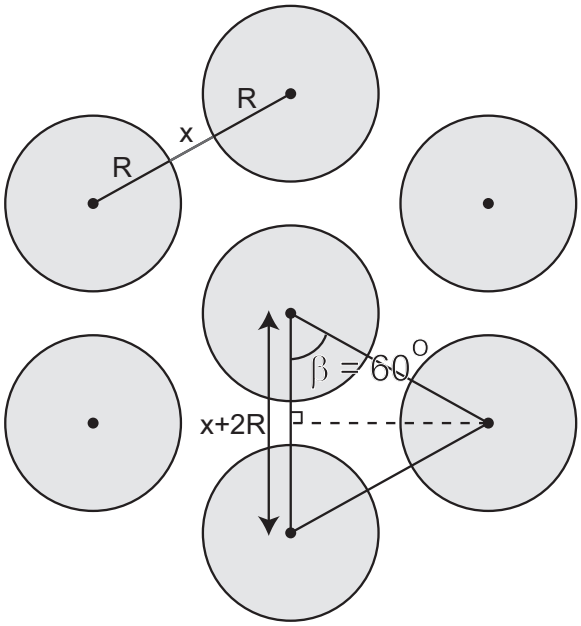

Figure 2. The particles (radius R) are assumed to be in a rigid 2-D lattice with a surface to surface distance of x. The centre of the particles are marked with a dot.

therefore $x = 2R\left(\sqrt{\phi_s^*/\phi_s} - 1\right)$, with $\phi_s^* = \phi_s(x=0) = \frac{1}{6}\sqrt{3}\,\pi$ the density of a closest packed layer of disks. Thus the electrostatic free energy reads

$$F_{el} = \frac{4\pi N z\alpha^2\sigma^2 R^3}{\varepsilon\varepsilon_0}(y^{-\frac{1}{2}} - 1)^{-1} \tag{4.13}$$

In the above equation we have defined $y = \phi_s/\phi_s^*$, which is the fraction of the available surface sites.

Again using $\mu = (\frac{\partial F}{\partial N})_{T,V}$ we can write the electrostatic contribution to the surface chemical potential as:

$$\mu_{el} = \frac{4\pi R^3 z\alpha^2\sigma^2}{\varepsilon\varepsilon_0(y^{-\frac{1}{2}} - 1)}\left(1 + \frac{1}{2(1-\sqrt{y})}\right) \tag{4.14}$$

2.2.3. *Van der Waals attraction.* While van der Waals interaction decays for atoms as the inverse distance to the sixth power, in the case of colloidal particles this decay is much slower[**7**], *i.e.*,

$$V_{vdW}(s) = \frac{-H}{6}\left(\frac{2}{s^2-4} + \frac{2}{s^2} + \ln\left(\frac{s^2-4}{s^2}\right)\right) \tag{4.15}$$

where H is the Hamaker constant and $s = (x+2R)/R = 2\,y^{-\frac{1}{2}}$.

The above result is correct for particles that are relatively close ($x \ll R$); at large interparticle distances V_{vdW} should be proportional to x^{-6}, whereas equation 4.15 predicts an x^{-2} dependence. Now using the same simplifications as in deriving the electrostatic free energy we get

$$F_{vdW}(s) \approx \frac{-zNH}{12}\left(\frac{y}{2(1-y)} + \frac{1}{2}y + \ln(1-y)\right) \tag{4.16}$$

The contribution of van der Waals interactions to the chemical potential of a particle at the water/heptane interface is obtained by differentiation, see equation 4.18.

2.2.4. *Translational entropy.* The translational entropy of dense systems is difficult to estimate, see, *e.g.*, Hoover *et al.* [**8**]. We will neglect the density dependence of the entropy of the two-dimensional system. However, in order to be consistent with the bulk contribution, we do take into account the two dimensional equivalence of the "ideal colloidal solution" term (the first term in equation 4.8), *i.e.*,

$$\mu_{tr}/kT = \ln\left(\frac{a_s}{a_p}\right) \tag{4.17}$$

In this equation, $a_s \approx v_w^{2/3}$ and $a_p \approx v_p^{2/3}$ are the molecular areas of a solvent molecule and a colloidal particle, respectively.

2.2.5. *Interfacial chemical potential.* When all the interfacial contributions are added, the chemical potential of a particle adsorbed at the water/heptane interface becomes

$$\mu_{int}/kT = \frac{\pi R^2}{kT}\left(\frac{2\gamma_l}{R} - \gamma_{o/w} + 4\gamma_{c/w}\right) + \frac{4\pi R^3 z\alpha^2\sigma^2}{\varepsilon\varepsilon_0 kT(y^{-\frac{1}{2}}-1)}\left(1 + \frac{1}{2(1-\sqrt{y})}\right) - \frac{zH}{12kT}\left[\frac{y^2}{2(y-1)^2} + y + \ln(1-y)\right] + \ln\left(\frac{a_s}{a_p}\right) \tag{4.18}$$

2.3. Combination. Setting $\mu_{bulk} = \mu_{int}$ leads to the interfacial density as a function of bulk density, charge density, Hamaker constant, particle size and interfacial tensions. By combining equations 4.8 and 4.18 we see that the contributions containing $\gamma_{c/w}$ cancel. Thus, the equilibrium surface fraction ϕ_s follows by numerically solving

$$\frac{\pi R^2}{kT}\left(\frac{2\gamma_l}{R} - \gamma_{o/w}\right) + \frac{4\pi R^3 z\alpha^2\sigma^2}{\varepsilon\varepsilon_0 kT(y^{-\frac{1}{2}}-1)}\left(1 + \frac{1}{2(1-\sqrt{y})}\right) - \frac{zH}{12kT}\left[\frac{y^2}{2(y-1)^2} + y + \ln(1-y)\right] = \ln\left(\frac{l_w}{l_p}\right) + \ln(\phi) + 2\frac{B_2}{v_p}\phi \tag{4.19}$$

In this equation we have defined $l_w \approx v_w^{1/3}$ and $l_p \approx v_p^{1/3}$. The first two terms on the right hand side of equation 4.19 contain the entropy of a particle in the bulk (3 dimensions) relative to that at the water/organic

interface (2 dimensions). In fact, ϕ and ϕ_s are equilibrium fractions and are related to the initial volume fraction (*i.e.* before adsorption takes place) in the water phase, ϕ_{init}, by matter conservation:

$$\phi_{init} = \phi + \frac{4AR}{3V}\phi_s \tag{4.20}$$

with V the volume of the aqueous phase, as before. In our case AR/V is always very small compared to ϕ_{init} so that in our calculations we set $\phi_{init} \approx \phi$.

3. Numerical Calculations and Observations

3.1. Interpretation of μ_{bulk} and μ_{surf}. Figure 3 curve A shows the bulk chemical potential as a function of the surface coverage ϕ_s. Since we have shown that $\phi_{init} \approx \phi$ (see equation 4.20), μ_{bulk} is constant with respect to the surface coverage. Its value is negative or positive, depending mainly on the value of $\gamma_{c/w}$. Curves B through E show four different solutions for the interfacial chemical potential μ_{int}.

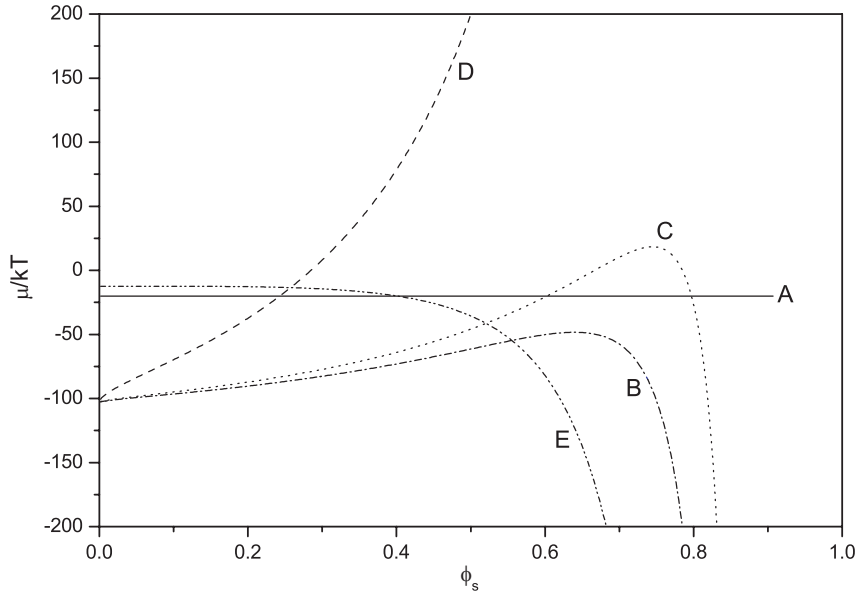

Figure 3. Solutions for the chemical potential of the bulk (see equation 4.8 and curve A) and the surface (see equation 4.18 and curves B through E). Values were $R = 8\ nm$ (A through D) and 2 nm (E), $\sigma = 0.0045\ C\,m^{-2}$ (B and E), $0.005\ C\,m^{-2}$ (C) and $0.01\ C\,m^{-2}$ (D), $\alpha = 0.027$, $\phi = 2\,10^{-5}$, $z = 6$, $B_2 = 0\ m^3$, $\varepsilon_{organic} = 2$, $T = 298\ K$, $\gamma_{o/w} = 2\ mN/m$, $\gamma_{c/w} = 0.01\ mN/m$ and $\gamma_l = 10^{-12}\ N$. Curve E was shifted down to match $\mu_{bulk}(R = 8\ nm)$ with curve A.

Curve B shows the interfacial chemical potential at a low residual surface charge density $\alpha\sigma$. At low surface coverage (y close to 0), μ_{int} is completely determined by the first (surface tension) term in equation 4.18. The sign of this term is determined by $\gamma_l/R - \gamma_{o/w}$. The water/organic surface tension can be easily measured with a Wilhelmy plate and is typically $1-50\ mN/m$, depending on the concentration of surface active species in the colloidal solution. In contrast, the line tension is difficult to determine experimentally and measured values range from 10^{-5} to $10^{-12}\ N$ (see Drelich *et al.* [**9**] and references therein). Model calculations suggest line tensions in the order of 10^{-10} to $10^{-12}\ N$ [**10**–**12**]. If the latter is correct, the "surface tension term" is negative for large R and positive for small R. When negative, the removal of surface tension by adsorption of colloidal particles at the interface forms a general driving force which is independent of the surface coverage. When ϕ_s is increased, μ_{int} increases. This is due to the "Coulomb repulsion" term, the second term in equation 4.18. Next, a maximum is reached followed by an exponential decrease of μ_{int}. In this last region, the van der Waals term (proportional to y), the second term in equation 4.18, dominates over the Coulomb repulsion (proportional to $\sqrt{y}$). For the case of curve B the equilibrium condition $\mu_{int} = \mu_{bulk}$ is never reached. Since $\mu_{int} < \mu_{bulk}$ the colloidal particles are likely to assemble spontaneously at the interface until the interface is saturated with particles.

When the Coulomb repulsion is increased, *e.g.* by increasing the surface charge σ, we obtain curve C of figure 3. Here the maximum of μ_{int} is larger than μ_{bulk} giving rise to two intersection points where $\mu_{bulk} = \mu_{int}$. Therefore, in principle, two equilibrium surface densities coexist. The position of the first equilibrium point (at low ϕ_s) depends mainly on the magnitude of the Coulomb repulsion, whereas the second depends on the interplay between Coulomb and van der Waals forces. The second "equilibrium" point is therefore a difference of two large quantities, allowing the inaccuracies of the model to become important. The asymptotic nature of μ_{int} close to $\phi_s = \phi_s^*$ does not have physical significance and is due to the assumptions made in the model.

In curve D of figure 3 the Coulomb repulsion is increased even further. The second term in equation 4.18 now completely overrules the van der Waals attraction. Contrary to curve C, μ_{int} goes to positive infinity at $\phi_s = \phi_s^*$. The second equilibrium point is therefore not present. Oddly enough, there is no intermediate case between curves C and D; a small increase of $\alpha\sigma$ causes the asymptotic behaviour of μ_{int} to change from minus infinity to plus infinity, which further underlines the fact that this asymptote has no physical meaning; At these small particle-particle separations other interactions might prevail, *e.g.* interactions between capping molecules, which are not included in the model. The other equilibrium surface

density (at low ϕ_s) remains present and is unaffected by the change from curve C to D.

The situation shown in curve E of figure 3 only occurs at very small R. Here the surface tension-term of equation 4.18 is too small to drive μ_{int} below μ_{bulk} at $y = 0$. Therefore, there is no initial driving force for layer formation. Coulomb repulsion is also very small due to the R^3 dependence. At higher ϕ_s an equilibrium is present due to van der Waals attraction, comparable to the second equilibrium point in curve C. Since van der Waals attaction is the main driving force at this point, it is likely that, besides 2-D aggregation at the interface, 3-D aggregation will also occur.

3.2. Calculating isotherms. In figure 4 the equilibrium surface fraction ϕ_s^{eq} is presented as a function of the surface charge at the particle/organic interface $\alpha\sigma$ for different sizes of gold nanocrystals.

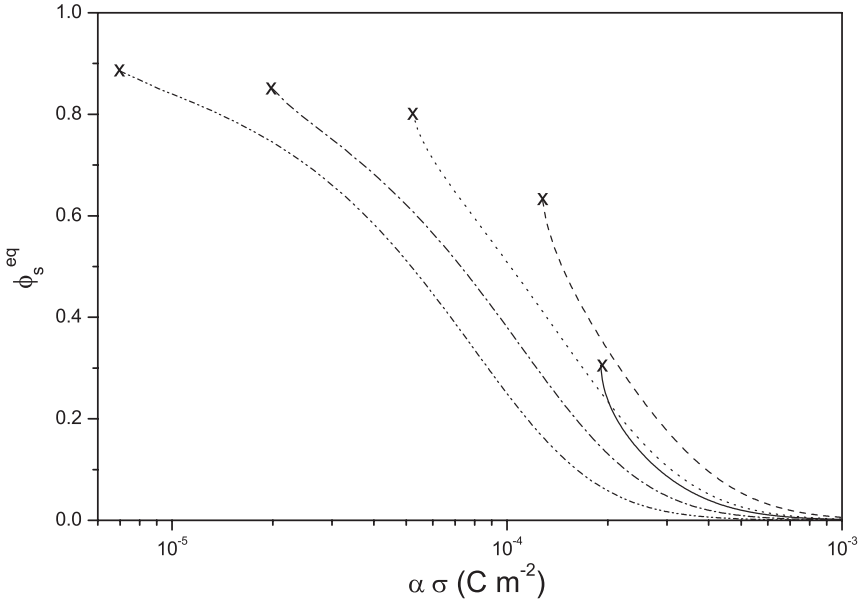

Figure 4. The equilibrium surface fraction ϕ_s^{eq} as a function of the surface charge in the organic phase $\alpha\sigma$ for particles with a radius of 4 (——), 8 (− − −), 16 (· · ·), 32 (− · − ·) and 64 nm (− · · −). Values used were: $\gamma_{o/w} = 2\ mN/m$, $\gamma_l = 10^{-12}\ N$, $\phi = 2.25\,10^{-5}$, $B_2 = 0\ m^3$, $z = 6$, $\varepsilon_{organic} = 2$. Points at which the transition between the situation of figure 3C to 3B occurs is marked with x.

Let us first look at the curve for particles with $R = 8\ nm$ (16 nm diameter). At relatively high surface charge, the interface is sparsely populated. As the charge is decreased below $\alpha\sigma = 4\,10^{-4}\ C/m^2$, ϕ_s^{eq} increases roughly

exponentially with decreasing charge until a transition point, marked by x in figure 4, is reached at $\alpha\sigma = 1.3\,10^{-4}\ C/m^2$. At this point the system changes from the situation of that in figure 3C to that in figure 3B. Since $\mu_{surf} = \mu_{int}$ has no solutions for situation 3B, equilibrium surface densities are not present beyond the transition point. All isotherms have this transition point, which occurs at higher surface fraction for larger particles. This is mainly due to the increase in Coulomb repulsion (proportional to R^3), which raises μ_{surf} relative to μ_{bulk}.

In order to obtain the same surface coverage, the surface charge density of smaller particles has to be lowered less than that of larger particles. This is also due to the fact that the Coulomb repulsion ($\sim R^3$) is stronger for larger particles. However, with 4 nm particles the surface charge needs to be reduced *more* than with 8 nm particles to reach the same surface coverage. This is due to the line tension ($\sim R$) which raises μ_{surf} with respect to μ_{bulk} and, therefore, counteracts particle adsorption at the interface. In these calculations $\gamma_l = 10^{-12}\ N$ was used; if the line tension is increased, *e.g.* to $10^{-10}\ N$, the isotherm shifts to even smaller $\alpha\sigma$.

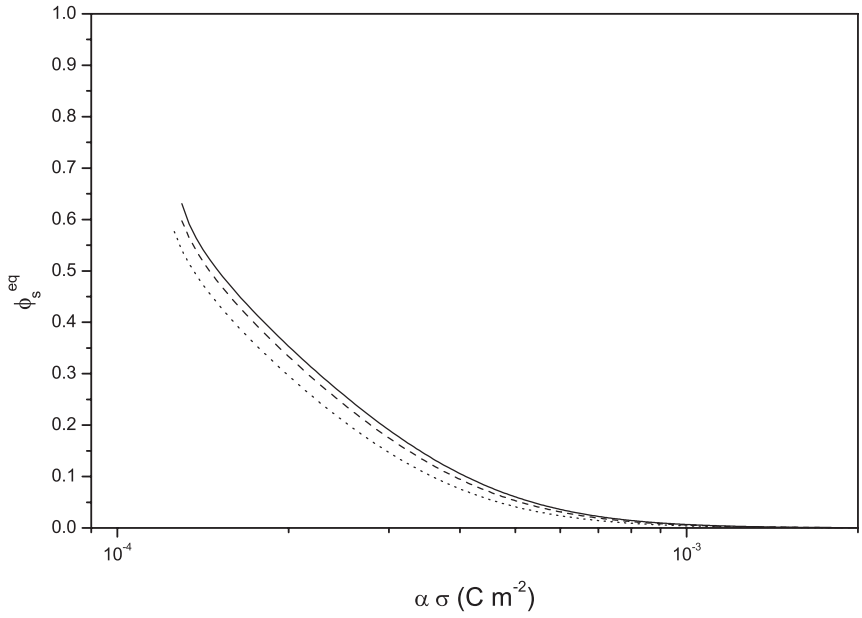

Figure 5. The equilibrium surface fraction ϕ_s^{eq} as a function of the surface charge in the organic phase $\alpha\sigma$ for a colloidal suspension with a bulk volume fraction of 10^{-2} (——), 10^{-5} (− − −) and 10^{-10} (· · ·). Other values were: $R = 8$, $\gamma_{o/w} = 2\ mN/m$, $\gamma_l = 10^{-12}\ N$, $B_2 = 0\ m^3$, $z = 6$ and $\varepsilon_{organic} = 2$.

With the Langmuir isotherm, the bulk concentration is the main driving force for layer formation. In the case of self-assembly at the water/heptane interface there are two driving forces: (the decrease of) interfacial surface energy and bulk concentration. Due to the logarithmic dependence of the bulk fraction ϕ on μ_{bulk} the bulk concentration term $\ln(\phi)$ is usually in the order of 5 to 50 kT, whereas the surface tension term is typically in the order of hundreds of kT. Therefore, the calculated isotherms depend only slightly on the bulk concentration. For 8 nm particles, a large change in the bulk fraction ϕ by 8 orders of magnitude only shifts the ϕ_s^{eq} by a few percent, as can be seen in figure 5.

Peculiarly, the non-ideal correction term for the bulk concentration $2B_2\rho$, see equation 4.19, is not dampened by a logarithm. Due to long-range electrostatic repulsion of particles in the bulk, B_2 is most likely to be positive. Since the concentration of colloidal suspensions is usually quite low and since the non-ideal term also has to compete with the surface tension term, just like the ideal term, the influence of the non-ideal term on the calculated isotherms is probably negligible.

The interfacial tension has a stronger influence on the isotherm, as can be seen in figure 6. When the interfacial tension is larger, a higher surface coverage is reached for the same surface charge. The transition point also occurs at higher ϕ_s for larger $\gamma_{o/w}$. The shape of the isotherm changes considerably when the surface tension is increased.

Temperature dependence in this model was not investigated since this would require knowledge of the dependence of many of the constants, *e.g.* $\varepsilon_{organic}$ and $\gamma_{o/w}$, on temperature.

4. Comparison with experimental results

We have described the formation of a dense layer of gold nanocrystals in chapter 3. We have shown that the colloidal particles are amphiphilic, *i.e.* they are half in the water, and half in the organic phase. Our experimental results show that a decrease of the surface charge by a factor of two leads to the formation of a dense ($\phi_s \approx 65\%$) layer of gold nanocrystals.

In figure 4, the data obtained from the system in chapter 3 were used to calculate isotherms. For 16 nm particles ($R = 8\ nm$), a decrease of the effective surface charge by a factor of two, *e.g.* from $\alpha\sigma = 3\ 10^{-4}$ to $1.5\ 10^{-4}\ C/m^2$, increases the surface density from 20 to 60 %. For 16 nm particles (32 nm diameter) the increase is from 10 to 40%. In contrast, the calculated isotherm for the smallest particles ($R = 4\ nm$) does not predict a high surface coverage, whereas experimentally the formation of a dense layer was observed.

Since the glass at the side of the flask is also polar (and most likely covered with water), the considerations that applied to the water/heptane interface also applies to the glass/heptane interface. Thus, our calculated

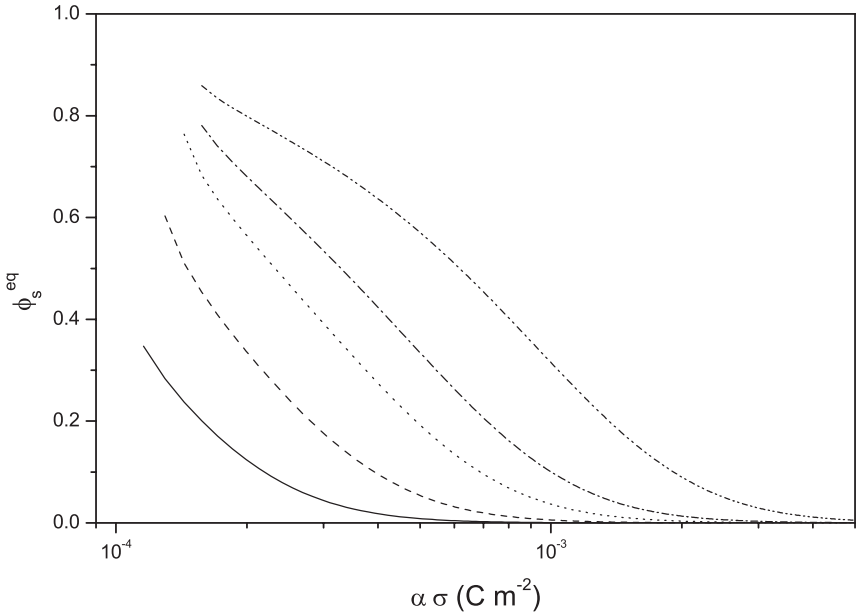

FIGURE 6. The equilibrium surface fraction ϕ_s^{eq} as a function of the surface charge in the organic phase $\alpha\sigma$ for water/organic interfacial tensions of 1 (——), 2 (− − −), 5 (· · ·), 10 (− · − ·) and 35 mN/m (− · · −). Other values were: $R = 8\ nm$, $\phi = 2 \cdot 10^{-5}$, $\gamma_l = 10^{-12}\ N$, $B_2 = 0\ m^3$, $z = 6$ and $\varepsilon_{organic} = 2$.

isotherms also provide an explanation for the fact that the layers extend vertically up the wall of the glass flask. The layer will not collapse when the driving force for layer formation is larger than the potential energy of the layer on the glass. Since the "surface tension" driving force is in the order of 100 kT, movement of the layer up the wall can be understood.

Another feature can, however, not be understood by this model: the existence of voids in the layer with an area equivalent to 10 to 100 particles. These voids might have several causes. Firstly, large clusters of slightly charged colloidal particles can be stabilised by a cumulative Coulomb repulsion[**13**]. As particles are added to the aggregate, this cumulative repulsion increases more than attraction until a maximum aggregate size is reached and no further aggregation occurs. Secondly, the system contained a second equilibrium point as depicted in curve C of figure 3. Since there are two equilibrium surface densities, the layer may have a dense and a diluted phase. The diluted phase is then interpreted as "holes". Since the observed density is an average of both phases, this could explain why the observed density is higher than the calculated density. Thirdly, the high polydispersity of the colloidal particles could disrupt ordering in the layer. According

to the model, the separation between particles in the layer is larger for larger particles, see *e.g.* figure 4, provided the effective surface charge density is constant. A monolayer consisting of differently sized particles would exhibit density fluctuations which might cause the creation of voids. However, the polydispersity is small ($\pm$ 10%) and the density fluctuations are expected to be small. Therefore, polydispersity is unlikely to explain fully the existence of these voids. Fourthly, there could be a chemical interaction between the capping molecules of the particle. For instance, with citrate-stabilised gold particles a dimer may be formed by hydrogen bonds between two protonated acid groups of the citrate. However, the distance between two particles seems to be too large for two citrate molecules. Finally, these layers are formed within seconds. It can be that after the initial disordered layer is formed and insufficient driving force is left to reach the better ordered equilibrium state (without voids).

There are two problems inherent in this model. Firstly, the remaining surface charge at the particle/organic interface is not known. Secondly, some assumptions had to be made regarding the Coulomb interaction between the particles adsorbed at the water/organic interface. These problems preclude a more quantitative consideration of the formation of these layers. However, although this model is rather crude, it gives considerable insight into the self-assembly of charged colloidal particles at the organic/aqueous interface. It is clear that the adsorption of particles at the water/organic interface is initiated primarily by a reduction of the particle surface charge in combination with a decrease of surface energy when the particle attaches to the interface.

References.

[1] B. P. Binks and S. O. Lumsdon. *Langmuir*, **17**-15 (2001) 4540–4547.

[2] D. F. Williams and J. C. Berg. *Journal of Colloid and Interface Science*, **152**-1 (1992) 218–229.

[3] R. Aveyard, J. H. Clint, D. Nees, and V. N. Paunov. *Langmuir*, **16**-4 (2000) 1969–1979.

[4] R. Aveyard, J. H. Clint, D. Nees, and N. Quirke. *Langmuir*, **16**-23 (2000) 8820–8828.

[5] V. N. Paunov, B. P. Binks, and N. P. Ashby. *Langmuir*, **18**-18 (2002) 6946–6955.

[6] H. Reiss, W.K. Kegel, and J. Groenewold. *Ber. Bunsenges. Phys. Chem.*, **100** (1996) 279.

[7] E.J.W. Verwey and J.Th.G. Overbeek. *Theory of stability of lyophobic colloids*. Dover, NY, 1999.

[8] W.G. Hoover and F.H. Ree. *J.Chem.Phys.*, **49** (1968) 3609–3617.

[9] J. Drelich. *Colloids and Surfaces a-Physicochemical and Engineering Aspects*, **116**-1-2 (1996) 43–54.

[10] F. Bresme and N. Quirke. *Physical Chemistry Chemical Physics*, **1**-9 (1999) 2149.

[11] T. Getta and S. Dietrich. *Physical Review E*, **57**-1 (1998) 655–671.

[12] F. Bresme and N. Quirke. *Physical Review Letters*, **80**-17 (1998) 3791–3794.

[13] J. Groenewold and W. K. Kegel. *Journal of Physical Chemistry B*, **105**-47 (2001) 11702–11709.

APPENDIX A

Dynamic Light Scattering

A light beam l can be characterised by a wavevector $\overrightarrow{k_l}$ which is pointing in the propagation direction of the beam. The length of the vector $\overrightarrow{k_l}$ is proportional to its wavelength:

$$k_l = |\overrightarrow{k_l}| = 2\pi/\lambda \tag{A.1}$$

where λ is the wavelength of the light.

Consider an experiment in which an incoming light beam with wavevector $\overrightarrow{k_{in}}$ is scattered off a sample and a scattered beam with wavevector $\overrightarrow{k_{out}}$ is collected by the detector. The angle between the incoming and scattered beam is Θ. The scattering vector $\overrightarrow{k}$ is defined as:

$$\overrightarrow{k} = \overrightarrow{k_{in}} - \overrightarrow{k_{out}} \tag{A.2}$$

If it is assumed that the scattering is elastic then the wavelength does not change during the scattering event, and the length of the scattering vector can be written as:

$$k = |\overrightarrow{k}| = \frac{4\pi n}{\lambda} \sin(\frac{1}{2}\Theta) \tag{A.3}$$

where n is the refractive index of the solvent.

For point scatterers with equal scattering strength, the instantaneous configuration of scatterers, termed the microscopic density $\rho(\overrightarrow{r}, t)$, at a given time t is given by:

$$\rho(\overrightarrow{r}, t) = \sum_{j=1}^{N} \delta(\overrightarrow{r} - \overrightarrow{r}_j(t)) \tag{A.4}$$

In equation A.4 the term $\overrightarrow{r} - \overrightarrow{r}_j(t)$ denotes the position of particle j ($\overrightarrow{r}_j(t)$). The Dirac delta function δ is used to show that these are really point scatterers. Next, these relative positions are summed over all N particles.

Using the Fourier transformed macroscopic density, denoted $\rho(\overrightarrow{k}, t)$, the intensity of the scattered light $i(\overrightarrow{k}, t)$ can be written as:

$$i(\overrightarrow{k}, t) = |\rho(\overrightarrow{k}, t)|^2 \tag{A.5}$$

For a fixed angle Θ and wavelength λ equations A.4 and A.5 show that the intensity of the scattered beam depends only on the positions of the particles at time t. However this configuration changes over time due to Brownian motion of the particles. Therefore, the intensity obtained will fluctuate over time. Conversely, by measuring the fluctuating intensity information about the diffusion of particles can be obtained. To investigate the time scale on which these fluctuations occur, the intensity auto correlation function $g_I(\overrightarrow{k}, t)$ is used.

$$g_I(\overrightarrow{k}, t) = \langle i(\overrightarrow{k}, t_0)\, i(\overrightarrow{k}, t + t_0)\rangle \tag{A.6}$$

The angular brackets denote an ensemble average. For each value of the sampling time t, the product of $i(t_0)$ and $i(t_0 + t)$ is evaluated for all possible values of t_0, *i.e.* from $t_0 = 0$ to $t_0 = t_{max} - t$, and the resulting values are averaged to obtain $g_I(\overrightarrow{k}, t)$. Because the two values are multiplied, the highest contribution is given when both factors are large. At short sampling time t the fluctuations cannot occur within this time frame and $i(t_0) \approx i(t + t_0)$. Hence $g_I \approx \langle i(t_0)^2\rangle$ at short t. When t is large $i(t_0) \neq i(t + t_0)$ and $g_I \approx \langle i(t_0)\rangle^2$. It is clear that $\langle i(t_0)^2\rangle \geq \langle i(t_0)\rangle^2$ so g_I is a decaying function. This decay takes place on the timescale of the intensity fluctuations caused by the Brownian motion of the particles.

For convenience the auto correlation function is normalized to the intensity:

$$\widehat{g}_I(\overrightarrow{k}, t) = g_I(\overrightarrow{k}, t)/I^2 \tag{A.7}$$

where I is the average scattered intensity, *i.e.* $I = \langle i(\overrightarrow{k}, t)\rangle$

Using Fick's laws, the relation between the diffusion constant D and the auto correlation function can be found[**1**]:

$$\widehat{g}_I(\overrightarrow{k}, t) \sim e^{-2Dk^2 t} + 1 \tag{A.8}$$

References.

[1] J. K. G. Dhont. *An Introduction to Dynamics of Colloids*. Studies in Interface Science. Elsevier (Amsterdam), 1996.

Summary

It has long been a wish in nanoscience to manipulate matter at the molecular level. However, current lithography cannot easily produce ordered structures smaller than 100 nm. The gap between the length scale accessible by lithography and the molecular scale might be bridged by self-assembly techniques. Interactions at the molecular level determine the assembly of nanometre-scaled building blocks (*e.g.* molecules, colloidal particles or nanocrystals) into well-defined, periodic structures of varying length scale (10-1000 nm). This thesis reports on the self-assembly of charge-stabilised gold nanocrystals (diameter 4-40 nm) on chemically modified gold substrates and at the aqueous/heptane interface.

In chapter 2 the structure and electrochemical properties of gold (substrate)/oligo(cyclohexylidene) SAM/gold nanocrystal junctions were studied. Such a junction was built up layer by layer. At each stage, the structure was investigated by scanning-probe methods and the electrochemical properties were studied.

The plot of interfacial capacitance (measured at 1000 Hz) vs. potential for a bare gold (111) electrode showed a maximum near the potential of zero charge E_{pzc}. The results of the electrochemical measurements on bare gold (111) can be explained using the jellium model. After immersion of the gold (111) electrode in an ethanolic solution of the two-ringed oxime cyclohexylidene, the interfacial capacitance was moderately reduced compared to that of the bare gold (111) electrode and the maximum in the plot of capacitance vs. potential was no longer present. However, the same effect was found when the gold (111) electrode was immersed in a pure ethanol solution. It was concluded that ethanol and the oxime cyclohexylidene are only physisorbed on the Au(111) surface, and a robust self-assembled monolayer (SAM) is not formed. In contrast, when the gold (111) electrode was pretreated with a monosulfide cyclohexylidene, the interfacial capacitance measured in aqueous solution was reduced considerably. It can be concluded that the monosulfide forms a robust SAM on the Au(111) surface. These observations were confirmed by cyclic voltammetry measurements on the electrodes in the presence of $Fe(CN)_6^{3-/4-}$.

Next, we investigated whether difunctionalized oligo(cyclohexylidene)s could give robust SAMs on gold (111). The disulfide cyclohexylidene, just like the monosufide cyclohexylidene, formed a well-ordered, robust SAM. Strikingly, the oxime-sulfide cyclohexylidene did not produce a well-ordered SAM. The nature of the oxime functionality seems to prevent the formation of the well-ordered SAM. The oxime functionality can form hydrogen bonds, whereas an oxime-sulfide molecule with a methylated oxime group cannot form hydrogen bonds. The methylated oxime-sulfide self-assembled onto gold (111) to produce a well-ordered SAM. In this way we have shown that slight changes in the chemical nature of the molecules can have a strong effect on molecular self-assembly. The electrochemical response of the gold (111)/cyclohexylidene interface is determined by the dielectric properties of the cyclohexylidene SAM, although a considerable influence of the oligo(cyclohexylidene) end-functionality was observed. The latter was most likely due to the wetting properties of the cyclohexylidene SAM.

Self-assembly of colloidal gold particles did not occur on a bare gold (111) surface; large aggregates were formed at the grain boundaries. On the gold (111)/disulfide cyclohexylidene SAM system, however, individual particles attached to the surface were observed. Aggregates did not occur. The maximum coverage of the layer was close to 10 %. Possibly, a higher surface coverage is prevented by Coulomb repulsion between the charged particles. The particles were not moved around by the tapping mode AFM tip, showing that they are securely attached to the surface. In contrast, when the gold nanocrystals were self-assembled on a monosulfide cyclohexylidene SAM (thus with a CH_2 end group), the individual particles could be displaced by the AFM tip, which indicates that they are only physisorbed on the SAM layer. Curiously, the disordered Au(111)/oxime-sulfide interface was able to firmly attach gold nanocrystals. This suggests that some oxime-sulfide dimers are present at the surface, allowing the surface to be partially sulfide-terminated.

After addition of colloidal gold nanocrystals, the electrochemical properties of the gold (111)/cyclohexylidene SAM/gold nanocrystal structure were similar to those of the naked gold electrode. For instance, the maximum in the capacitance vs. potential curve was again present. This shows that the gold nanocrystals can be addressed electrically through the oligo(cyclohexylidene) layer, which hence acts as a molecular electronic bridge between the gold substrate and the nanocrystal. Using the potential step method the attachment of the colloidal particles could be measured *in situ*. It was found that the attachment rate is equal to the product of the available space and a Frumkin-type exponential term($d\theta/dt \propto (1-\theta)e^{-f\theta}$, where θ is the relative particle coverage).

In chapter 3 we report on the self-assembly of colloidal gold nanocrystals at the water/heptane interface. When the aqueous colloidal gold solution (16 nm diameter particles) is brought into contact with heptane, no significant changes are observed. However, after addition of several millilitres of ethanol a blue interfacial layer is formed at the water/heptane interface. When the water/heptane interface is full, the layer can extend up the glass for several centimetres without breaking. The interfacial gold nanocrystal layer was studied with both *in-situ* and *ex-situ* methods.

First, pictures made by optical microscopy showed that at low ethanol concentrations islands of colloidal gold nanocrystals are formed at the water/heptane interface. When the ethanol concentration is increased, these islands grow until an optically dense film is formed. Second, using a Langmuir trough, the layer was compressed laterally and the surface pressure was measured. The isotherm of surface pressure vs. area indicates the point at which the individual islands transform into a continuous layer. Upon further compression, the layer collapsed. Thus reversible compression isotherms with a variable interparticle distance as observed with uncharged, alkanethiol-capped gold nanocrystals could not be observed here. Finally, the mobility of the gold nanocrystals in the bulk solution and interfacial layer was measured with the dynamic light-scattering method. The mobility of the colloidal gold nanocrystals in (bulk) solution was that expected for freely diffusing particles. The mobility of the colloidal particles in the interfacial layer was several orders of magnitude lower than in the bulk solution.

TEM images of the layer collected by the Langmuir method show a dense interfacial layer which consists of unordered, individual nanocrystals separated by large voids. The distance between two neighbouring particles was typically smaller than the Debye screening length L_D. The TEM images showed that the interfacial layer contained voids, even when the pressure was high enough to collapse parts of that layer. These results were confirmed with tapping mode AFM. AFM was also performed on layers of larger (diameter 40 nm) and smaller (diameter 8 nm) gold particles. The same type of unordered, dense monolayer with voids was found.

To investigate the wetting properties of the colloidal gold particles at the water/heptane interface, a drop of water+ethanol was placed onto a gold (111) sample, and the sample with droplet was immersed in heptane. The three-phase contact angle between the water, heptane and gold is clearly negative indicating that the bare gold (111) surface is hydrophobic. It is known from the literature that the gold nanocrystals are charge-stabilised due to citrate ions adsorbed at the particle surface. The gold substrates were therefore immersed in a trisodium citrate solution at $60°C$ for 30 min, rinsed and subjected to the same experiment. The three-phase angle

changed to approximately 90°. The citrate-capped nanocrystals are therefore amphiphilic and are, when self-assembled at the interface, positioned approximately halfway in the water/heptane interface.

The factors influencing the formation of a dense layer of gold nanocrystals at the water/heptane interface were investigated. Since repulsion between the double-layers of the nanocrystals hinders layer formation, it is logical to assume that a change of the double-layer structure can trigger layer formation. The double-layer structure can be changed in two ways: by a decrease of the particle surface charge or by a decrease of the double-layer width L_D.

The effect of ethanol on the double-layer structure around the gold particles was studied by the *Doppler Effect Light Scattering Analyser* (DELSA). It was shown that the particle surface charge density was reduced after addition of ethanol. This result agrees with the results reported in chapter 2 which showed that the ethanol adsorbs on the gold surface. Thus, very probably the ethanol displaces the citrate. Unfortunately, the wetting properties are also changed by the addition of ethanol. In order to distinguish the effects of wetting and charge reduction, the pH of the colloidal gold solution was lowered. In this way the gold nanocrystal surface is discharged due to protonation of the citrate, while the wetting properties stay unchanged (the citrate remains on the surface). Addition of hydrochloric and sulfuric acid to the gold sol/heptane mixture resulted in the formation of an interfacial layer which closely resembled the layers formed after ethanol addition.

Reduction of the double-layer width by addition of salt ($NaClO_4$) also leads to a layer at the water/heptane interface. However, AFM showed that this layer consisted of aggregates. The height of these aggregates was typically 100 nm or more, whereas the particle diameter was 16 nm. Thus, with a decrease in the width of the double-layer, three-dimensional aggregation occurs simultaneously with the formation of an interfacial layer, leading to a 'clumpy layer'.

Finally, we have reduced the surface charge by adsorbing species other than ethanol. Several thiols and sulfides were added to the gold sol/heptane two-phase system. The interfacial layers that were formed consisted partly of gold nanocrystal monolayers and partly of clumps.

It has been shown that a dense interfacial monolayer of gold nanocrystals is formed at the water/heptane interface after a slight reduction of the particles surface charge. Since reduction of the surface charge can be achieved by a variety of chemical methods, layer formation by charge reduction should be applicable to a wide range of charge-stabilised particles.

In chapter 4 a model is described aimed at explaining the observations made in chapter 3. In this model it is assumed that the gold nanocrystals are completely monodisperse and spherical.

In this model the chemical potential of the bulk (aqueous) phase μ_{bulk} is composed of three terms:

- a term describing a solution of non-interacting colloidal particles (much like an ideal-gas);
- a correction term, containing the virial coefficient, which corrects for attraction and/or repulsion between the particles;
- and finally an interfacial energy term, containing the surface tension of the nanocrystal/water interface.

The chemical potential of colloidal particles at the interface μ_{surf} is composed of four terms:

- an interfacial energy term, accounting for the interfacial tension of all three interfaces. A line tension term was also included here;
- an electrostatic repulsion term. It was assumed that, after assembly at the interface, a fraction α of the original surface charge remained at the organic/nanocrystal interface. Since this charge is not screened by the organic phase, it was assumed that the charge is responsible for electrostatic repulsion. The interaction was calculated using a 2-D hexagonal packing of nanocrystals.
- a term accounting for van der Waals attractions between the nanocrystals.
- and finally a translational entropy term.

Using the equilibrium condition, $\mu_{bulk} = \mu_{surf}$ an adsorption isotherm was derived which takes into account the particle size, the surface tension of the water/organic interface (and line tension), and the charge at the organic/nanocrystal interface. Due to the fact the gold nanocrystals are truly amphiphilic (*i.e.* are located half in the organic and half in the water phase), the surface tension contributions of the water/nanocrystal and nanocrystal/organic interface cancel.

The surface fraction was plotted vs. the residual charge at the nanocrystal/organic interface, $\alpha\sigma$. It was found that both the interfacial tension term(s) and the van der Waals attraction promoted surface attachment, whereas Coulomb repulsion counteracted surface attachment. Since the Coulomb repulsion term increases more strongly with increasing particle size than the van der Waals attraction and interfacial tension terms, larger particles are less prone to surface adsorption than small particles. In other words: large particles require a lower surface charge to reach the same surface coverage at the water/heptane interface than small particles. Despite somewhat crude approximations, the model was able to explain the results in a semi-quantitative way.

Samenvatting

Al langere tijd probeert men in de nanowetenschappen de materie te manipuleren op atomair niveau. Het belangrijkste doel van de nanowetenschap is het maken van geordende structuren van slechts enkele nanometers[a] groot. Zulke nanostructuren kunnen de actieve component vormen in een aantal nieuwe toepassingen zoals super-efficiënte lasers, harde schijven met een zeer grote opslagcapaciteit en de allerkleinste (en daarom allersnelste) computerchips. De huidige lithografische technieken kunnen geen geordende structuren creëren die kleiner zijn dan ongeveer 100 nanometer. Beneden de 100 nm kunnen geordende structuren worden gecreëerd door zelf-assemblage. Hierbij organiseren kleine hoeveelheden materie (zoals moleculen, colloïden en nanokristallen) zichzelf in goed gedefinieerde, geordende structuren met een grootte van 10 tot meer dan 1000 nanometer[b]. Zelf-organisatie is gebaseerd op interacties tussen moleculaire bouwstenen. In dit proefschrift wordt de zelf-assemblage van goudnanokristallen, van enkele nanometers groot, op chemisch gemodificeerde goudsubstraten en op het water/heptaan oppervlak beschreven.

In hoofdstuk 2 worden de elektrochemische eigenschappen van goud (111)/oligo(cyclohexylideen)/goudnanokristal systemen besproken. Deze structuren worden laag voor laag opgebouwd. Allereerst zelf-assembleren oligo(cyclohexylideen) moleculen, of kortweg 'cyclohexylidenen', zich op een goud (111) oppervlak. Deze moleculen vormen een laagje van één oligo-(cyclohexylideen) molecuul dik, ook wel een zelf-geassembleerde monolaag (self-assembled monolayer, SAM) genoemd. Hierna assembleren ladingsgestabiliseerde goudnanokristallen (diameter 16 nm) zichzelf op het goud

[a] Om een idee te krijgen hoe klein 1 nanometer is: In 1 nanometer passen ongeveer 4 goudatomen.

[b] Het 'uit zichzelf' vormen van geordende structuren is het best uit te leggen aan de hand van een voorbeeld: Neem een aantal moleculen en een vlak stukje substraat. De moleculen binden zeer sterk met het substraat. Omdat er niet genoeg plaats is voor alle moleculen op het substraat ordenen de moleculen zich in een mooi regelmatig patroon zodat er zoveel mogelijk moleculen op het substraat passen. Bij zowel het vormen als de ordening van de laag vindt geen (directe) beïnvloeding van de mens plaats; de moleculen 'doen het zelf'. Voor moleculen in dit voorbeeld zou ook colloïden of nanokristallen gelezen kunnen worden.

(111)/cyclohexylideen oppervlak. Bij elke fase van de assemblage werd het oppervlak elektrochemisch onderzocht. Ook werd de topologie van het oppervlak vastgelegd met behulp van atomaire kracht microscopie (Atomic Force Microscopy, AFM).

De grensvlakcapaciteit (gemeten bij 1000 Hz) van een onbedekte goud (111) elektrode vertoont een maximum bij de ladingsvrije potentiaal (the potential of zero charge, E_{pzc}). Dit maximum kan worden verklaard met behulp van een oppervlakdipool model, dat in het vakgebied als het "jellium model" bekend staat. Uit de literatuur is bekend dat de grensvlakcapaciteit van een goed geordende SAM zeer laag en vrijwel onafhankelijk van de potentiaal is. Na onderdompeling van de goud (111) elektrode in een oplossing van een oxime-cyclohexylideen in ethanol verminderde de capaciteit lichtelijk (t.o.v. onbedekt goud) en verdween het maximum uit de capaciteit-potentiaal grafiek. Dezelfde respons werd gevonden toen de goud (111) elektrode werd ondergedompeld in zuiver ethanol. Er werd geconcludeerd dat het ethanol en de oxime slechts fysisch geadsorbeerd zijn en de moleculen geen goed geordende moleculaire monolaag vormen op de goud (111) elektrode. Na behandeling van de goud (111) elektrode met een monosulfide cyclohexylideen daarentegen, werd de grensvlakcapaciteit van de electrode, gemeten in een waterige oplossing, zeer klein en vrijwel onafhankelijk van de potentiaal. De monosulfide cyclohexylideen vormt dus wel een goed geordende SAM op goud (111). De vorming van een goed geordende SAM is het gevolg van een sterke goud-zwavel binding en sterke van der Waals interacties tussen naburige cyclohexylideen-eenheden in de "stoel" conformatie[c]. De voorgaande resultaten werden bevestigd door cyclische voltammetrie in aanwezigheid van het redoxkoppel $Fe(CN)_6^{3-/4-}$.

Hierna werd de zelf-assemblage van oligo(cyclohexylidenen) voorzien van twee functionele eindgroepen onderzocht. De disulfide cyclohexylideen vormde, net als het monosulfide, een goed geordende SAM op de goud (111) elektrode. Verrassend was dat oxime-sulfide cyclohexylideen geen goed geordende SAM vormde, ondanks de aanwezigheid van de zwavelfunctionaliteit. De oxime functionaliteit lijkt de vorming van een goed geordende laag te voorkomen. Eén van de eigenschappen van de oxime functionaliteit is het vormen van waterstofbruggen. Daarom werd getracht een SAM te vormen met een gemethyleerd oxime-sulfide cyclohexylideen, welke niet de mogelijkheid heeft om waterstofbruggen te vormen. De gemethyleerde oxime-sulfide cyclohexylideen moleculen bleken zichzelf te assembleren tot een goed geordende SAM op goud (111). De elektrochemische respons van het goud

[c]Voor een gedetailleerde uitleg zie het proefschrift van Albert W. Marsman, *"Functionalized Oligo(cyclohexylidenes) : semi-rigid molecular rods forcrystal engineering, through-bond orbital interactions and self-assembly"*, Universiteit Utrecht, 1999, ISBN 90-393-2265-1.

(111)/cyclohexylideen grensvlak wordt hoofdzakelijk bepaald door de dielektrische eigenschappen van de cyclohexylideen SAM, alhoewel de eind-functionaliteit van de oligo(cyclohexylideen) een aanzienlijke invloed heeft. De eind-functionaliteit heeft waarschijnlijk een sterke invloed op de structuur van de eerste paar lagen watermoleculen.

Tenslotte assembleerden de goudnanokristallen zichzelf op de hierboven beschreven elektrodes door deze elektrodes simpelweg in een colloïdale oplossing van goudnanokristallen te dompelen. De structuren die zo ontstonden werden onderzocht met atomaire kracht microscopie in de niet-contact modus (tapping mode Atomic Force Microscopy, tm-AFM). Een tikkende naald tast het oppervlak af en daardoor kan de morfologie van het oppervlak bepaald worden. Zelf-assemblage van colloïdale gouddeeltjes op goud (111) zonder aanwezigheid van een cyclohexylideen SAM slaagde niet: Er verzamelden zich grote aggregaten ('klonten' van meerdere gouddeeltjes) op het goud (111) oppervlak. Op het goud (111)/disulfide cyclohexylideen oppervlak daarentegen, zetten zich alleen losse gouddeeltjes af; er was geen clustering of aggregatie te zien op het oppervlak. De maximale bezettingsgraad was ongeveer 10 %, zelfs als de elektrode gedurende zeer lange tijd in de colloïdale oplossing werd gehangen. Een grotere bedekking wordt hoogstwaarschijnlijk geblokkeerd door Coulomb-repulsies tussen de geladen nanokristallen. De deeltjes zaten stevig vast, want de tikkende AFM naald (tapping mode AFM tip) kon de deeltjes niet over het oppervlak bewegen. Dit is logisch want een goud (111)/disulfide cyclohexylideen SAM is zwavel getermineerd ('er zit zwavel aan de buitenkant'). Dit zwavel vormt een binding met de goudnanokristallen. Goudnanokristallen daarentegen, die afgezet werden op een monosulfide cyclohexylideen kunnen wel door de naald verplaatst worden. Omdat de zwavelfunctie aan de goudelektrode gebonden is, is de monosulfide cyclohexylideen SAM CH_2 getermineerd. De zwaveltermination van het oppervlak is dus belangrijk voor het stevig verankeren van de deeltjes. Verbazingwekkend was dat de goudnanokristallen die zichzelf assembleerden op een oxime-sulfide SAM wel stevig verankerd waren. Dit suggereert dat sommige oxime-sulfide cyclohexylidenen, die op het oppervlak verankerd zijn, dimeren vormen d.m.v. waterstofbruggen met vrije oxime-sulfide cyclohexylidenen. Hierdoor kan het oppervlak gedeeltelijk zwavel getermineerd zijn.

Na zelf-assemblage van goudnanokristallen op het goud (111)/cyclohexylideen oppervlak, werd de grensvlakcapaciteit gemeten door middel van potentiaal-stap metingen (potential step measurements). Er was (net als bij een onbedekte goud (111) elektrode) weer een maximum te zien in de capaciteit-potentiaal-grafiek. Dit betekent dat de elektrische respons van het nanokristal/electrolyt oppervlak te meten is door de SAM heen. De cyclohexylideen moleculen vormen dus een elektrische moleculaire brug tussen het goudsubstraat en de nanokristallen. De verankering van de nanokristallen

kon ook *in situ* worden gemeten. De additiesnelheid bleek evenredig te zijn met het aantal beschikbare plaatsen maal een Frumkin-achtige exponentiële term.

In hoofdstuk 3 wordt de zelf-assemblage van goudnanokristallen aan het water/heptaan oppervlak bestudeerd. Als de oplossing van colloïdale goudnanokristallen (16 nm diameter) in water in contact wordt gebracht met heptaan, wordt er geen (dichte) laag van goudnanokristallen gevormd aan het grensvlak. Echter, na toevoeging van enkele milliliters ethanol aan dit systeem ontstaat er een blauwe laag aan het water/heptaan grensvlak. Deze laag klimt tegen de glaswand op zodra er te weinig plaats is aan het water/heptaan oppervlak. De laag kan zelfs enkele centimeters tegen de glaswand opklimmen zonder te breken of in elkaar te storten. De zo ontstane film werd onderzocht met zowel *in-situ* als *ex-situ* methoden.

Allereerst werden er met een optische microscoop foto's gemaakt van de laag aan het water/heptaan oppervlak. Bij een lage ethanol concentratie ontstaan er drijvende eilanden van goudnanokristallen. Wanneer de concentratie van ethanol verhoogd wordt dan groeien deze eilanden uit tot één laag.

Vervolgens werd de laag samengeperst door middel van een Langmuir-trog, terwijl de laterale druk[d] gemeten werd. De grafiek van de oppervlakdruk tegen de oppervlakte, ook wel de compressie-isotherm genoemd, liet duidelijk het moment zien waarop de eilanden samenkwamen en er een continue laag werd gevormd. In deze laag blijven er trouwens gaten aanwezig, ook als de laterale druk verder verhoogd wordt. Als de laterale druk te ver werd opgevoerd, vouwde de laag zich op (klapte in elkaar). De laag gedraagt zich dus niet als een monolaag van ongeladen, met alkaanthiol bedekte goudnanokristallen. In de laatstgenoemde laag neemt de afstand tussen de deeltjes af als de laterale druk toeneemt. Bij afnemende druk neemt zo'n laag zijn oorspronkelijke vorm weer aan.

Tenslotte werd de mobiliteit van de goudnanokristallen bepaald met dynamische lichtverstrooiing (Dynamic Light Scattering). De mobiliteit van de deeltjes in de waterige fase had een waarde die overeen kwam met wat verwacht kon worden op basis van colloïdale diffusie. De mobiliteit van de nanokristallen in het water/heptaan grensvlak was enige ordes van grootte lager dan in de waterige fase. Het is dus waarschijnlijk dat de deeltjes in de laag niet vrijelijk door de laag heen kunnen bewegen.

Er werden TEM (Transmissie Electron Microscopie) foto's gemaakt van lagen die door middel van de Langmuir techniek waren overgebracht op een substraat. Deze foto's toonden een (sub-)monolaag van niet-versmolten (individuele) deeltjes in een chaotische, dichte stapeling onderbroken door grote gaten. Een nette ordening van de nanokristallen aan het oppervlak

[d] De druk langs het oppervlak.

werd niet verwacht omdat de variatie in deeltjesgrootte ($\geq 10\%$) daarvoor te groot was. De afstand tussen twee aangrenzende deeltjes was over het algemeen kleiner dan de dikte van de elektrische dubbellaag (gegeven door de Debye afschermingslengte). De TEM foto van een laag na laterale compressie toonde gebieden waar de laag was opgevouwen tezamen met gebieden met een monolaag, waarin nog steeds gaten waren te zien. Deze bevindingen werden bevestigd door tikkende naald AFM metingen. Lagen van kleinere (diameter 8 nm) en grotere (diameter 40 nm) nanokristallen werden ook onderzocht met AFM. Dezelfde ongeordende, dichte lagen met gaten werden gevonden.

Om te onderzoeken hoe een deeltje zich gedraagt aan het water/heptaan oppervlak werd een serie bevloeiingsexperimenten uitgevoerd. Een druppel water+ethanol werd voorzichtig op een goud (111) substraat geplaatst, waarbij zowel de druppel als het goudsubstraat waren ondergedompeld in heptaan. De drie-fasen contacthoek (three-phase contact angle) was duidelijk negatief (het water vormde een bolletje) wat aantoont dat het goud (111) oppervlak hydrofoob is. Omdat de goudnanokristallen in oplossing bedekt zijn met citraat(de geconjugeerde base van citroenzuur), werd het goudplakje ondergedompeld in een trinatrium citraat oplossing gedurende 30 minuten bij $60°C$, voor gebruik. De drie-fasen hoek veranderde naar ongeveer 90 graden (de druppel had de vorm van een halve bol). De met citraat bedekte goudnanokristallen zijn dus amphifiel: ze willen even graag in de waterige als de heptaanfase zitten en bevinden zich daarom ook half in de water- en half in de heptaanfase.

Nu is het tijd om de factoren te identificeren die de vorming van een dichte laag van geladen goudnanokristallen stimuleren. Omdat afstoting van de elektrische dubbellaag rond de goudcolloïden de vorming van een dichte laag tegengaat is het logisch te veronderstellen dat een verzwakking van de dubbellaag de vorming van een dichte laag tot gevolg kan hebben. De dubbellaag kan op twee manieren worden verzwakt: verkleining van de oppervlaklading en vermindering van de dikte van de dubbellaag.

Gebruik makend van de DELSA (Doppler Effect Lichtverstrooiings Analysator) werd het effect van het ethanol vastgesteld. Na toevoeging van 4 ml ethanol op 10 ml colloïdale goudoplossing verminderde de oppervlakladingsdichtheid met ongeveer de helft. In hoofdstuk 2 werd gevonden dat ethanol aan het goudoppervlak adsorbeert. Het kan dus zijn dat op deze manier het geladen citraat van het goudnanokristal oppervlak wordt vervangen door ethanol. Jammer genoeg zullen de bevloeiingseigenschappen van de nanokristallen veranderen door de adsorptie van het ethanol. Om het effect van ladingsvermindering te onderscheiden van bevloeiingseffecten werd de pH van de colloïdale goudnanokristal oplossing verlaagd. Door het toevoegen van protonen (H^+) wordt het negatief geladen citraat omgezet in het ongeladen citroenzuur, zonder dat het citraat/citroenzuur van het

oppervlak verdwijnt. Na toevoeging van zoutzuur of zwavelzuur aan het colloïdale goud oplossing/heptaan systeem ontstond er een dichte monolaag op het water/heptaan oppervlak die sterk leek op de lagen gevonden na het toevoegen van ethanol.

Vermindering van de dikte van de dubbellaag geschiedt door middel van het toevoegen van zout (natriumperchloraat, $NaClO_4$). De laag die op deze manier gevormd werd bestond echter uit grote aggregaten. De aggregaten hadden een grootte van 100 nm of meer, terwijl de diameter van één deeltje slechts 16 nm was. Het dunner maken van de dubbellaag leidt dus niet alleen tot de vorming van een laag aan het water/heptaan oppervlak, maar tevens tot aggregatie van deeltjes. Deze twee effecten tezamen zorgen ervoor dat een laag bestaande uit grote aggregaten gevormd wordt.

Tot slot hebben wij geprobeerd de oppervlaklading van de deeltjes te verminderen door stoffen die aan goud adsorberen aan het colloïdale goud/heptaan systeem toe te voegen. Wij hebben de proef herhaald met verschillende moleculen met zwavel en/of thiol functionaliteit. De grensvlak-laag bevatte naast gebieden met aggregaten ook gebieden met goudnanokristal monolagen.

Hierboven is aangetoond dat dichte monolagen van goudnanokristallen gevormd worden aan het water/heptaan oppervlak na een kleine vermindering van de oppervlaklading van de goudnanokristallen. Omdat reductie van de oppervlaklading op vele manieren kan plaatsvinden, zou de vorming van een grensvlak-laag door ladingsvermindering bruikbaar zijn bij een groot scala van ladings-gestabiliseerde deeltjes.

In hoofdstuk 4 wordt een model besproken die de bevindingen van hoofdstuk 3 probeert te verklaren. In dit model wordt aangenomen dat de goudnanokristallen allemaal gelijk van grootte en perfect rond zijn. In dit model wordt de chemische potentiaal van de goudnanokristallen in de bulk (waterige) fase, μ_{bulk}, en de goudnanokristallen in het grensvlak, μ_{surf}, afgeleid.

De chemische potentiaal van de bulk fase bestaat uit drie termen:

- Een ideale oplossing term, waarbij wordt aangenomen dat de deeltjes geen interacties met elkaar vertonen. Deze term heeft veel weg van de beschrijving van een ideaal gas.
- Een correctie term, welke een viriaal coëfficiënt bevat, die de aanwezigheid van attracties/repulsies tussen de deeltjes beschrijft.
- En tenslotte een oppervlak-energie term, die de oppervlakspanning van het water/nanokristal grensvlak bevat.

De chemische potentiaal van de nanokristallen aan het water/heptaan grensvlak wordt beschreven door vier termen:

- Een grensvlak term, die de oppervlakspanning van de drie grensvlakken (water/nanokristal, nanokristal/heptaan en water/heptaan)

in rekening brengt. Tevens wordt ook de lijnspanning in rekening gebracht.

- Een elektrostatische repulsie term. Er werd aangenomen dat, na zelf-assemblage van de goudnanokristallen aan het oppervlak, een fractie α van de originele oppervlak-ladingsdichtheid σ op het nanokristal/heptaan grensvlak achterblijft. Omdat de heptaan fase deze lading niet afschermt, wordt aangenomen dat alle elektrostatische repulsie veroorzaakt wordt door deze ladingen. De interactie werd berekend voor deeltjes in een 2D hexagonale ordening van nanokristallen.
- Een term die de van der Waals attractie beschrijft tussen de nanokristallen. Hierbij wordt aangenomen dat de deeltjes aan het water/heptaan oppervlak geordend zijn volgens een hexagonaal rooster.
- En tenslotte een translationele entropie term.

Wanneer een evenwicht wordt bereikt, is de chemische potentiaal van de bulk en die van het grensvlak aan elkaar gelijk, $\mu_{bulk} = \mu_{surf}$. Hieruit wordt een adsorptie isotherm afgeleid die de volgende variabelen bevat: De grootte van de nanokristallen, de oppervlakspanning van het water/heptaan oppervlak (en de lijnspanning), en de resterende lading aan het nanokristal/heptaan grensvlak $\alpha\sigma$. Doordat de goudnanokristallen volledig amphifiel zijn (d.w.z. de goudnanokristallen bevinden zich half in de water- en half in de heptaanfase) vallen de oppervlakspanningen van het water/nanokristal en nanokristal/heptaan oppervlak tegen elkaar weg.

Uit de berekeningen volgt dat zowel de grensvlak-energie term als de van der Waals attractie term de vorming van een dichte laag bevorderen, terwijl Coulomb repulsies deze tegengaat. Omdat de Coulomb repulsie term sneller toeneemt bij toenemende deeltjesgrootte dan de van der Waals en grensvlak-energie termen, zullen grote goudnanokristallen zichzelf minder snel assembleren aan het water/heptaan oppervlak dan kleine nanokristallen. Met andere woorden: Er is voor grote deeltjes een sterkere verlaging van de oppervlaklading $\alpha\sigma$ nodig om dezelfde concentratie van nanokristallen aan het grensvlak te krijgen dan voor kleine deeltjes. Ondanks de ruwe aannames in het model konden de bevindingen uit hoofdstuk 3 semikwantitatief verklaard worden.

List of Publications

F. Reincke, S.G. Hickey, J.J. Kelly, T.W. Braam, L.W. Jenneskens, and D. Vanmaekelbergh,
Electrochemical and topological characterization of gold(111) | oligo(cyclohexylidene) | gold nanocrystal interfaces,
Journal of Electroanalytical Chemistry **522** (2002) 2-10

F. Reincke, S.G. Hickey, W.K. Kegel and D. Vanmaekelbergh,
Spontaneous Assembly of a Monolayer of Charged Gold Nanocrystals at the Water/Oil Interface,
Angewandte Chemie, International Edition **43** (2004) 458-462

F. Reincke, W.K. Kegel and D. Vanmaekelbergh,
A thermodynamic evaluation of self-assembly of charged nanometre-sized crystals at the water/heptane interface,
To be submitted to Langmuir

Dankwoord

Onbewust heb ik toch de meeste moeite met dit gedeelte van mijn proefschrift, omdat je het eigenlijk nooit goed kan doen: Als je te veel voorbij gaat aan de dingen die iemand voor je gedaan heeft dan ben je respectloos, terwijl als je iemand te veel ophemelt dan vindt men het klef, of nog erger, sarcastisch. En als je iemand vergeet dan is helemaal de boot aan! Toch wil ik iedereen bedanken voor hun bijdrage aan de gezellige sfeer gedurende de afgelopen 4 jaar en een beetje (zeg maar 4.5).

Allereerst wil ik mijn promotor, Daniël Vanmaekelbergh, bedanken. Je hebt altijd een zeer grote interesse getoond in mijn werk en je hoofd liep altijd over van nieuwe dingen die leuk waren om te onderzoeken.

John Kelly, mijn co-promotor, wil ik bedanken voor een plezierige samenwerking. Je vindt het altijd vreselijk als mensen je vousvoyeren. Ik heb lang nagedacht waarom ik dat altijd deed en volgens mij is het je gentlemanachtige uitstraling, ondanks het feit dat je *roots* in Ierland liggen.

Ten slotte wilde ik mijn andere co-promotor, Willem Kegel, bedanken voor alle steun. Jouw enthousiasme voor je vak is bijkans nog groter dan dat van Daniël. Mede door je recht-door-zee mentaliteit heb ik een plezierige samenwerking met je gehad.

En laat ik ook de andere hoogleraren in onze vakgroep Andries Meijerink en Cees Ronda niet vergeten te bedanken voor de vele colleges die zij hebben gegeven en Andries in het bijzonder voor het lenen van zijn digitale camera zodat ik dit proefschrift van mooie illustraties kon voorzien.

Tijdens mijn promotie heb ik in de loop der jaren drie kamergenoten gehad. Allereerst was daar Willem Tjerkstra die mij de liefde voor Linux heeft bijgebracht. En ik moet zeggen dat mij dat nog steeds niet heeft bezuurd, alhoewel ik wel regelmatig nog die verdorven software uit Redmond, Washington, gebruik. Na een tijd kamergenootloos te zijn geweest en na een verbouwing kreeg ik Alexander Germeau als kamergenoot. Alexander, je bent een toffe kamergenoot geweest en ik wens je veel succes bij SRON (Stichting Ruimtevaart Onderzoek Nederland). En tevens hoop ik dat er nooit meer konijnen op de sofa mogen komen. Peter Liljeroth, you were the last person I shared a room with, and I hope I didn't annoy you too

much that last few months. I never could tell behind that patented Finnish undercooled facade.

Nu wij toch dicht bij 'huis' zijn wil ik ook mijn (kantoor)buren bedanken. Steven 'the Hickmeister' Hickey, your door was always open for a chat about my results and some good advice, or just for some fun and laughs. And if it wasn't for your keen eye there wouldn't be a chapter 3 and 4. And of course Celso de Mello Donegá, my other 'neighbour'. I will always remember you discussing articles and problems with Steven. These talks used to last a good part of the monday morning and somehow, despite the serious topics that were discussed, there was always a very friendly and good-spirited atmosphere.

Het sociale leven van deze vakgroep draaide vooral om een tafelvoetbaltafel. In een grijs verleden aangekocht, is er zo vaak op gespeeld dat de stangen nu zo krom zijn dat de blauwe aanvallers de bal bijna niet meer kunnen raken. Een goede investering me dunkt. Aangezien je na een tijd op elkaar ingespeeld raakt, werd er door Arjan Houtepen de *mayhem*-factor even opgekrikt. Hij voerde namelijk de variant *duoball* in, oftewel het spelen twee ballen. Terloops had Arjan even het eerste jaarlijkse Ornstein tafelvoetbaltoernooi georganiseerd, dat hij ook pardoes won (toeval?). Deze liefde voor het tafelvoetbal werd je met de paplepel ingegoten door je exkamergenoot, Aarnoud 'de roestbak' Roest, die zich voor laat staan op zijn verwoestende schoten van achteruit.

En niet vergeten de andere AIO's die ik enige of langere tijd heb meegemaakt, Erik 'Diaz' Bakker, Ageeth Bol, Addy van Dijken, Marcel Di Vece, Floris van Driel, Petra de Jongh, Paul Peijzel, Liesbeth van Pieterson, Harold Philipsen, Freek Suyver, Peter Vergeer, Arjan Vink, Bert van Vught, René Wegh en Sander Wuister. En natuurlijk ook de postdocs Zeger Hens, Monica Giesselbach en Xinghua Xia.

Dan nog een aantal mensen van de 'supporting staff': Hans 'discrip' Lighthart, jij kon bijna alle problemen oplossen. Een idee, hoe vaag ook, wist je altijd tot een werkend geheel te maken. Stephan, jij was vooral de stille kracht van de vakgroep. Van het schrijven van de besturingsprogramma's voor de potentiostaten tot het urenlang bedienen van de Scanning Electron Microscope (SEM). Paul Jurrius, ik was een tijd regelmatig in je werkplaats te vinden om een goud plakje te 'annealen' (lees: rustig verwarmen). Uiteindelijk is het ons toch gelukt om de waterstofgenerator, waarmee wij annealden, bij ons op de kamer te krijgen. Maar als ik ooit nog ergens een gaatje in wil laten boren, dan weet ik je te vinden. En niet te vergeten de secretaresses Jessica en Clarien. Jessica, sorry je zult nu verder zonder mijn overheerlijke taart door het leven moeten en Clarien ik hoop dat je geen slapeloze nachten hebt gehad van het samenstellen van het AIO Boekje. Tot slot wil ik de glasblazers bedanken, want van hen hebben ik en mijn

mede-vakgroepsgenoten nog het meeste gevraagd: De meest vreemdvormige elektrochemische cellen, 1500 stukjes glas van 13 bij 13 bij 1 millimeter. En oh als je dan toch bezig bent doe dan maar 1000 borosilicaat(lees: pyrex) glas van 11x11x1 en 200 van 30x11x1. En niet te vergeten het polijsten van al die aluminium substraten.

Ik wil ook 'mijn' student, René de Waele, bedanken, want het is waar: je bouwt toch iets persoonlijks op met je 'eigen' student. Je was altijd zeer hardwerkend en zeer nieuwsgierig. Ik weet dat dit erg clichématig klinkt, maar ik meen het echt. Naast René bedank ik ook de vele andere studenten die het Ornstein gebouw bevolkten en voor sfeer op de vakgroep zorgden.

Tot slot wil ik mijn ouders en mijn zus bedanken, zonder hun onvoorwaardelijke steun zou ik nooit zover zijn gekomen.

Curriculum Vitae

De schrijver van dit proefschrift werd op 30 augustus 1976 geboren te Leidschendam. Na het behalen van het VWO-diploma op de RK Scholengemeenschap Alfrink College te Zoetermeer in 1994, begon hij aan de studie Scheikunde aan de Universiteit van Utrecht. In augustus 1999 werd het doctoraalexamen Scheikunde afgelegd. Het laatste jaar van zijn doctoraalstudie bestond uit een onderzoek naar het elektrochemisch reactiemechanisme van zink en chroom-EDTA complexen aan druppelende kwik (micro)elektrode bij de (inmiddels opgeheven) sectie 'Electrochemie'. Op 1 september 2003 trad hij in dienst bij de faculteit Scheikunde van de Universiteit van Utrecht als onderzoeker in opleiding bij de sectie 'Gecondenseerde Materie' van het Debye Instituut. De resultaten van dit onderzoek zijn beschreven in dit proefschrift en gepresenteerd op de conferentie "Joint International Meeting of the Electrochemical Society and the International Society of Electrochemistry" (San Francisco, California, USA in september 2001). Naast onderzoek begeleidde hij eerstejaars studenten Scheikunde bij het practicum scheikunde en eerstejaars studenten Natuurwetenschap en Innovatiemanagement in het vak 'Scheikunde 1b: Thermodynamica'. Daarnaast was hij actief binnen de Debye AIO Commissie.